IMM 394
April 1973

Courant Institute of
Mathematical Sciences

Some Problems in Geophysics

J. J. Stoker

Prepared under Contract N00014-67-A-0467-0030
with the Office of Naval Research NR 041-446

New York University

NR 041-446

IMM 394
April 1973

New York University

Courant Institute of Mathematical Sciences

SOME PROBLEMS IN GEOPHYSICS

J. J. Stoker

This report represents results obtained at the Courant Institute of Mathematical Sciences, New York University, with the Office of Naval Research, Contract N00014-67-A-0467-0030.

Table of Contents

Preface

This report gives somewhat abbreviated versions of talks in a seminar on geophysics that was held once a week during the academic year 1970-71 at the Courant Institute of Mathematical Sciences of New York University.

The talks were presented for the most part by applied mathematicians rather than by professionals in the field of geophysics, but a number of professionals attended the seminar. It was hoped that both groups would find it interesting and rewarding to look at the problems together, based on the well-founded experience in science that progress has often resulted by bringing disciplines together that at first sight might not seem to have much in common. It was also thought desirable to examine a rather wide variety of physical problems, which in turn required the use of a variety of mathematical ideas and methods. For example, more emphasis was put on problems with formulations from the theory of elasticity in its linear version than is usual in the literature on geophysics.

Some of the ideas advanced may well be found highly speculative by professionals, but it is hoped that they may nevertheless be found amusing and stimulating. Of course, it is also hoped that applied mathematicians may find it worthwhile to become acquainted with the highly attractive and varied field of geophysics.

Lecture 1

The Gyroscopic Motions of the Earth

J. J. Stoker

A variety of phenomena in geophysics, such as the diurnal variation of the tides in the ocean, and seasonal changes in the atmosphere, are caused by gyroscopic motions of the earth, which in turn are the result of gravitational action by the sun and the moon. In this first lecture the salient features of the gyroscopic motions of the earth are described.

In geocentric coordinates, the earth spins with a period $T_0 = 1$ day, the sun moves about the earth with a period $T_1 = 1$ year and the moon moves about the earth with a period $T_2 = 27.2$ days. The earth's spin axis rotates with a retrograde precession about the normal to the ecliptic (the plane of the sun's orbit) with a period $T_3 = 26{,}000$ years, whereas the moon's node (the line in which the plane containing the moon's orbit intersects the ecliptic) precesses with a period $T_4 = 18\frac{2}{3}$ years. Finally, the earth's axis executes small oscillations of amplitude measured in seconds of arc, called nutations, which have various periods and which have various causes.

A description of these motions based on rigid body dynamics will be given, but without detailed analysis. For such an analysis the book of Klein-Sommerfeld: Die Theorie des Kreisels, should be consulted.

The orbital motions of the sun and the moon relative to the earth come from the gravitational forces between them. The

gyroscopic motions of the earth arise from the gravitational torques exerted on it by both the sun and the moon. These torques owe their existence to the departure of the earth from sphericity. In fact the ellipsoidal earth with mass m_o has an axial moment of inertia C larger than its transverse moment of inertia A such that $(C-A)/C \cong 1/305$. The earth's radius is small compared with the distances to the sun and the moon. As a consequence the gravitational potential energy of the ellipsoidal earth may be replaced with good accuracy by that of a homogeneous sphere plus a thin uniform ring around its equator in such a way that the total mass, m_o, and the moments of inertia of this combination are the same as those of the earth. The ring must have a radius r_o and a mass m, and the sphere must have a mass M, such that $M + m = m_o$, $\frac{1}{5}Mr_o^2 + mr_o^2 = C$ and $\frac{1}{5}Mr_o^2 + \frac{1}{2}mr_o^2 = A$, i.e. $M = 5(2A-C)/r_o^2$ and $m = 2(C-A)/r_o^2$. As the sun moves in an orbit which is very nearly circular and hence with constant velocity, its gravitational potential is a periodic function and can be expanded easily in a Fourier series. The time-independent secular term in the Fourier series can be interpreted with good accuracy as the potential due to a uniform thin ring with a mass m_1 equal to the sun's mass and a radius r_1 equal to the average distance between the sun and the earth. Similarly, the moon may be replaced by a uniform thin ring with a mass m_2 equal to the moon's mass and a radius r_2 equal to the average distance between the moon and the earth. These approximations can afterwards be improved by considering the effects of eccentricity of the orbits and of nonuniform velocities as small perturbations.

The sun's ring lies in the ecliptic, but the earth's ring is inclined to the ecliptic at an angle θ approximately equal to $23\frac{1}{2}^\circ$. Thus the gravitational attraction of the sun's ring on the earth's ring produces a torque about the earth's node (the line in which the plane containing the earth's ring intersects the ecliptic). A similar torque is produced by the gravitational attraction due to the moon's ring. Neglecting the small inclination angle (approximately 5°) between the moon's ring and the ecliptic, the resultant torque on the earth's ring is found to be given approximately by

$$\frac{3}{4}Gmr_o^2\left(\frac{m_1}{r_1^3}+\frac{m_2}{r_2^3}\right)\cos\theta\sin\theta$$

where G is the gravitational constant. This torque, acting on the earth's ring, which spins with the period of T_o, produces a precession of the earth's axis. The angular velocity of the precession is

$$\frac{3}{8\pi}G\,\frac{mr_o^2T_o}{C}\left(\frac{m_1}{r_1^3}+\frac{m_2}{r_2^3}\right)\cos\theta\ .$$

It is worth mentioning that the contribution due to the moon's attraction is larger than that due to the sun by a factor of 2.13 because the distance to the moon is small enough to outweigh its much smaller mass. (This is also the reason why the moon's effect is predominant in creating the tides in the oceans.) Using the relationships

$$\left(\frac{2\pi}{T_1}\right)^2 = G\,\frac{m_1}{r_1^3}\left(1+\frac{M}{m_1}\right) \quad \text{and} \quad \left(\frac{2\pi}{T_2}\right)^2 = G\,\frac{m_2}{r_1^3}\left(1+\frac{M}{m_2}\right)$$

as given by Kepler's laws we obtain the period of the earth's precession as

$$\frac{1}{T_3} = \frac{3}{2}\,\frac{C-A}{C}\left[\frac{T_o}{T_1^2\left(1+\frac{m_o}{m_1}\right)} + \frac{T_o}{T_2^2\left(1+\frac{m_o}{m_2}\right)}\right]\cos\theta\ .$$

If the value of $(C-A)/C$ is taken as 1/305, we get T_3 equal to 26,000 years (i.e. $51\frac{1}{2}''$ of arc per year). In fact, however, the above formula was really used to calculate $(C-A)/C$, by using the observed value of T_3. The result is in agreement with other methods. Moreover, the precession of the earth's axis is retrograde, i.e. the equinoxes (the points where the earth's node intersects the sun's ring) move in a sense opposite to that of the earth's spin. This is so because the torques tend to pull the earth's ring into the ecliptic.

In the same manner, due to its inclination to the ecliptic, the rotating moon's ring precesses under the gravitational torque produced by the sun's ring (the torque produced by the earth's ring is negligible). The calculated period is 18 years under the assumption made here, which is considerably smaller than the observed value of $18\frac{2}{3}$ years. The discrepancy arises in the main from the rather large eccentricity of the moon's orbit.

The steady precession of the earth's axis is subject to various small amplitude nutations. The component due to the free

oscillation (as the initial conditions do not fit the exact precession) has an amplitude of the order of tenths of a second of arc and a period of 304 days, which is much smaller than the observed value of 428 days. The discrepancy is attributed to the elasticity of the earth. It appears that the earth should have the rigidity of steel to reconcile the discrepancy. More important components, because of larger amplitudes, come from the forced oscillations due to external periodic torques with periods equal to those of the precession of the moon's ring, and the fact that the orbits of the sun and the moon are not circular. These terms arise from the harmonic components in the Fourier series for the time-dependent gravitational potentials of the precessing moon's ring and the orbiting sun and moon.

To summarize, we combine the various gyroscopic motions linearly in the following expressions (time t is measured in years) for the inclination angle θ and the azimuthal angle ψ, both with reference to the ecliptic, which specify the orientation of the earth's axis.

$$\psi = 50''.3714\ t - 17''.251 \sin \frac{2\pi t}{T_4} + 0''.207 \sin \frac{4\pi t}{T_4} - 1''.269 \sin \frac{4\pi t}{T_1} - 0''.204 \sin \frac{4\pi t}{T_2} ,$$

$$\theta = 23^\circ 27' 32''.0 + 9''.223 \cos \frac{2\pi t}{T_4} - 0''.090 \cos \frac{4\pi t}{T_4} + 0''.551 \cos \frac{4\pi t}{T_1} + 0''.089 \cos \frac{4\pi t}{T_2} .$$

The perturbation due to the second harmonic of the precession of the moon's ring is included here. More correction terms can be added to account for the ellipticity of the orbits, motions of the perihelia,and interaction of other planets.

Lecture 2

Flood Waves in Rivers and Reservoirs

J. J. Stoker

Flow problems in rivers and reservoirs were treated in the past by hydraulic engineers using the flood-routing method.[1] Owing to its oversimplification of the dynamic behavior of the flows, the method was not always applicable. With the advent of high speed digital computers it became feasible to solve the flow problems numerically by finding the solutions for the governing nonlinear partial differential equations. The first attempts were made by Stoker, Isaacson and Troesch[2] in 1953-1956 on a UNIVAC computer (see also [3]). Three test cases were made, with the object of comparing the observed flood stages with those computed numerically:

(1) Flow in a long river: the flood of 1945 in the 375-mile stretch of the Ohio River between Wheeling, W. Va., and Cincinnati, Ohio,

(2) Flow through a junction of two rivers: the flood of 1947 through the junction of the Ohio and Mississippi Rivers at Cairo, Ill., about 35 miles in each branch, and

(3) Flow in a long reservoir: the flood of 1950 through Kentucky Reservoir, about 184 miles long, in the Tennessee River.

In each case, the flood stages (the height of the water surface above sea level) and the flow velocities (averaged over the cross section) were assumed known everywhere at some arbitrarily selected initial time. For subsequent times the inflow from

tributaries and the local run-off in the main valley were taken from the actual records, and the progress of the flood in the main stream at various locations along the river was then computed for future times of the order of weeks. The numerically calculated flood stages were then compared with those actually observed along the river. The results as shown in Figures 1, 2, and 3 were very satisfactory. Thus, it was demonstrated that numerical flood predictions have become possible in a practical way (in contrast with the earlier failure in the much more complicated case of numerical weather predictions*) as it is conceivable that it might take longer to predict a flood numerically than the duration of the flood itself. Even on the UNIVAC the computing time needed to compute flows for periods of three weeks was about six hours; with the equipment available now, the CDC 6600, the time would be reduced to seconds. After some initial hesitation, hydraulics engineers have accepted the method as practical and useful, and it has superceded the building of very expensive hydraulic models — which, in any case, were not true models but rather analogue computers.

The laws of conservation of mass and momentum for flow in an open channel are formulated in the following two partial differential equations for H (the flood stage, e.g. the height above sea level) and u (the flow velocity) in terms of the distance x along the river and the time t:

---

* At the present time, numerical prediction of various quantities important in weather forecasting is carried out successfully, at least for times of the order of days.

$$B(x,H)\,\frac{\partial}{\partial t}\,H + \frac{\partial}{\partial x}[A(x,H)u] = q(x,t) \ ,$$

$$\frac{\partial}{\partial t}\,u + u\,\frac{\partial}{\partial x}\,u + g\,\frac{\partial}{\partial x}\,H = -F(x,H)u|u| \ .$$

In these equations g is the acceleration of gravity, A is the cross-section area of the river, B ($= \frac{\partial A}{\partial H}$) is the breadth of the river at its surface, and F is the friction coefficient. As indicated A, B, and F are functions of x and H. In any given case they are quantities that must be determined empirically; the first two, of a geometric nature, were obtained from topographic maps of the river valley, while the friction coefficient was determined by using flow data for past floods from $F = g|\frac{\partial H}{\partial x}|/u^2$, by neglecting the inertia term in the equation of motion. The source term q represents the rate of the inflow into the main channel per unit length of the river, either from tributaries or by the flow over its bank from the main valley; this quantity was estimated from actual records in our test cases. The term $Fu|u|$ represents a resistance which is in the direction opposite to the flow.

In addition to the differential equations, it is necessary to prescribe initial data and boundary data to have a completely formulated problem with a definitely determined solution. As initial data, the values of the stage and velocity at some instant of time were taken from flood records. As the boundary data for the first test case, the inflow at the upper end (Wheeling) and a rating curve (a relation between H and u obtained from previous floods) at the lower end (Cincinnati) were used. For the second

test case, the continuity conditions for the stages and discharges at the junction were used, in addition to the boundary data at the three ends. For the third test case the discharge rate at the dams at the two ends of the reservoir from actual records were used.

The two partial differential equations for u and H are a hyperbolic system possessing two real characteristics. In fact, the following characteristic form

$$\left[\frac{\partial u}{\partial t} + \left(u \pm \sqrt{\frac{gA}{B}}\right)\frac{\partial u}{\partial x}\right] \pm \sqrt{\frac{gB}{A}}\left[\frac{\partial H}{\partial t} + \left(u \pm \sqrt{\frac{gA}{B}}\right)\frac{\partial H}{\partial x}\right] = -Fu|u| \pm \sqrt{\frac{g}{AB}}\,(q - u\,\frac{\partial A}{\partial x})$$

indicates that the two characteristics are given by curves in the x,t plane as defined by $\frac{dx}{dt} = u \pm \sqrt{\frac{gA}{B}} \equiv c_{\pm}$. Thus $\sqrt{\frac{gA}{B}}$ can be interpreted as the velocity at which a small disturbance in the flow propagates downstream and upstream relative to the flow. The hyperbolic character of the governing equations has an important consequence in the numerical scheme for solving the problem. Namely, for a given space interval Δx for the net points, the time interval Δt must be small enough so that, $\frac{\Delta x}{\Delta t} > c_{\pm}$, with $c_{\pm}$, the quantity defined above. In all three test cases, Δx was chosen as 10 miles and Δt was taken as 9 minutes in order to be within the necessary bound.

Finally, we remark that the success of the present method over the flood routing method for some problems (for which the dynamical equation of motion is replaced by a kinematic empirical relation that is based in part on the idea that flood waves

progress downstream, thus backwater effects are ignored) is caused by the fact that propagation of waves upstream as well as downstream has been taken into account.

References

1. H. A. Thomas, The Hydraulics of Flood-Movements in Rivers, Carnegie Institute of Technology, Pittsburgh, Pennsylvania, 1937.

2. E. Isaacson, J. J. Stoker, and A. Troesch, Numerical Solution of Flow Problems in Rivers, Proceedings of the American Society of Civil Engineers, Journal of the Hydraulics Division, 1958.

3. J. J. Stoker, Water Waves, Wiley-Interscience, New York, 1957.

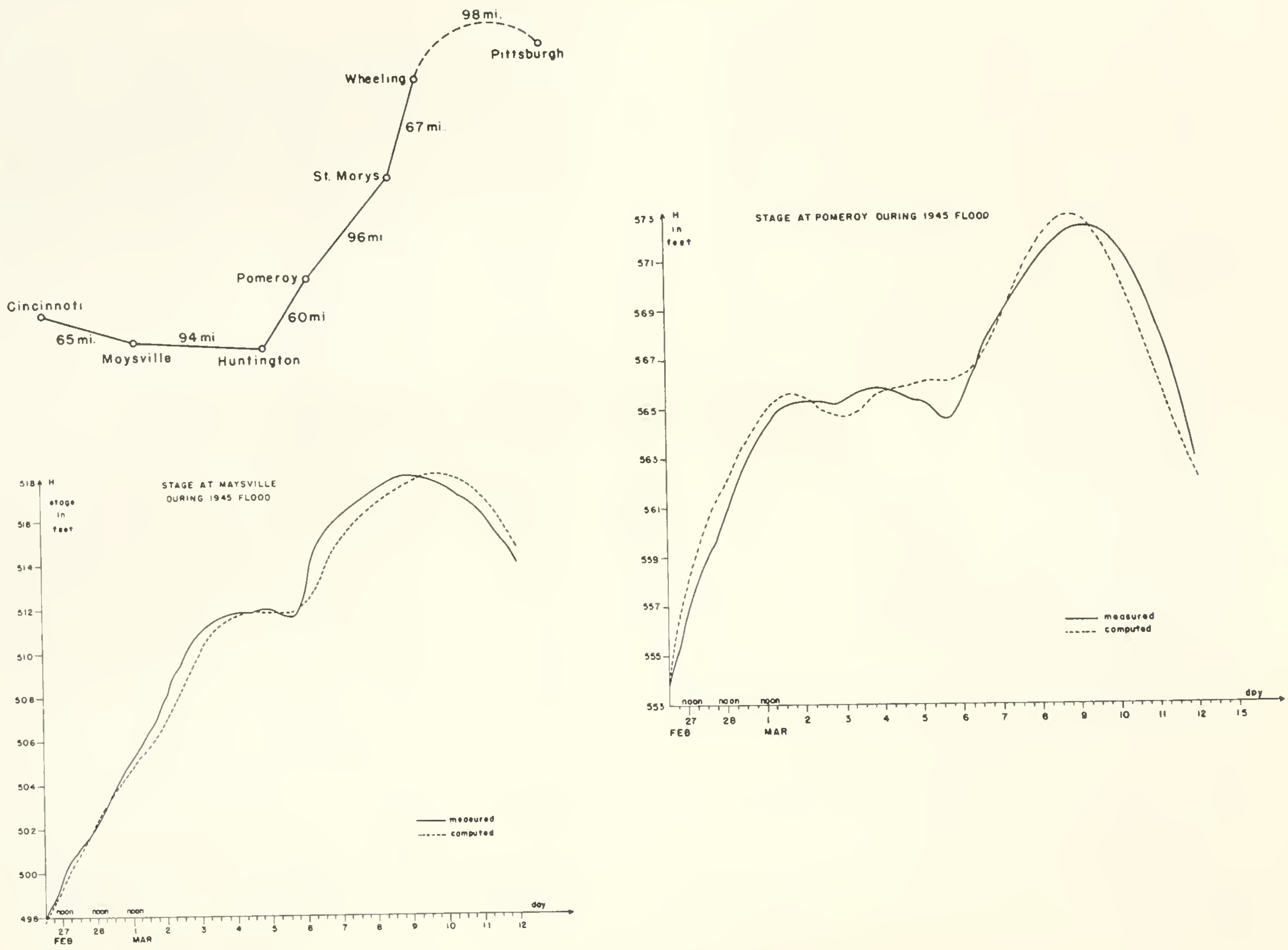

Fig. 1. Flow in a long river

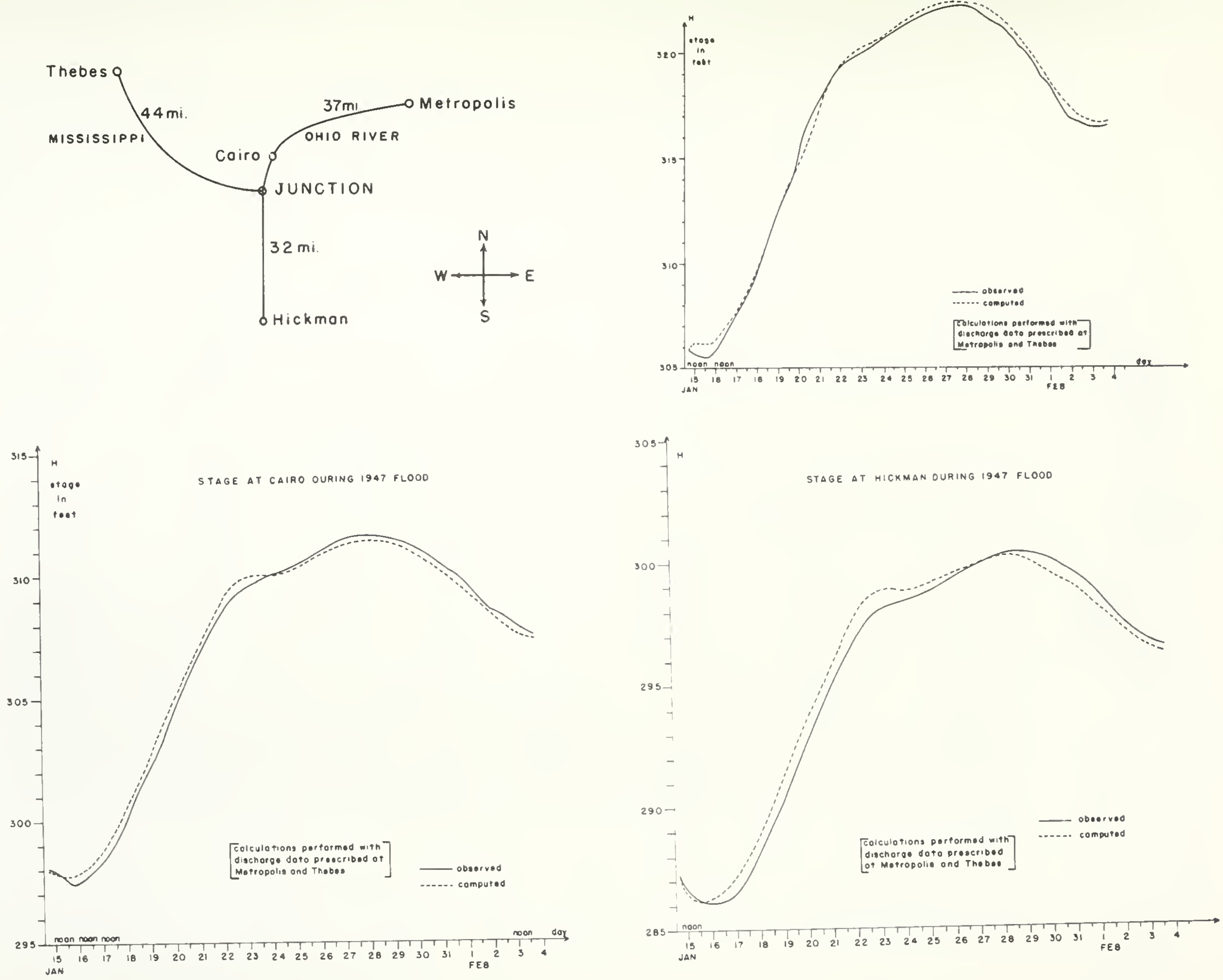

Fig. 2. Flow through a junction of two rivers

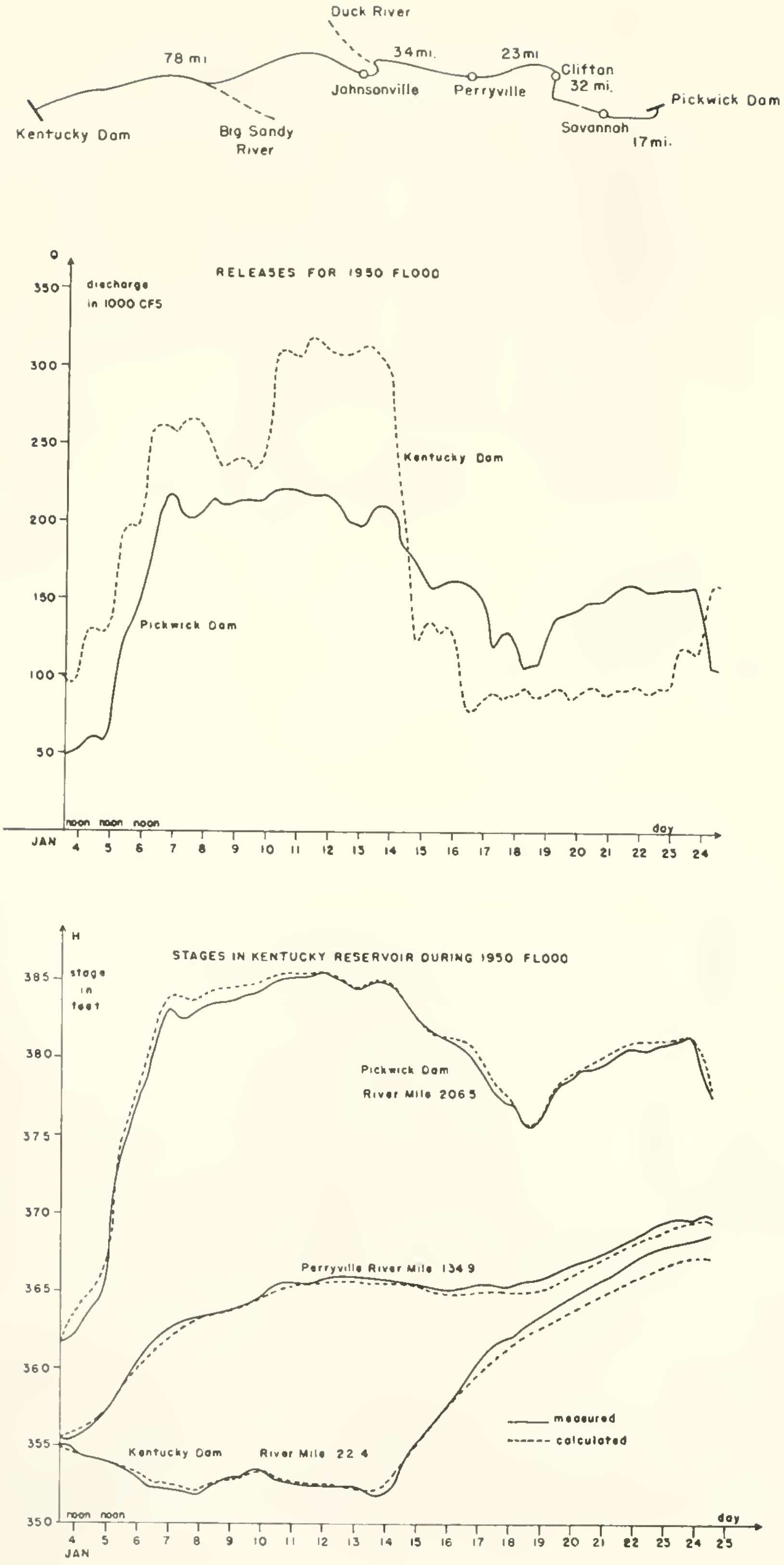

Fig. 3. Flow in a long reservoir

Lecture 3

Frontal Motion in the Atmosphere

J. J. Stoker

The weather in middle latitudes is determined primarily by events associated with the development and propagation of frontal cyclones between tropical and polar air masses in the atmosphere. Before the advent of computers, mathematical studies were limited to small perturbations to a quasistationary front with the aim of finding solutions whose patterns resemble those of observed nascent cyclones. As a prelude to study the nonlinear effects in the dynamical equations, Stoker (1957) formulated a two-layer model for the frontal motion. Then, Kasahara, Isaacson and Stoker (1965) made the first successful attempt in showing the evolution toward an occlusion from a developing frontal cyclone.

Before describing the mathematical model and the results of numerical computation, a brief mention of some of the meteorological observations about weather fronts should be made. In the middle latitudes the upper layer of warm air is separated from the lower layer of cold air by a thin transition zone (a discontinuity surface) across which both the density and the tangential velocity of the air change abruptly. The intersection of this discontinuity surface with the ground forms the "front". The front moves eastward as a whole. The portions of the front where the cold air pushes the warm air off the ground are called cold fronts, and the portions where the cold air is receding from

the warm air are called warm fronts. Since a cold front usually moves faster than its adjacent warm front, what is called an occlusion may develop eventually.

Figure 1 shows the dynamical system to be studied. The cold air at the ground occupies a wedge-like domain with warm air over it. The interface is given by $z = h(x,y,t)$, with x in the eastward direction and y in the northward direction. The top of the warm layer, where atmospheric pressure is essentially zero, is given by $z = h'(x,y,t)$. The fluid in each layer is assumed to be inviscid and incompressible, with constant density ρ and ρ' in the cold and warm layers respectively, and subject to gravity. For large scale motions in meteorology the hydrostatic pressure law holds quite well, and this means that the acceleration of the fluid in the vertical direction can be neglected. Hence the pressure in the warm layer is given by

$$p'(x,y,z,t) = \rho' g(h' - z) ,$$

and the pressure in the cold air by

$$p(x,y,z,t) = \rho' g(h' - h) + \rho g(h - z) ,$$

g being the gravitational constant. It follows that the horizontal pressure gradient is independent of z. Since the Coriolis force due to the rotation of the earth may also be regarded as independent of z without serious error, it follows that the horizontal acceleration of fluid particles is independent of z, and hence that the horizontal components of velocities u, v and u', v' will remain independent

of z if they were so initially, which is assumed here. The equations of motion, in Eulerian form, are

$$\frac{\partial u'}{\partial t} + u' \frac{\partial u'}{\partial x} + v' \frac{\partial u'}{\partial y} + g \frac{\partial h'}{\partial x} = fv' ,$$

$$\frac{\partial v'}{\partial t} + u' \frac{\partial v'}{\partial x} + v' \frac{\partial v'}{\partial y} + g \frac{\partial h'}{\partial y} = -fu'$$

for the warm air, and

$$\frac{\partial u}{\partial t} + u \frac{\partial u}{\partial x} + v \frac{\partial u}{\partial y} + g\left(\frac{\rho'}{\rho} \frac{\partial h'}{\partial x} + \frac{\rho-\rho'}{\rho} \frac{\partial h}{\partial x}\right) = fv ,$$

$$\frac{\partial v}{\partial t} + u \frac{\partial v}{\partial x} + v \frac{\partial v}{\partial y} + g\left(\frac{\rho'}{\rho} \frac{\partial h'}{\partial y} + \frac{\rho-\rho'}{\rho} \frac{\partial h}{\partial y}\right) = -fu$$

for the cold air. Here f is the Coriolis parameter, given by $f = 2\omega \sin \phi$ with ω the angular velocity of the earth and ϕ a reasonable latitude for the region under consideration. Since the fluids in both layers are assumed to be incompressible, the equations of continuity can be written as

$$\frac{\partial}{\partial t} (h' - h) + \frac{\partial}{\partial x}[u'(h' - h)] + \frac{\partial}{\partial y}[v'(h' - h)] = 0 ,$$

$$\frac{\partial}{\partial t} h + \frac{\partial}{\partial x}[uh] + \frac{\partial}{\partial y}[vh] = 0 .$$

The treatment can be simplified further by assuming that u', v', and h' do not change in time. The reason that the dynamics of the perturbations in the warm air relative to the initial stationary state can be neglected as a first approximation is that the warm layer can adjust itself through a slight change in the vertical

velocity without a substantial change in the horizontal velocity. Therefore, when the warm air is in a stationary state given by

$$u' = u'_o \text{ (const.)} , \quad v' = 0 , \quad h' = -\frac{f}{g} u'_o y + \text{const.}$$

the governing equations for the cold air become

$$\frac{\partial}{\partial t} h + \frac{\partial}{\partial x}[uh] + \frac{\partial}{\partial y}[vh] = 0 ,$$

$$\frac{\partial u}{\partial t} + u \frac{\partial u}{\partial x} + v \frac{\partial u}{\partial y} + g \frac{\rho - \rho'}{\rho} \frac{\partial h}{\partial x} = fv ,$$

$$\frac{\partial v}{\partial t} + u \frac{\partial v}{\partial x} + v \frac{\partial v}{\partial y} + g \frac{\rho - \rho'}{\rho} \frac{\partial h}{\partial y} = f\left(\frac{\rho'}{\rho} u'_o - u\right) .$$

The interface between the two layers is a free surface in the problem. Any point $(x_c(t), y_c(t))$ on the front moves with the particle velocity on it. This follows from the continuity equation, since at $h = 0$ the equation $\left(\frac{\partial}{\partial t} + u \frac{\partial}{\partial x} + v \frac{\partial}{\partial y}\right)h = 0$ holds.

To solve the partial differential equations for u, v, and h a rectangular domain $(0 < x < X, 0 < y < Y)$ in the xy plane is taken (see Fig. 2). For the boundary conditions, $v = 0$ is assumed for all time on the northern boundary $(y = Y)$ and u, v, h are assumed to be periodic in x, viz. $h\big|_{x=0} = h\big|_{x=X}$ etc. The boundary condition on the front is that $\frac{dx_c}{dt} = u$ and $\frac{dy_c}{dt} = v$. Two sets of initial conditions were actually considered.

<u>Case A.</u> The initial conditions are:

$$u = u_o \text{ (const.)} , \quad v = 0 ,$$

$$h = \frac{f}{g} \frac{\rho}{\rho - \rho'} \left(\frac{\rho'}{\rho} u_o' - u_o\right)(y - y_c) \quad \text{for} \quad y_c \leq y \leq Y ,$$

$$y_c = C_2 - C_1 \cos \frac{2\pi}{X} x_c .$$

<u>Case B.</u> The initial wind field is geostrophic:

$$u = u_o , \quad v = 0 ,$$

$$h = \frac{y - y_c}{Y - y_c} \frac{f}{g} \frac{\rho}{\rho - \rho'} \left(\frac{\rho'}{\rho} u_o' - u_o\right)(Y - C_1 - C_2) ,$$

$$y_c = C_2 - C_1 \cos \frac{2\pi}{X} x_c .$$

In the computation, it is convenient to use the moving coordinates ξ and η instead of x and y as defined by

$$\xi = x - u_o t , \quad \eta = y .$$

The increment sizes Δt = 10 minutes, $\Delta\xi$ = 76.2 km, $\Delta\eta$ = 76.2 km were chosen and $X = 20\Delta\xi$, $Y = 20\Delta\eta$, $C_1 = 2\Delta\eta$, $C_2 = 9.5\Delta\eta$, u_o = 10ft/sec, $\frac{\rho'}{\rho} u_o'$ = 50ft/sec, $f = 10^{-4}\text{sec}^{-1}$, $g = 32.15\text{ft/sec}^2$, $g(1 - \frac{\rho'}{\rho}) = .6\text{ft/sec}^2$ were used. The above magnitude of the density discontinuity corresponds to a temperature discontinuity of 5°C. The results of numerical calculation are shown in Fig. 3 for Case A and in Fig. 4 for Case B. In Fig, 3c the numerators and the denominators represent respectively the ξ-component and the η-component of the velocities of points on the front relative to the moving coordinate system, which has an eastward velocity of 10ft/sec.

It is seen that particles on the cold front moved southeastward and those on the warm front moved northwestward on the average, whereas both fronts themselves propagated eastwards. The movement of particles on the front clearly indicates the production of a cyclonic circulation around a center near the junction of the cold front with the warm front. The converging motion of the cold air near the circulation center will produce moist convections. This implies that severe storms are likely to be associated with cold fronts. In conclusion, the two cases studied indicate that the action of the purely mechanical forces, gravity and the Coriolis force, are primarily responsible for the gross features of the occlusion process for the weather fronts.

References

J. J. Stoker (1957): Water Waves, Interscience Publishers, New York.

A. Kasahara, E. Isaacson and J. J. Stoker (1965): Numerical studies of frontal motion in the atmosphere - I, Tellus, 17, pp. 261-276.

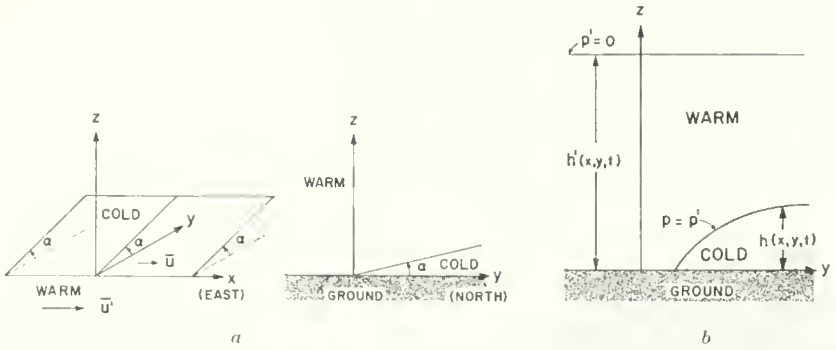

FIG. 1. (*a*) A stationary front. (*b*) Vertical cross section of the two layers.

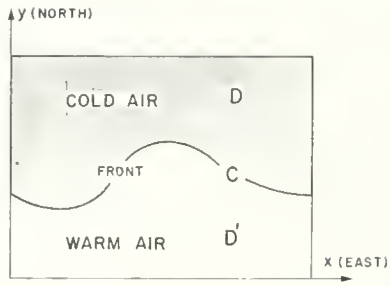

Fig. 2. The rectangular domain of numerical integration.

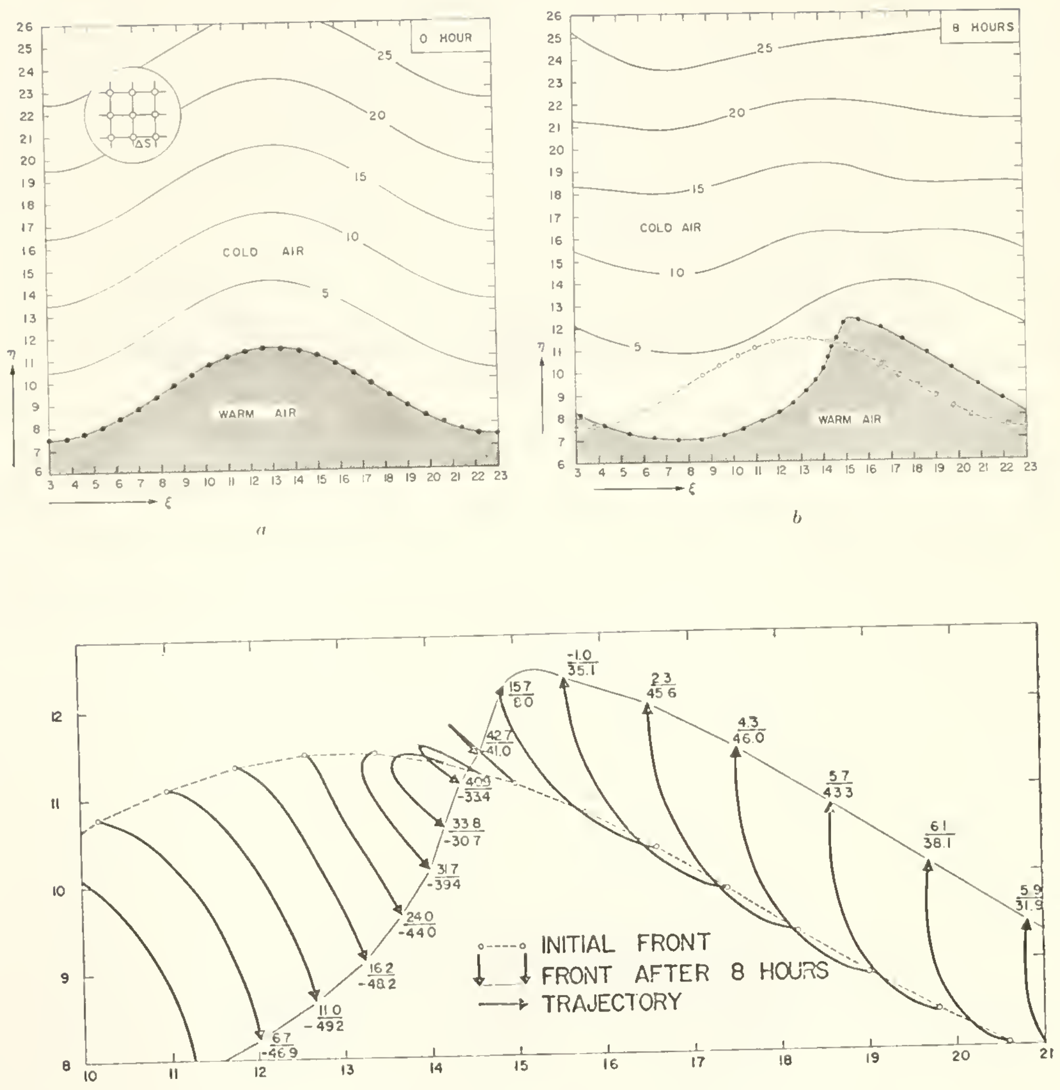

Fig. 3. Case A. Height contours (at 5000 ft. intervals) in the cold air layer and trajectories of front points during the period of 8 hours.

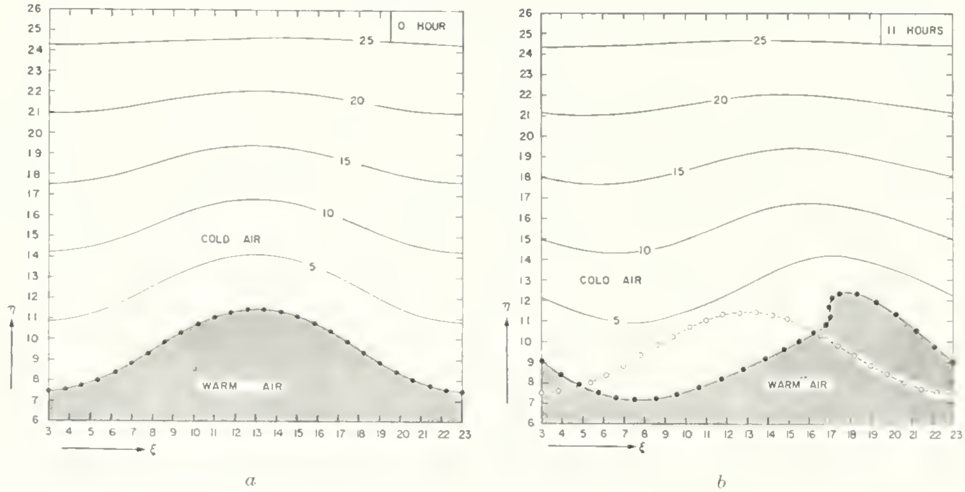

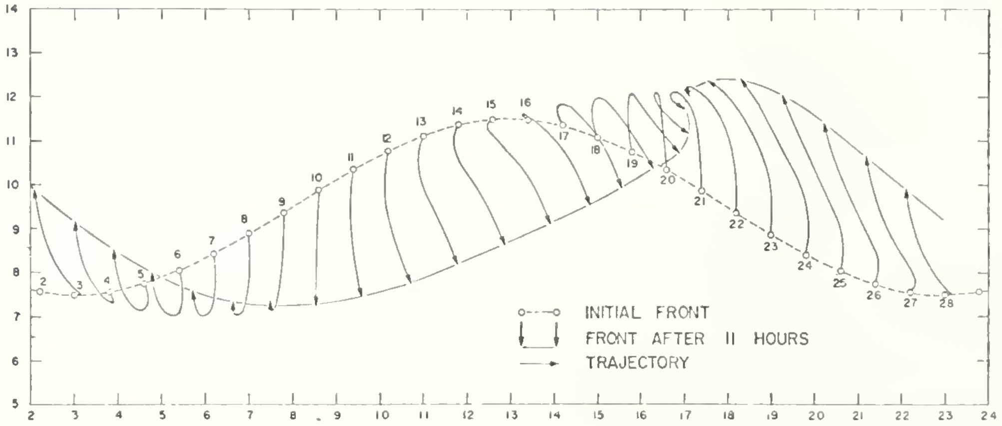

Fig. 4. Case B. Height contours (at 5000 ft. intervals) in the cold air layer and trajectories of front points during the period of 11 hours.

Lecture 4

Frontal Motion in the Atmosphere

E. Turkel

The equations, derived in a previous lecture, for a single layer model of the atmosphere are to be discussed here. Those equations are

$$u_t + uu_x + vu_y + g(1 - \frac{\rho'}{\rho})h_x = fv$$

(1) $$v_t + uv_x + vv_y + g(1 - \frac{\rho'}{\rho})h_y = f(u - \frac{\rho'}{\rho}\,\overline{u}')$$

$$h_t + (hu)_x + (hv)_y = 0$$

where u and v are the velocities of the cold air in the x and y directions respectively, while h is the height of the cold air. ρ and ρ' are the densities of the cold and warm air masses, f is the Coriolis parameter and $\overline{u}'$ is the speed in the x direction of the warm air.

It is assumed that the cold air lies above a region D of the x, y plane and that this region is bounded on three sides by straight lines and on the fourth side by a curve C(t) as illustrated in Fig. 1. The curve $C(t) : (x_C(t), y_C(t))$ is defined as the line along which h = 0. The points of C move in time with the velocity (u_C, v_C) of the particles on the front: Hence the following conditions hold along C:

$$h = 0$$

(2) $$\frac{d}{dt}(x_C(t)) = u_C(x_C, y_C, t)$$

$$\frac{d}{dt}(y_C(t)) = v_C(x_C, y_C, t)$$

where $\frac{d}{dt}$ is the particle derivative.

The quantities u, v and h must be prescribed along the other three boundaries. Two different situations are considered for the distance between the east and west boundaries. For simplicity it is first assumed that the dependent variables are initially sinusoidal in the x direction with a wavelength, λ, equal to the distance between the east and west boundaries. In the second situation, the east-west boundaries are taken to be three times more distanct than in the first situation, while the initial data are chosen to be constant for $0 \leq x \leq \lambda$ and $2\lambda \leq x \leq 3\lambda$, but in the region $\lambda \leq x \leq 2\lambda$ the dependent variables are chosen to be sinusoidal with wavelength λ, so as to lessen the boundary influence on the occlusion process. Along the northern boundary the north-south component of the velocity, v, is specified; and is not necessarily zero as was assumed in the preceding lecture.

A complete formulation of the problem requires appropriate initial data for u, v and h. It is also necessary to specify the initial position of the curve C(t) and the values of u and v along the front. In Case 1, u and v are taken initially the same as for the constant steady state zonal solution, while h varies linearly in y and sinusoidally in x.

The initial conditions are thus:

Case 1: (Non-geostrophic)

$$y_C = C_2 - C_1 \cos\left(\frac{2\pi}{X} x\right)$$

$$u = \bar{u}$$

$$v = 0$$

$$h = (y - y_C)H , \qquad y_C \leq y \leq Y$$

where

$$H = \frac{f}{g\left(1 - \frac{\rho'}{\rho}\right)} \left(\frac{\rho'}{\rho} \bar{u}' - \bar{u}\right) ; \qquad \frac{\rho'}{\rho} \bar{u}' > \bar{u} .$$

X, Y denote the lengths of the sides of R in the x and y directions respectively. The contour lines of the initial value of h, at 5000 foot intervals, are plotted in Figure 2a.

As a second case, a physically more realistic condition is assumed, namely that the wind field is initially geostrophic. Thus, at t = 0 there is no acceleration in either the x or y directions, i.e. $\frac{du}{dt} = \frac{dv}{dt} = 0$. This leads to the initial conditions.

Case 2: (Geostrophic)

$$h = \frac{y - y_C}{Y - y_C} (Y - b)H$$

$$u = -\frac{g\left(1 - \frac{\rho'}{\rho}\right)}{f} \frac{\partial h}{\partial y} + \frac{\rho'}{\rho} \bar{u}'$$

$$v = \frac{g\left(1 - \frac{\rho'}{\rho}\right)}{f} \frac{\partial h}{\partial x}$$

where $b = C_1 + C_2$ and H, Y, y_C are as in Case 1. The contour lines of the initial value of h for Case 2 is plotted in Figure 5a.

Subcases 1a and 2a denote the problems with periodic east-west boundary conditions and v = 0 at the northern boundary. Subcases 1b and 2b denote the same problems but with v specified (nonzero) at the north. Finally, subcases 1c and 2c concern the problems with the extended x domain, while v is taken as zero at the north.

Difference Equations

Consider the rectangle R with sides L_1, L_2. A dimensionless moving coordinate system is introduced so that in dimensionless units the unrefined mesh has length and width equal to 1 (see [3,5]). By D_Δ is meant the connected set of net points in the interior of D, the region under the cold air. By a regular point is meant a point in D_Δ whose eight nearest neighbors are all in D_Δ. All other points in D_Δ are called irregular points. At regular points, two different second order schemes are considered. The first is a one-step method that is a nonlinear generalization of the Lax-Wendroff method [4]. The second method is a two-step scheme due to Burstein [2]. At the northern boundary and at irregular points sufficiently far from the front, variations of the Lax-Wendroff method were used. At irregular points too close to the front the values of u, v and h were found by interpolation.

Boundary Conditions

The finite difference approximations at the boundaries are considered next. The east and west boundaries consist of regular

net points upon using the periodicity condition. Along the northern boundary v is given, while u and h are calculated by using one-sided differences.

Along the front the sound speed is zero and so the characteristic directions coincide with the particle path. Thus, u and v cannot be found by extrapolation along the characteristics but must be found by solving the differential equations (2) for u and v along the front.

An implicit method, based on the trapezoidal rule, is used to solve the ordinary differential equations. The accuracy of this method is consistent with the second order accuracy of the Lax-Wendroff method. Furthermore, the trapezoidal method does not require information at previous time levels and so presents no difficulties when the points along the front are redistributed.

It was found that as the occlusion process continued the individual particles on the front converged toward the place where the warm and cold fronts join. Therefore, the spacing between the points on the front becomes small in comparison with the grid size. It was thus found necessary, on occasion, to select new equidistant points along the front. The values of x, y, u, v at the new points on the front are found by interpolation from their values at the old points.

Results

Figure 2b shows subcase 1a after 18 hours. Evidently the entire front progresses to the east with the cold front moving eastward faster than the warm front. It is noticed that the front

is no longer a single-valued function of the x coordinate and that the front is curling counterclockwise. The development of this asymmetry suggests the occlusion process of frontal cyclones.

Subcase 1a assumes that no air enters from the north. The problem was then solved for subcase 1b where cold air enters the region from the north simulating a polar wind. As in Alterman and Isaacson [1], the velocity v was assumed given by

$$(3) \qquad V(t,Y,x) = \begin{cases} V_p[\cos(\frac{\pi t}{T}) - 1] , & t < 2T , \\ 0 , & t \geq 2T . \end{cases}$$

Figure 3 shows the result after 18 hours with T = 7 hours and V_p = 10 ft/sec. As is natural, it is seen that the polar air forces the front southward. With cold air entering from the north, the front becomes steeper and the cyclonic activity increases.

The periodic east-west boundary conditions are not realistic for a single wave of period X. Thus, in subcase 1c a larger region was introduced to simulate an infinite domain in the x direction. That is, X was chosen as 60 dimensionless units; while the initial data was chosen to be: a single wave of period $\frac{X}{3}$ over the center twenty units and extended to the right and left as having values independent of x, see Figure 4a. As seen in Figure 4b the main occlusion process is almost unchanged by the new boundary conditions after 18 hours. In Figure 4c we plot the contour lines of h, for the midportion $(20 \leq x \leq 40)$, to facilitate their comparison with the corresponding lines in Figure 2b.

Note that in the regions away from the center of the occlusion process, the front remains closer to its initial state and even moves slightly southward. The propagation of disturbances is faster towards the north since the sound speed is proportional to the square root of the height of the cold air. This height increases approximately linearly towards the north.

In Case 2 the initial velocities and height field distribution were assumed to be geostrophic. The initial shape of the front is again sinusoidal with the height contour lines flattening out towards the north as is seen in Figure 5a. Figure 5b shows the position of the front together with the height contour lines after 24 hours. As before the entire frontal system progresses eastward. It takes more time for the occlusion process to occur since the initial accelerations are zero. However, after a complete day the occlusion process is apparent and large cyclonic motions have developed.

Subcase 2b considers the effect of a polar wind entering from the north as given by equation (3). Figure 6 shows the contour levels for the height field for this case after 24 hours. As before the boundary conditions were then changed with the east-west boundaries taken as three times further apart and with no wind entering from the north. In Figure 7a is shown the initial configuration for subcase 2c. In Figure 7b it is seen that the occlusion process is not greatly affected, after 24 hours, by this change in boundary conditions. Since the height levels are relatively independent of x toward the north the wave motion is not as well developed as it was in Case 1. Figure 7c shows

the center portion of Figure 7b to facilitate comparisons with Figure 5b.

Conclusions

The general motion of cold fronts in the atmosphere can be qualitatively described by a system of nonlinear equations for the motion of a single layer of fluid. These equations include gravitational and Coriolis forces but ignore thermodynamic variables. By changing the initial and boundary conditions, the shape of the front, the cyclonic pattern of the air and the time variation can all be varied. Within one day the cyclonic pattern is clearly developed for realistic initial conditions. Thus, this model indicates that the action of purely mechanical forces, i.e. gravity and the Coriolis effect, are primarily responsible for the gross features of the occlusion process.

Bibliography

[1] Alterman, Z. S. and E. Isaacson, "A method for calculating frontal motion, 1. One dimensional tests," Journal of Computational Physics, Vol. 4, pp. 67-96 (1969).

[2] Burstein, S., "Finite difference calculations for hydrodynamic flows containing discontinuities," Journal of Computational Physics, Vol. 1, pp. 198-222 (1966).

[3] Kasahara, A., E. Isaacson, and J. J. Stoker, "Numerical studies of frontal motion in the atmosphere," Tellus, Vol. 17, pp. 261-276 (1965).

[4] Lax, P. D. and B. Wendroff, "Difference schemes for hyperbolic equations with high order accuracy," Comm. Pure Appl. Math., Vol. 17, pp. 381-398 (1964).

[5] Turkel, E., "Frontal motion in the atmosphere," Courant Inst. Math. Sci., NYU, Report IMM-385 (1970).

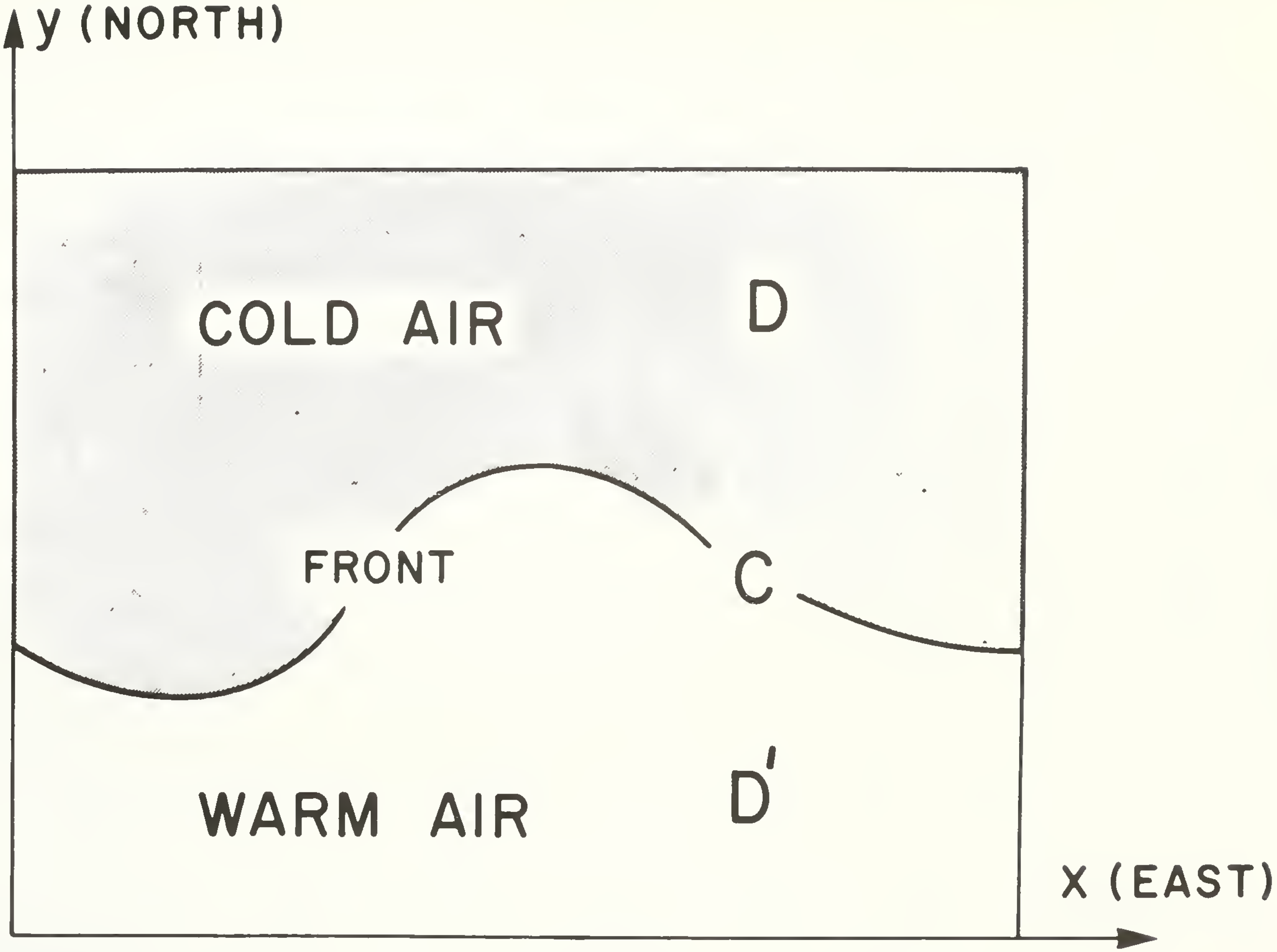

Fig. 1: Rectangular domain of integration.

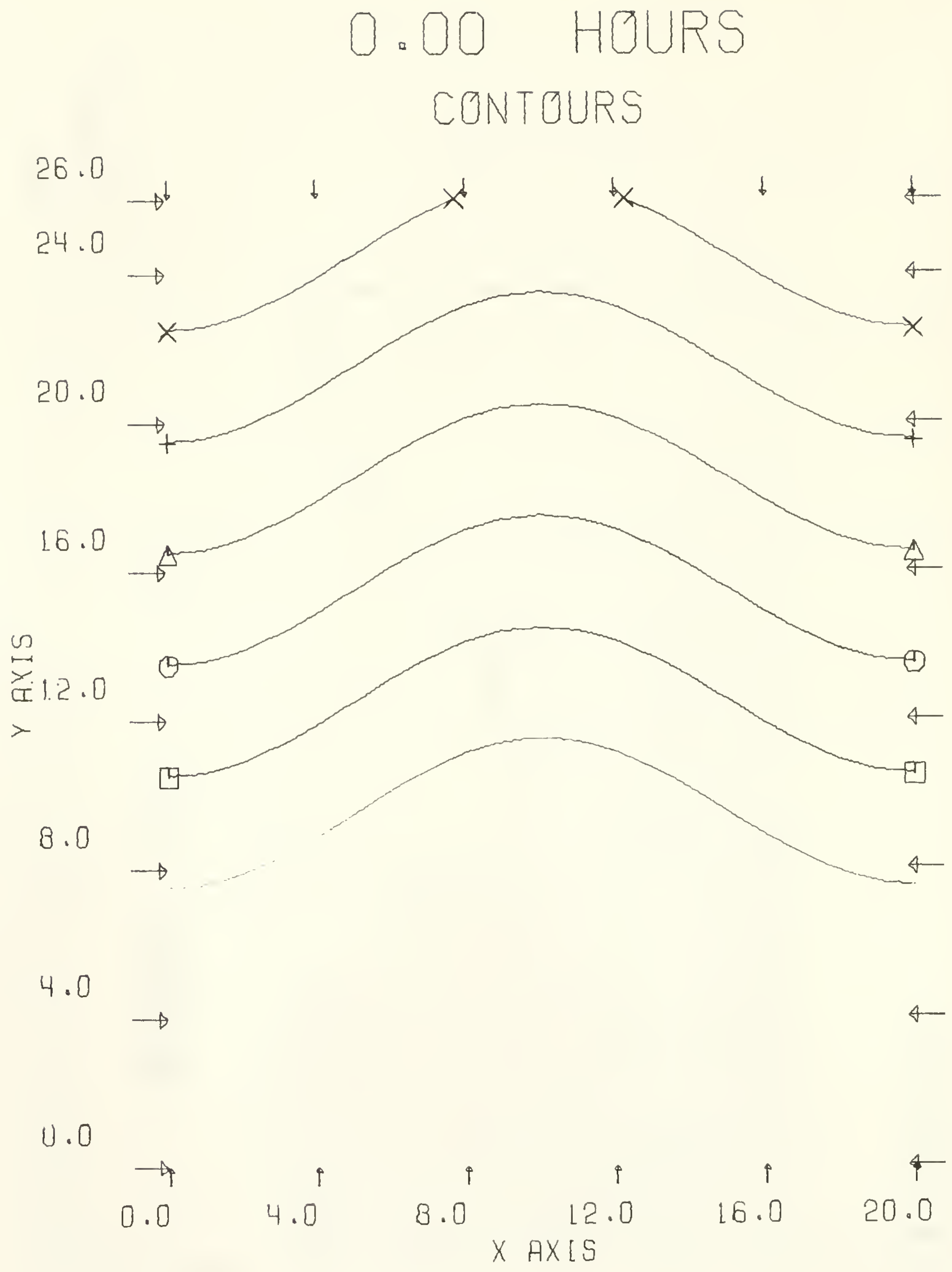

Fig. 2a: Initial height contour pattern, in 5 thousand foot intervals, for case 1a with no air entering from the north.

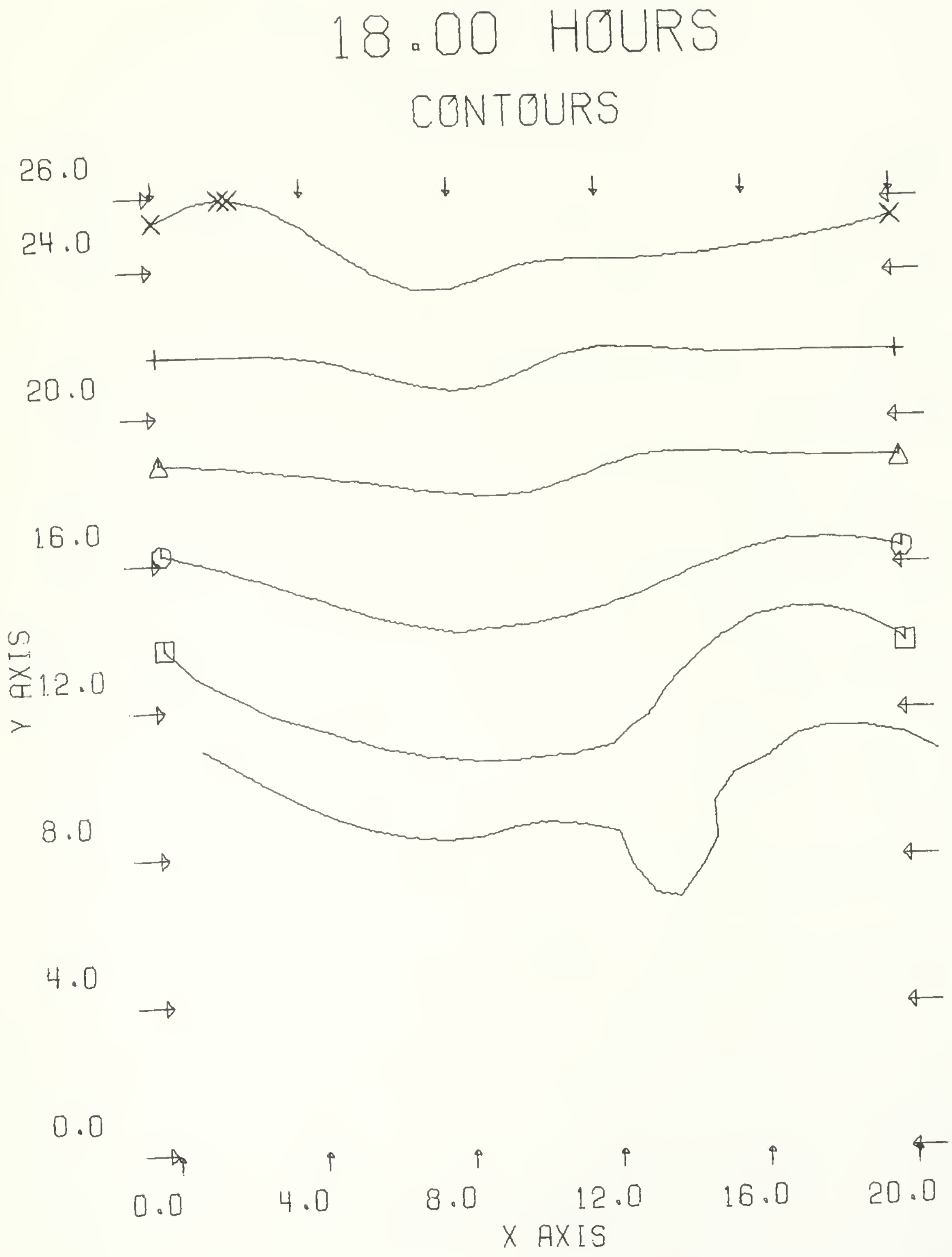

Fig. 2b: Height contour pattern for case 1a after 18 hours.

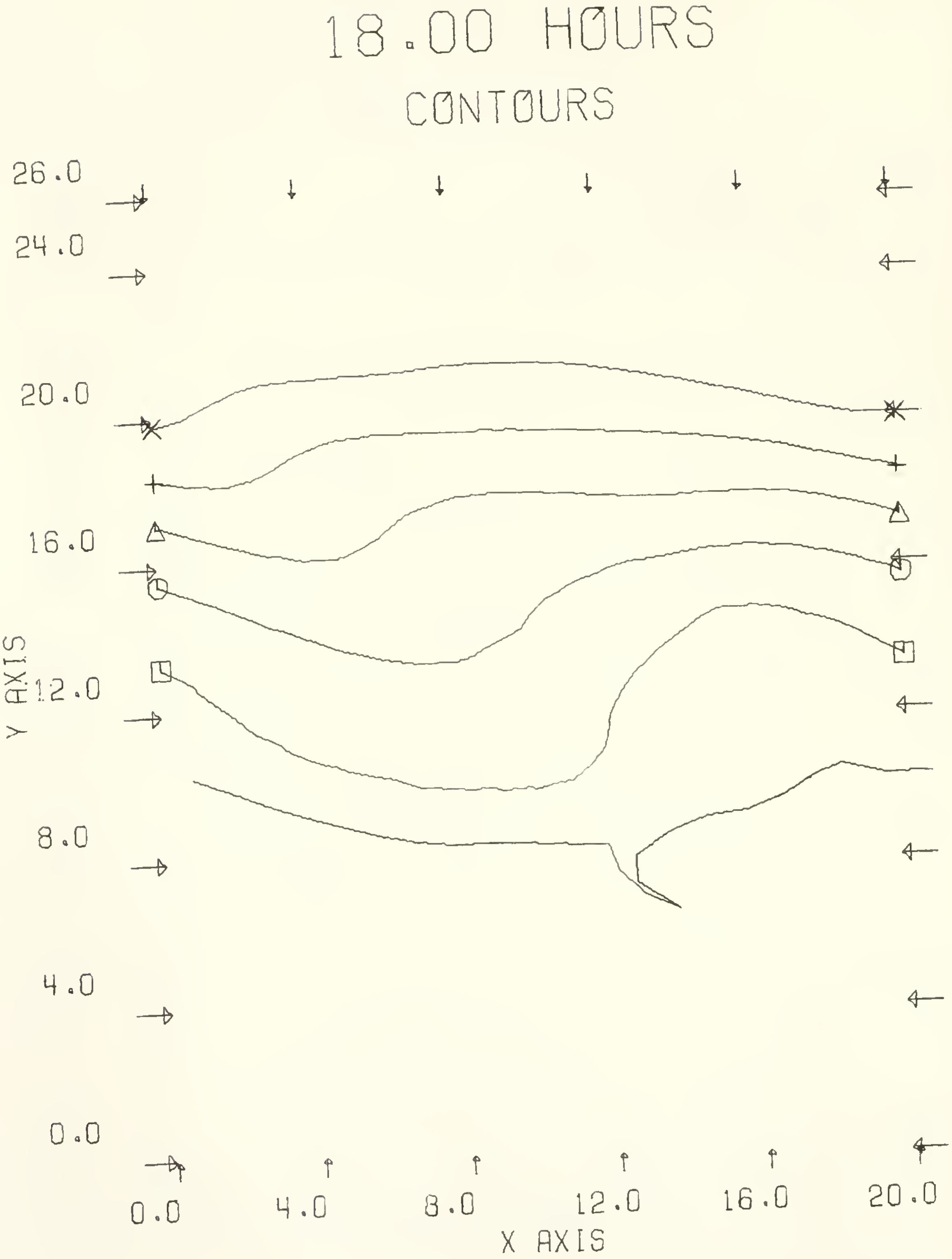

Fig. 3: Height contour pattern for case 1b, air entering from the north, after 18 hours.

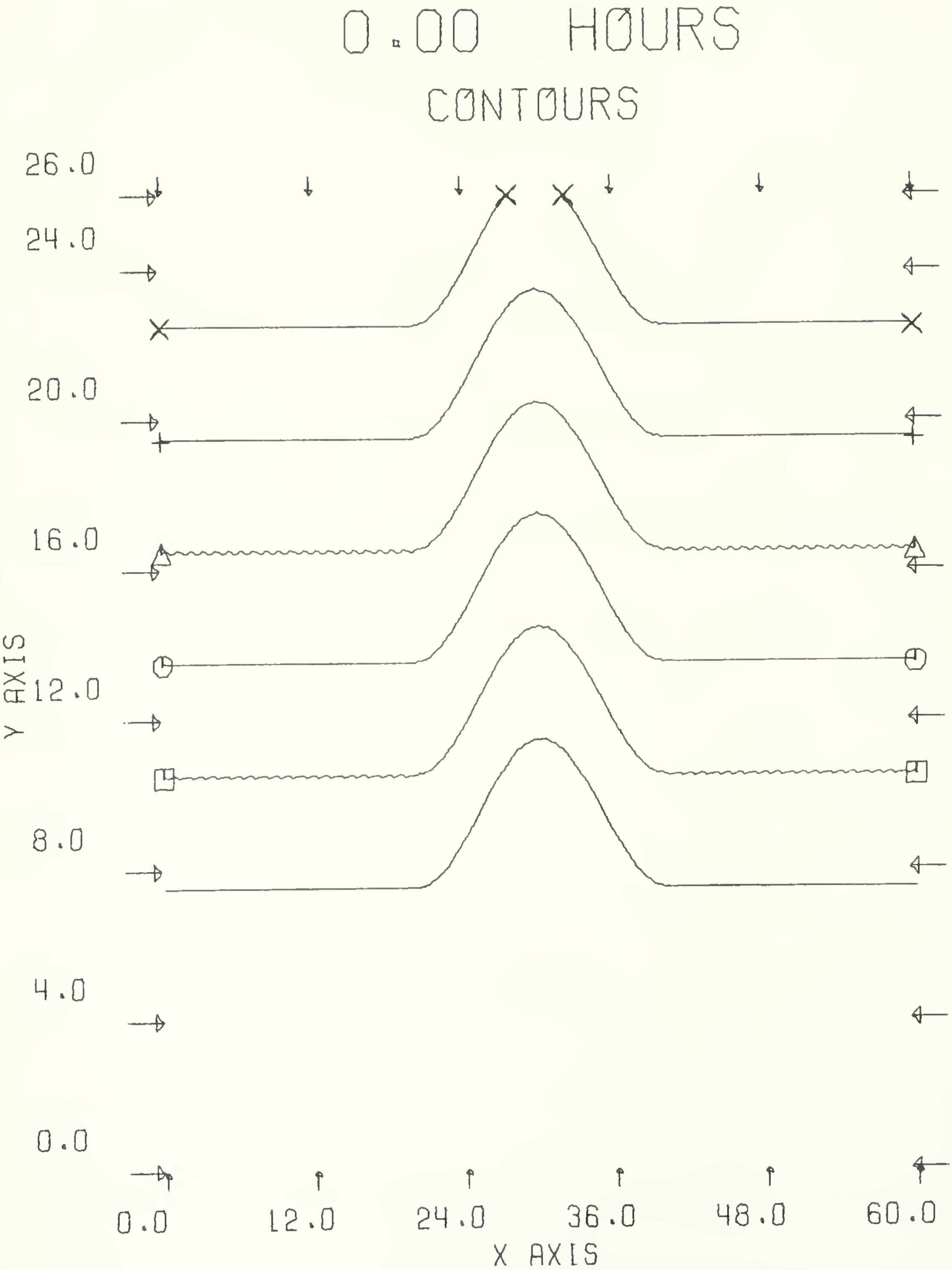

Fig. 4a: Initial height contour pattern, in 5 thousand foot intervals, for case 1c with the east-west boundaries three times further apart.

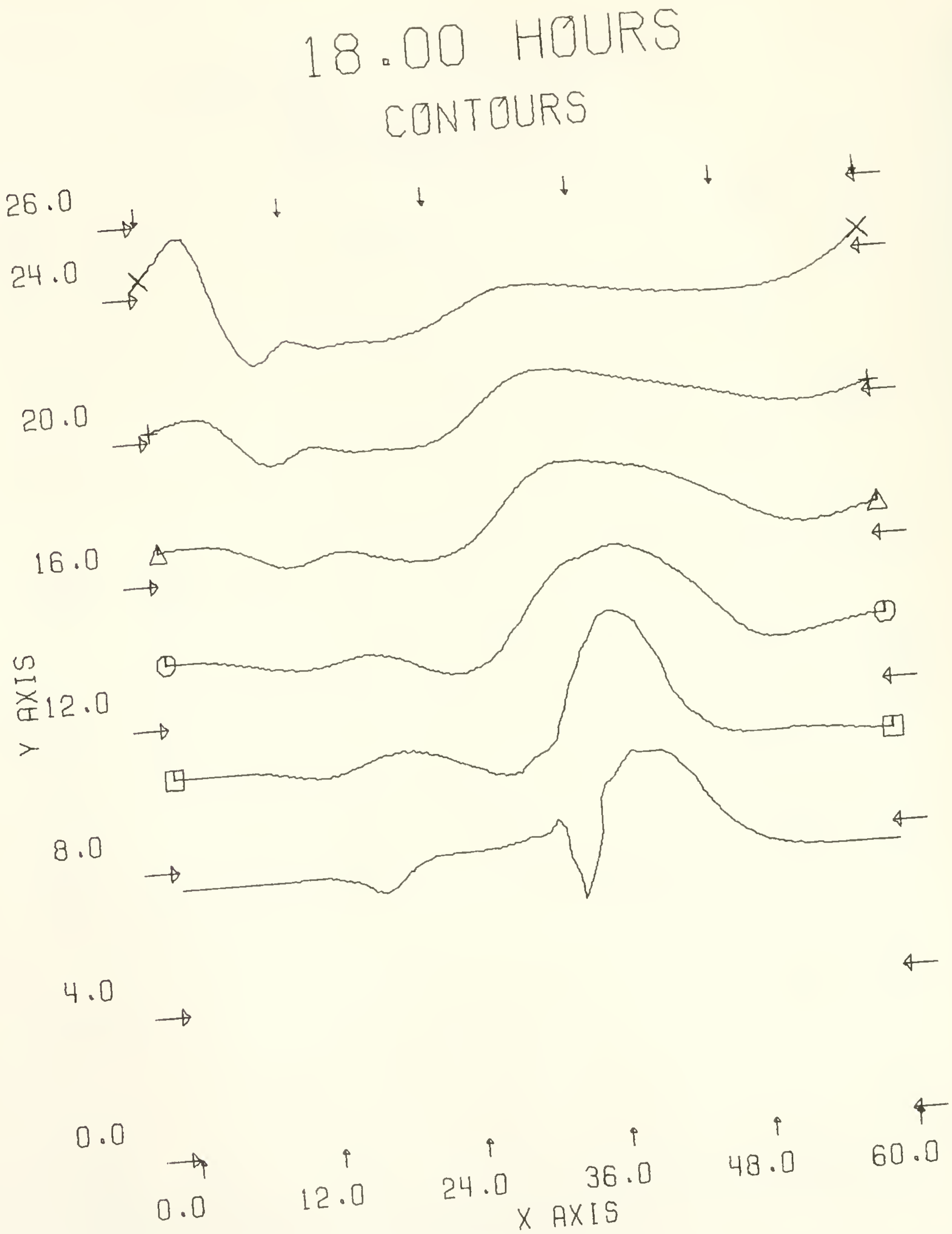

Fig. 4b: Height contour pattern for case 1c after 18 hours.

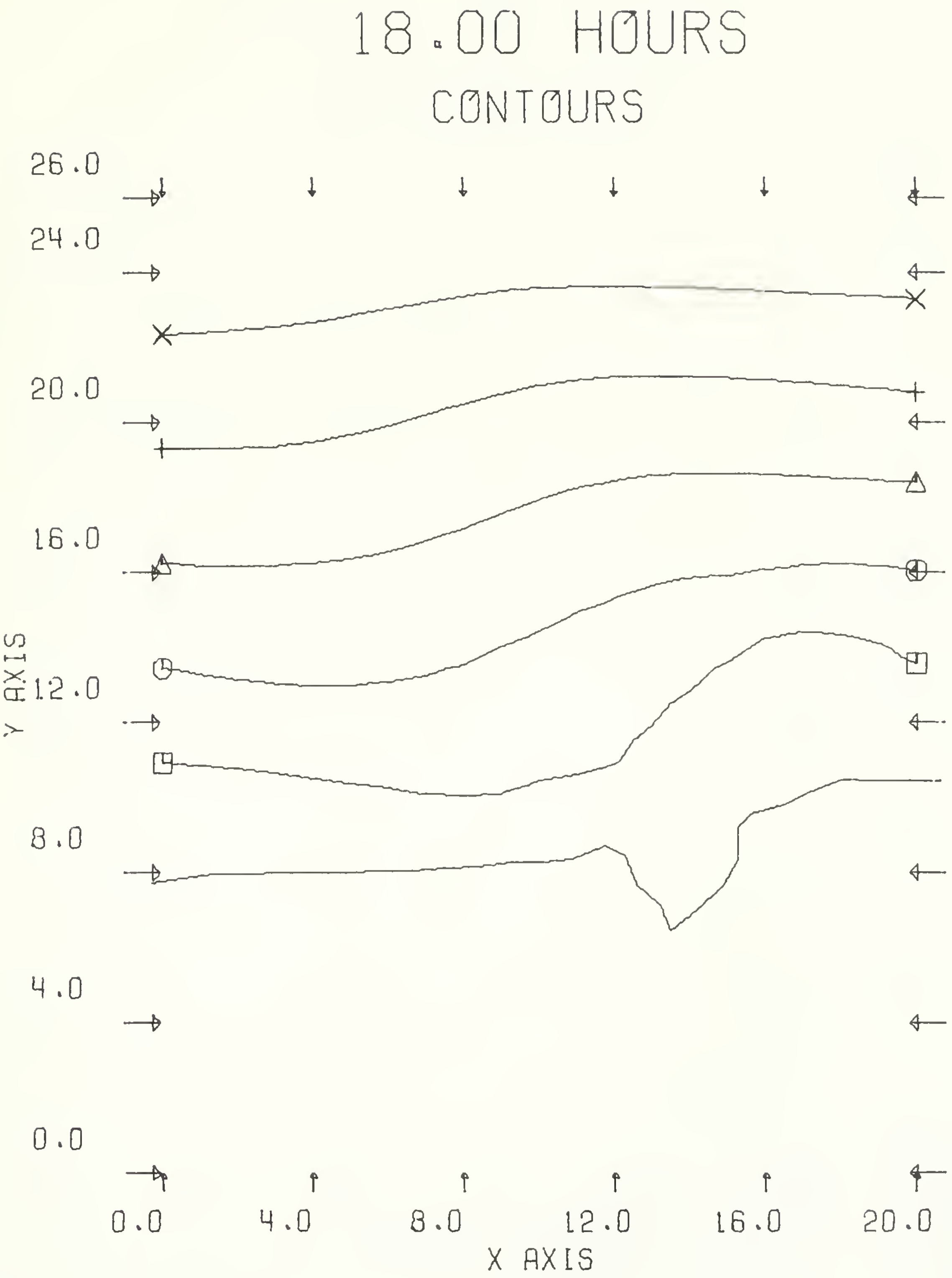

Fig. 4c: Central portion of Fig. 4b to facilitate comparison with 2b.

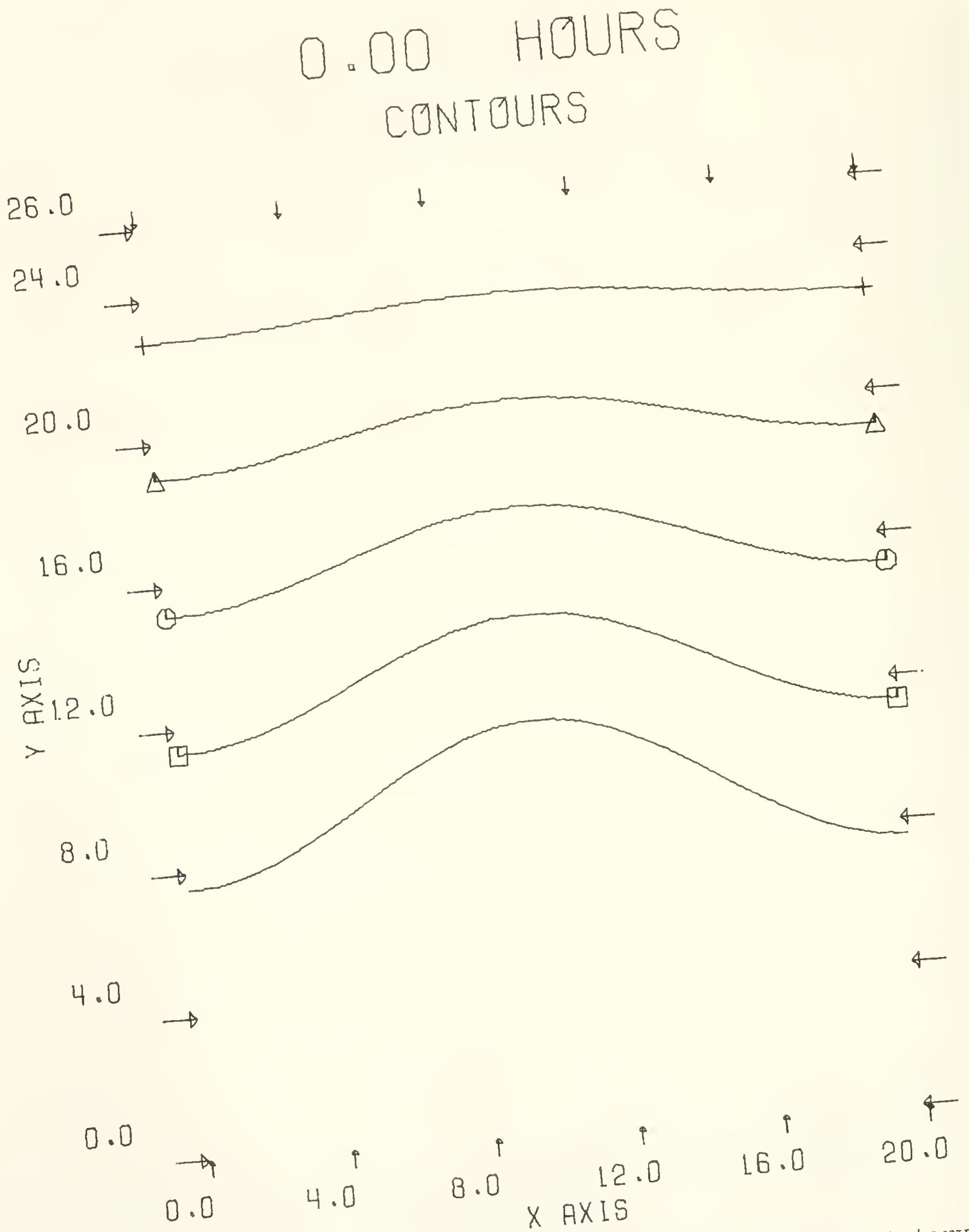

Fig. 5a: Initial height contour pattern, in 5 thousand foot intervals for case 2a with geostrophic initial conditions.

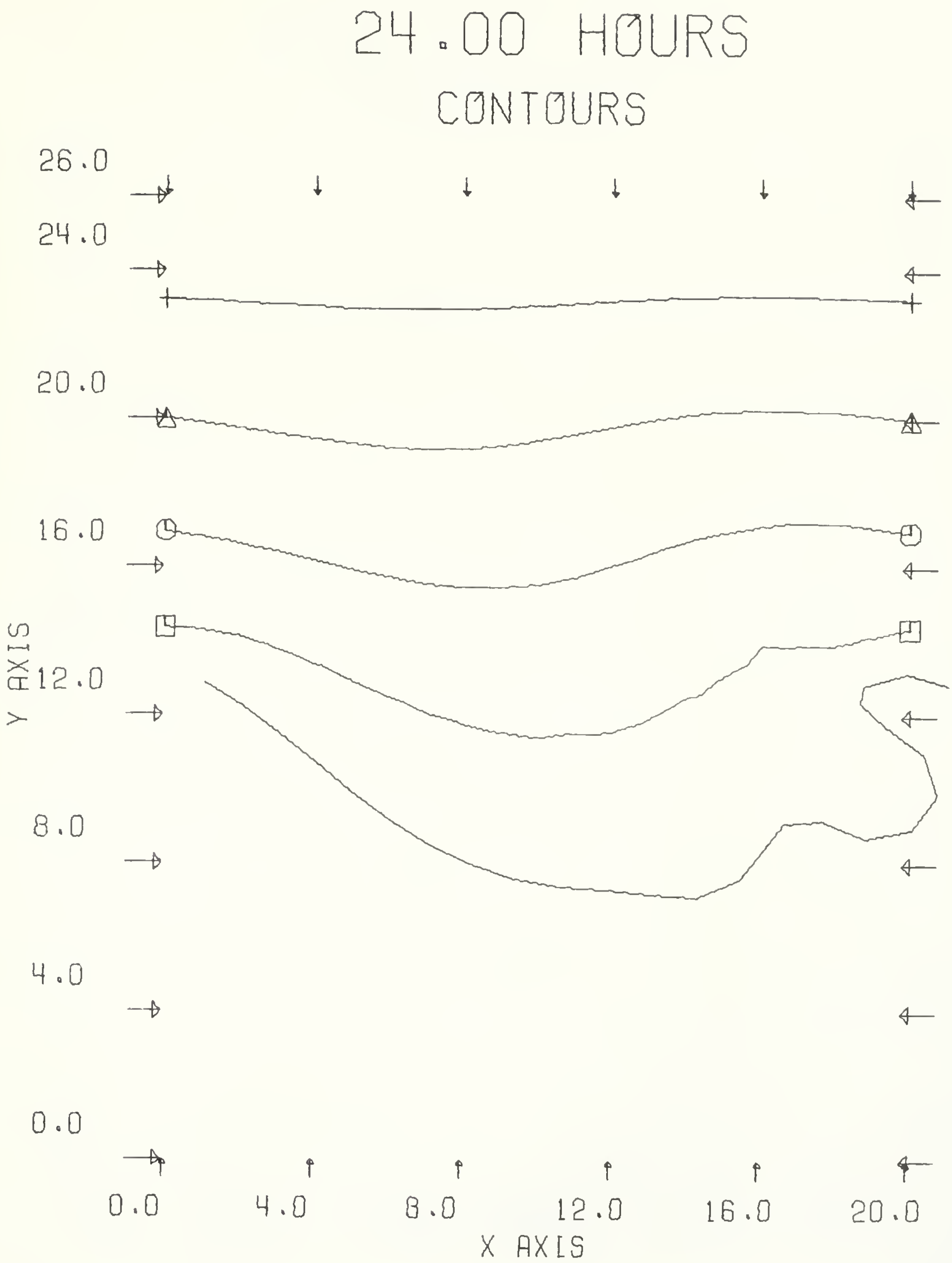

Fig. 5b: Height contour pattern for case 2a after 24 hours.

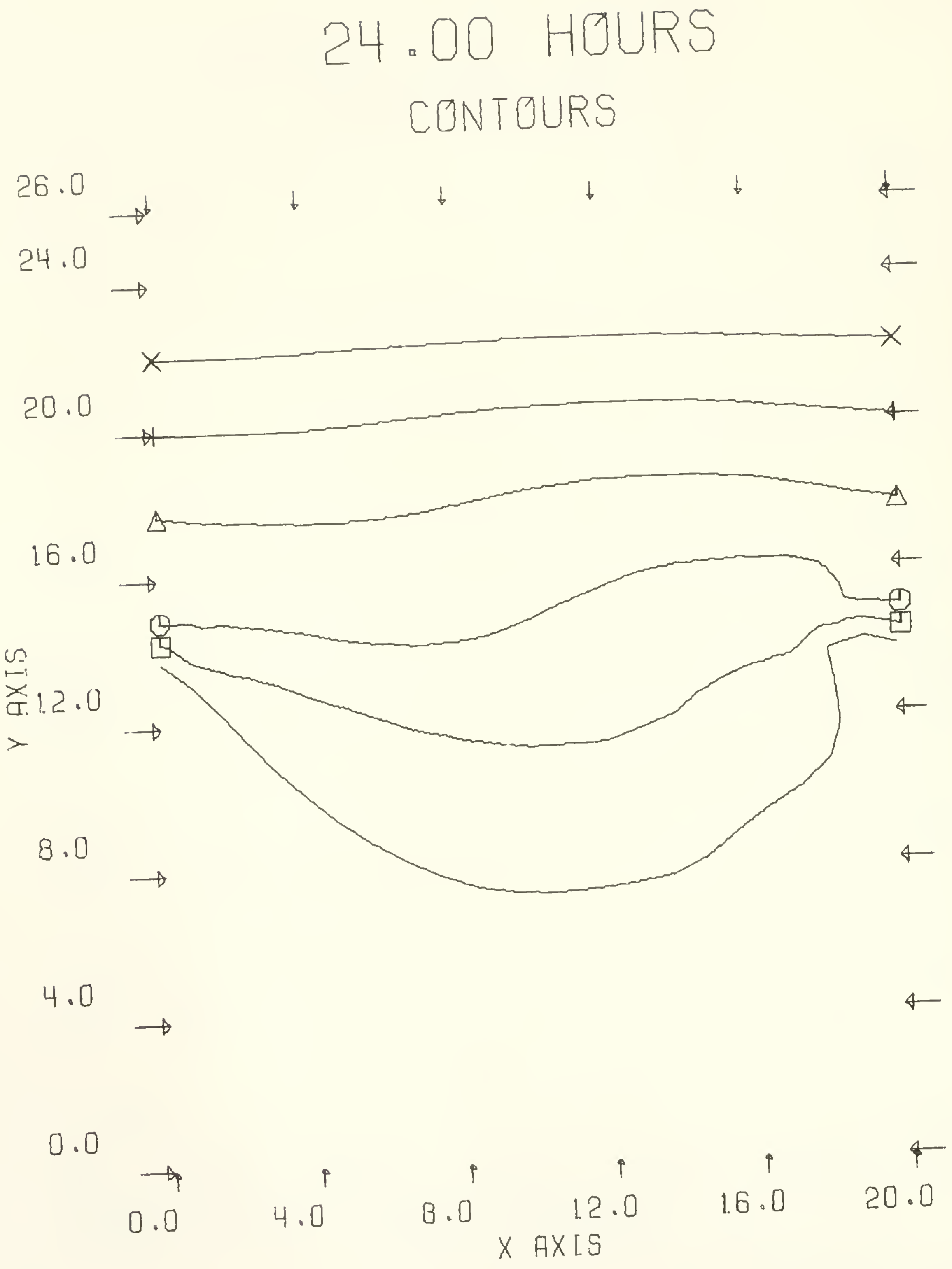

Fig. 6: Height contour pattern for case 2b after 24 hours.

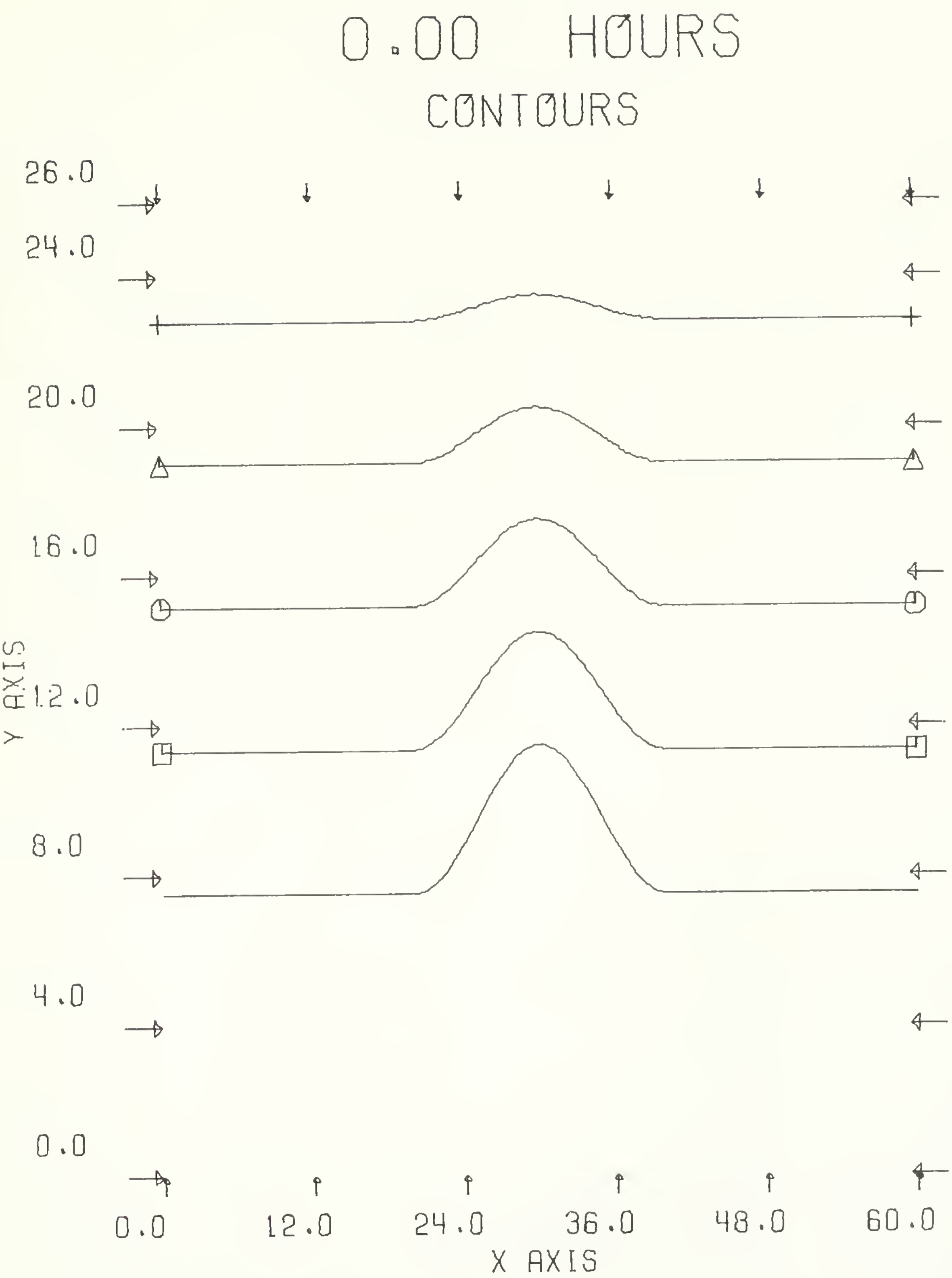

Fig. 7a: Initial height contour pattern for case 2c.

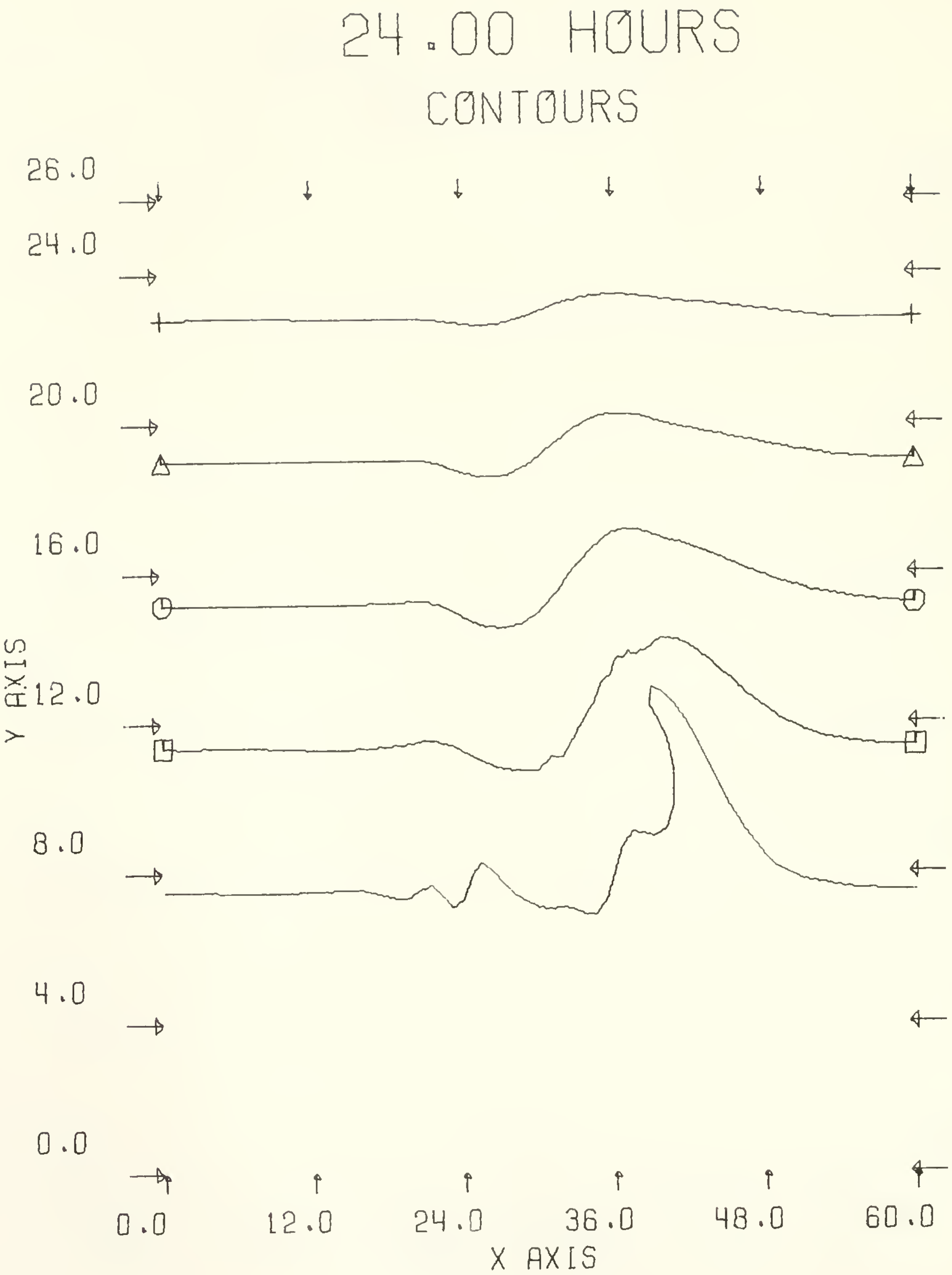

Fig. 7b: Height contour pattern for case 2c after 24 hours.

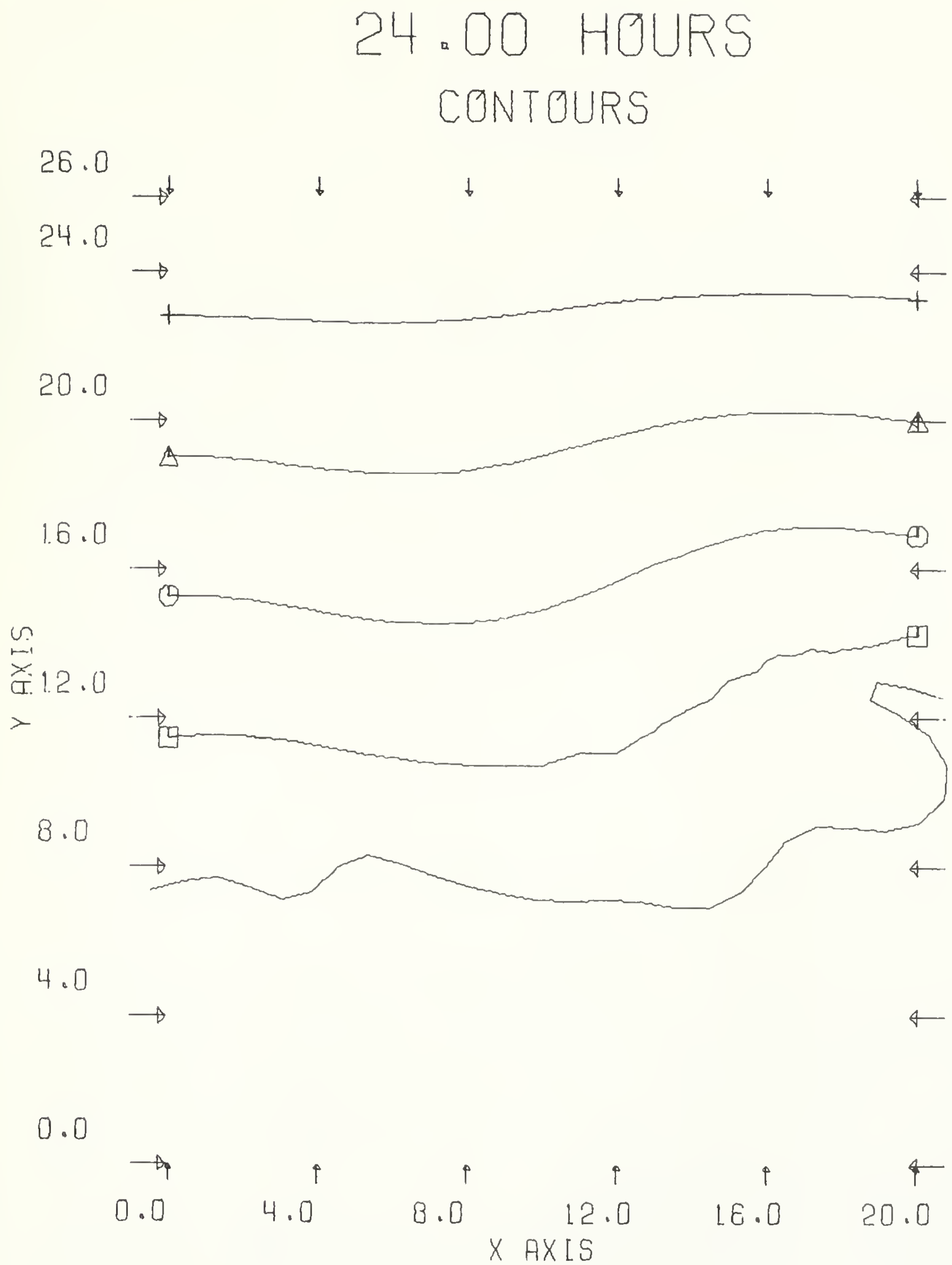

Fig. 7c: Central portion of Fig. 7b.

Lecture 5

Mountain Winds

E. Isaacson

The occurrence of dangerous, high speed winds on the lee slope of a mountain (e.g. the east slope of the Rocky Mountains) is still unpredictable. To understand such strong mountain winds, Houghton and Kasahara (1968) studied a one-layer atmospheric model over a symmetrical mountain to determine the steady asymptotic states of the mountain flows arising from a family of problems in which the west to east wind is perpendicular to the mountain ridge and instantaneously constant at the initial time. They found that if this initial velocity is large enough (but not extremely large), then the flow is asymmetrical and the asymptotic state contains a hydraulic jump. Such a jump either remains stationary on the lee side of the mountain or moves downwind with a small constant velocity depending on the magnitude of the initial velocity. This one-layer model gives an excellent explanation of the hydraulic jump, often seen as white turbulence, on the downstream side of a large boulder immersed in a shallow, rapid stream. In order to simulate nature more closely, Houghton and Isaacson (1969) studied a two-layer model of the atmosphere. Their aim was to find the asymptotic states of the asymmetrical flows that may arise and to compare these with observed flows.

Based on observations by Harrison, the atmosphere between the surface of the earth and the tropopause is assumed to consist of two layers, separated by a very thin mid-tropospheric interface.

Each layer is treated as an incompressible fluid subject to the hydrostatic pressure law. The lower layer, between the ground, $z = H(x)$, and the mid-troposphere interface, has a depth $\phi(x)$ and an average horizontal flow velocity $u(x)$ with a constant density ρ. Whereas the upper layer, between the mid-tropospheric interface and the tropopause, has a depth $\phi'(x)$ and an average horizontal flow velocity $u'(x)$ with a constant density $r\rho$ $(r < 1)$. The stratosphere on top of the tropopause is assumed to be at rest with a horizontal upper surface. This passive stratospheric layer has a constant density $s\rho$ $(s < 1)$. The governing equations for ϕ, u, ϕ', and u' are

$$\frac{\partial}{\partial t}\phi + \frac{\partial}{\partial x}(\phi u) = 0 ,$$

$$\frac{\partial}{\partial t}u + u\frac{\partial}{\partial x}u + g(r-s)\frac{\partial}{\partial x}\phi' + g(1-s)\frac{\partial}{\partial x}\phi = -g(1-s)\frac{\partial H}{\partial x} ,$$

$$\frac{\partial}{\partial t}\phi' + \frac{\partial}{\partial x}(\phi' u') = 0 ,$$

$$\frac{\partial}{\partial t}u' + u'\frac{\partial}{\partial x}u' + g(1-\frac{s}{r})\frac{\partial}{\partial x}\phi' + g(1-\frac{s}{r})\frac{\partial}{\partial x}\phi = -g(1-\frac{s}{r})\frac{\partial H}{\partial x} ,$$

g being the acceleration of gravity.

Here, for the case of a symmetrical mountain, the nature of the asymptotic states (as $t \to \infty$), that arise from initially constant velocities and horizontal atmospheric interfaces, is more complex than for the case of the single layer flow. In fact, except for the case of quite low initial velocity, in which the flow is again symmetrical, there is a regime of steady asymmetric flow over the mountain, only for a narrow neighboring range of

higher initial velocities (region B in [2]). If the initial velocity is chosen to be still somewhat higher (region B' in [2]), then the flow over the mountain fails to become steady, but instead behaves roughly as if periodic waves are created over the mountain and sent downstream.* Nevertheless, both this steady asymmetric flow, with its hydraulic jumps on the lee side, and the unsteady flow, occur for physically realistic atmospheric velocities.

With this study of flow over a symmetrical mountain completed, a calculation of the flow over a realistic profile of the Rocky Mountains was undertaken. The ground is assumed to have the average profile of a ten mile wide strip, running east-west through Colorado at a latitude between Denver and Boulder, Colorado. If initially each of the two layers has a horizontal upper surface and a uniform eastward flow velocity as indicated in Fig. 1, the state after 5.17 hours is shown in Fig. 2 for the heights of the upper surfaces of the two layers and the flow velocities in the two layers. The solution shows a severe decrease in depth of the lower layer on the lee side of the mountain, and a correspondingly high wind velocity, u, in the Boulder area. In fact, u is 100% larger than u'; and u is close to the 125 mph winds observed at Boulder in [5]. In [2], a comparison is made of another calculated flow, with carefully made observations of the atmosphere on Feb. 20, 1968.

---

* Subsequent work by Isaacson and Zwas [4] shows that this unsteady, almost periodic behavior was caused by the numerical scheme. In fact, the flow for such data (called B' in [2]) does become steady, but it contains a secondary weak shock on the lee side of the crest. The numerical schemes to carry out this calculation are studied in [4].

It is pointed out that this model is easy to use for local wind forecasting purposes. Further high wind observations are needed to justify more fully the use of this two-layer model, which predicts the occurrence of a high shear in the wind.

References

1. D. D. Houghton and A. Kasahara, Nonlinear shallow fluid over an isolated ridge, Comm. Pure Appl. Math. 21, pp. 1-23, 1968.

2. D. D. Houghton and E. Isaacson, Mountain winds, Studies in Num. Anal. 2, pp. 21-52, 1969.

3. H. T. Harrison, Synoptic features of the mountain wave at Denver, Colorado, UAL Meteorology Circular 41, United Air Lines, Inc., Denver, Colorado, 1956.

4. E. Isaacson and G. Zwas, Mountain Winds, in preparation.

5. L. T. Julian and P. R. Julian, Boulder's Winds, Weatherwise, 22, pp. 108-112, 126, 1969.

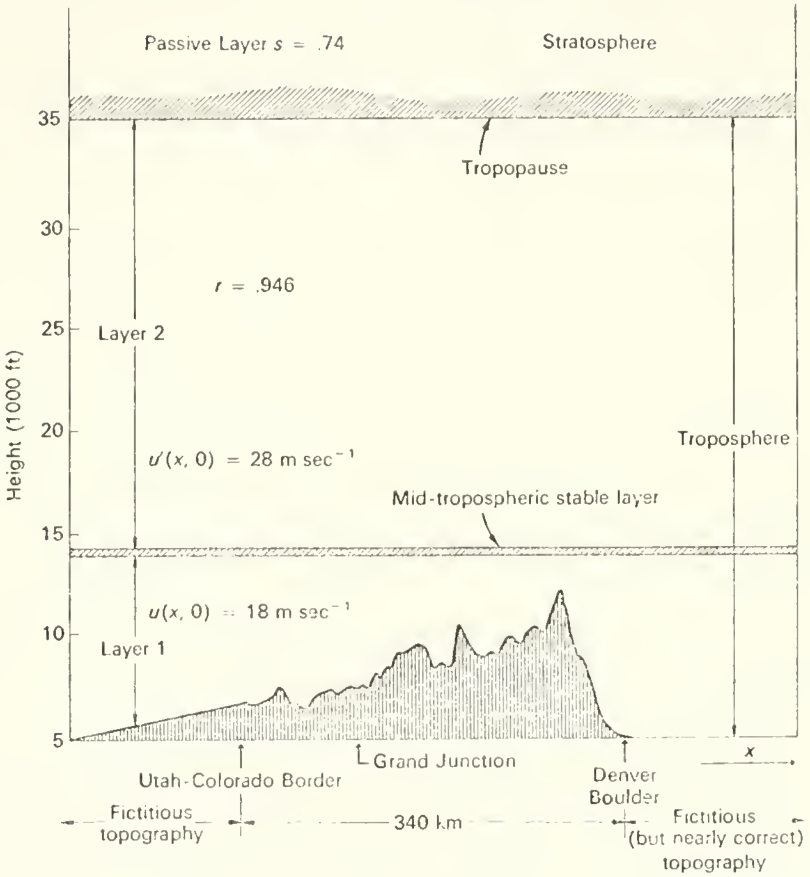

Fig. 1. Initial conditions in the two layers

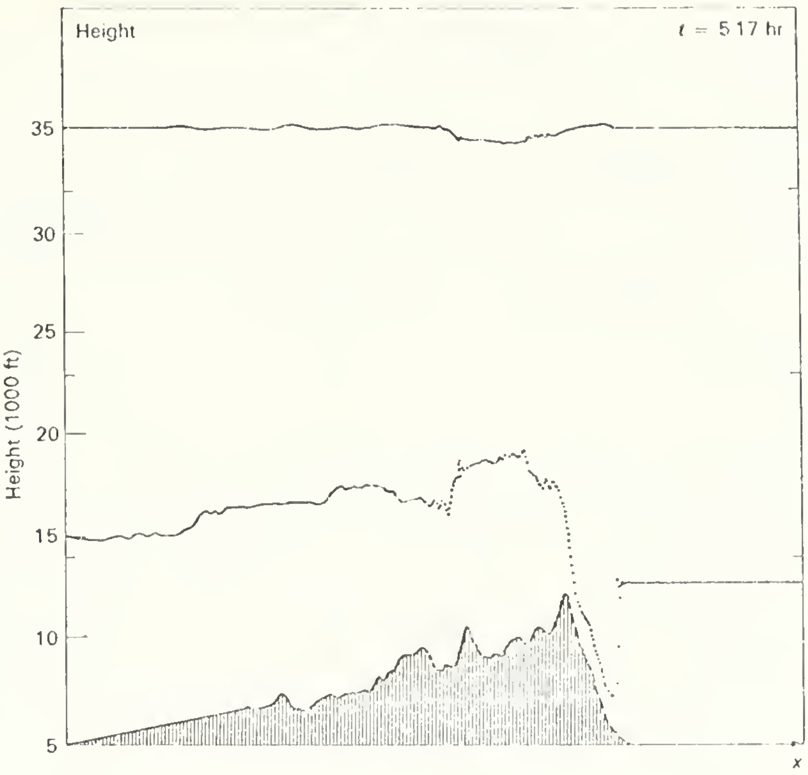

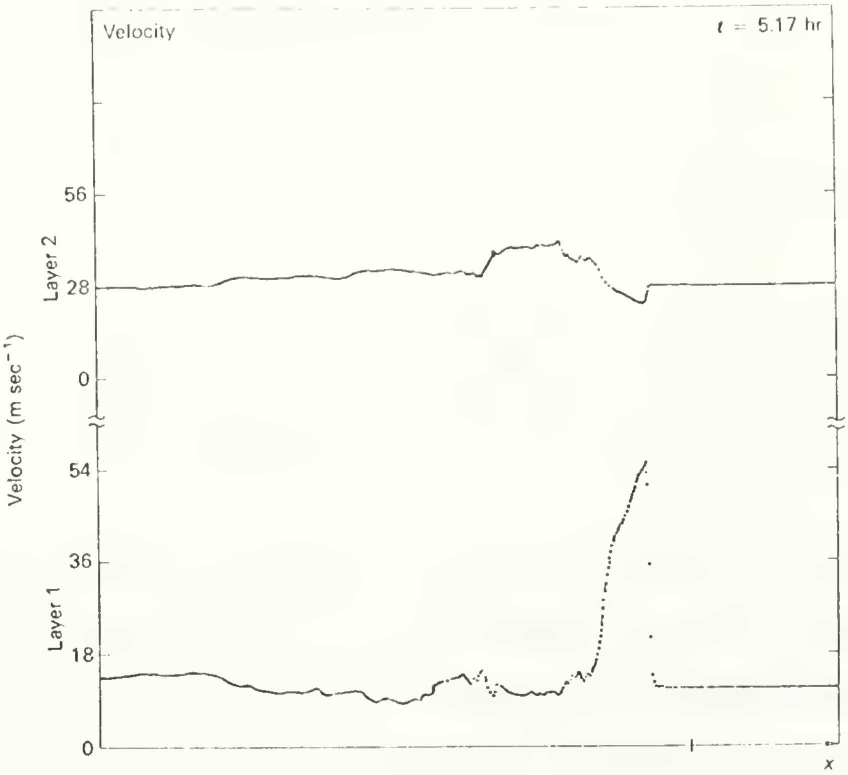

Fig. 2. Steady states in the two layers. The height of the upper surfaces of the two layers and the flow velocities in the two layers.

Lecture 6

Atmospheric Predictability
(an introduction to large-scale numerical meteorology)

Richard C. J. Somerville

Introduction

Suppose that one possessed perfect knowledge of the physical laws which describe the behavior of the earth's atmosphere and of the appropriate mathematical expressions of these laws. Suppose too that the numerical methods and computational machinery necessary for an essentially errorless integration of the resulting initial- and boundary-value problem were available. Also suppose that one could obtain all the observational data needed to define the initial and boundary conditions. With such perfect models, methods, and data, for how long a time could one "accurately" (defined in some appropriate sense) forecast the weather?

Alternatively, for the imperfect models, methods, and data actually available today, in what respects are forecasts deficient, and for how long a time can forecasts presently be said to be accurate?

Finally, to produce an accurate forecast for some arbitrary length of time, intermediate between the presently practicable and the ultimately possible lengths of time, what sorts of models, methods, and data would be required?

Atmospheric predictability is the subject which is concerned with such questions. It is a subject of practical importance as well as theoretical interest, because while the economic benefits of improved weather forecasts are immense, so are the costs of super-computers, satellites, etc. In the following sections, we shall first describe the problem a little more concretely and then briefly survey several separate lines of attack on it. The survey is by no means exhaustive, but the bibliographies contained in the references provide an extensive set of entry points to the literature.

Basic Equations

The appropriate fundamental laws are thought to be representable by the following system:

$$\frac{d}{dt}\underset{\sim}{V} = -2\underset{\sim}{\Omega}\times\underset{\sim}{V} - \alpha\nabla p + \underset{\sim}{g} + \underset{\sim}{F}$$

$$\frac{d}{dt}\alpha = \alpha\nabla\cdot\underset{\sim}{V}$$

$$\frac{d}{dt}T = (1-\gamma)T\,\nabla\cdot\underset{\sim}{V} + \frac{Q}{c_v}$$

$$p\alpha = RT\ .$$

These are, respectively, Newton's second law, the statement that mass is conserved, the first law of thermodynamics, and an equation of state. The individual time derivative $\frac{d}{dt}$ means $(\frac{\partial}{\partial t} + \underset{\sim}{V}\cdot\nabla)$, $\underset{\sim}{V}$ is the velocity relative to the earth rotating at angular velocity $\underset{\sim}{\Omega}$,

α is the reciprocal of density, p is pressure, $\underset{\sim}{g}$ is the apparent gravitational acceleration, R is the gas constant, γ is the ratio of specific heats $(\frac{c_p}{c_v})$, and T is temperature. The frictional force $\underset{\sim}{F}$ and net heating Q per unit mass are very complicated and imperfectly known functions of other variables (cf. Lorenz, 1967).

Since World War II, much effort has been devoted to the numerical solution of these equations, with a great variety of domains, boundary conditions, numerical methods, initial data, assumptions about $\underset{\sim}{F}$ and Q, etc. (e.g., Thompson, 1959; Gavrilin, 1965; Phillips, 1970). Today, such models, run on a routine operational basis, comprise the core of the process by which regular weather forecasts are produced in the technologically advanced countries. The more complicated models, which cannot meet the operational real-time requirement, are used for research purposes. Quite aside from the fact that the archive of meteorological observations constitutes what must be among the largest data sets in all science, the sheer computational magnitude of these efforts is awesome by conventional standards. The largest models (general circulation models) saturate the memories of the largest computers and may require several hundred hours of machine time for a single experiment. The verisimilitude of the results is sometimes purchased at a steep price, not only in dollars but also in loss of insight and intelligibility — the model, like the atmosphere itself, may be so complicated that specific effects cannot easily be attributed to specific causes. Before examining the results of the large models, therefore, we

shall first survey three somewhat simpler approaches to the predictability problem.

Analogues

We shall first briefly mention some fluid systems designed to resemble the atmosphere in certain important respects but to differ from it in size, simplicity, and susceptibility to observation and control. The most extensively studied of such systems are the "rotating annulus" experiments (Fultz, et al., 1959), which consist of two concentric right circular cylinders mounted on a turntable and rotated together at a constant rate about their common (vertical) axis. If the cylinders are maintained at different constant temperatures, water contained in the space between them has been found to exhibit many of the features of large-scale atmospheric flow, for certain ranges of values of the external parameters. Many of these features (which include fronts, jet streams, and "planetary" waves) have been shown convincingly to bear a more than superficial resemblance to their atmospheric counterparts. These features, in both annulus and atmosphere, are due to the horizontal temperature contrast and the dominant constraint of rotation (Greenspan, 1968). Several qualitatively different regimes of flow can be produced in the annulus by varying the external parameters. These range from regimes of infinite predictability (steady flows and flows which appear to vary perfectly periodically in time) to irregular and turbulent regimes which are often supposed to correspond most closely to the

atmosphere. The annulus experiments have provided insight into the dynamics of the atmosphere, but the analogy is too crude to supply detailed quantitative answers to questions of predictability.

A very different kind of analogue may be sought in the meteorological records themselves. The idea is to find two actual observed states of the atmosphere, widely separated in time, which resemble each other so closely that the differences between them are typical of the small errors which might be due to an imperfect observing system. Following the subsequent history of these two states might then reveal the evolution of the "error," an estimate of the doubling time of such errors, and ultimately the predictability time (after which the two histories are essentially uncorrelated, the states of one differing from those at the corresponding times of the other by the same amount as would two randomly chosen states).

A search of the existing aerological records by Lorenz failed to produce any such pairs of states but did produce pairs of states which differed from one another by amounts which might be typical of errors larger than errors of observation. The observed growth rates of these "errors" could be extrapolated to yield estimates of the growth rate of smaller errors. The result (a doubling time of under three days) is not incompatible with results obtained by other methods, which we shall now describe.

Simple theoretical models

The mechanism implicit in the previous discussion (a limitation on predictability due to the instability, growth, and eventual dominance of initially small observational errors in a turbulent atmosphere) has been further explored in several theoretical studies. We shall briefly describe that of Lorenz (1969). He considers a flow governed by the inviscid two-dimensional barotropic vorticity equation, which in terms of a stream function ψ is

$$\frac{\partial}{\partial t} (\nabla^2\psi) = -J(\psi,\nabla^2\psi) .$$

This equation, while much simpler than the system described earlier, served as the successful basis for early short-term numerical weather forecasts. From it Lorenz derives expressions for ensemble averages of quantities identifiable as the "error energy" of separate scales of motion. After making several statistical assumptions and simplifications, a system of ordinary differential equations (in time) results, the coefficients of which may be evaluated from estimates of the atmospheric energy spectrum. Numerical integration of this system is easy, and estimates of predictability times are obtained by noting the times at which the error energy of a particular scale of motion reaches the amplitude of the total energy of that scale. With the chosen values of the coefficients, motions on the scale of cumulus clouds can be predicted for about an hour, "synoptic-scale" motions

(those of typical weather map features, several hundred miles in size) for a few days, and the largest (planetary) scales for "a few weeks." The predictability times, however, depend crucially on the estimates of the atmospheric energy spectrum, and may be much longer if energy per unit wavenumber k falls off faster than the $k^{-5/3}$ Kolmogoroff spectrum assumed for short wavelengths. Neither observations nor present theories of quasi-two-dimensional turbulence are sufficient to determine the spectrum shape with any certainty, but it is almost surely steeper than the Kolmogoroff spectrum (Charney, 1969). To escape the necessity of such assumptions and simplifications, one must resort to the numerical models. In this subject, simple approaches provide insight, but realistic quantitative answers seem to come only from less tractable procedures.

Numerical models

As an example, we cite the results of Smagorinsky (1969), who describes his model as follows:

"Briefly, the model is governed by the primitive equations and has 9 vertical levels. The domain is hemispheric and the computational grid is mapped stereographically. The model is 'moist' with a condensation criterion of 80% relative humidity; the parameterized convection scheme is a moist adiabatic temperature adjustment. Long and short wave radiation are accounted for, with water vapor, carbon dioxide and ozone as absorbers of radiant energy which at most are functions of height and latitude and

constant with time. Large scale mountains and the thermal consequences of land-sea contrast are accounted for. The surface drag coefficient is constant irrespective of land and sea; the availability of water for evaporation is 0.5 over land and 1.0 over sea; the temperature specification is different over land-ice and sea ice; the snow line is constant with time. The effective Karman constant for the internal non-linear lateral viscosity is 0.4."

Using this model, with horizontal resolutions as fine as 40 grid points between pole and equator (a grid size of 320 km at the pole and 160 km at the equator), pairs of 3-week integrations were carried out. One run of a pair used initial data from observations for a particular day and time, and the other used this data set perturbed by a random temperature disturbance of 0.5 deg C amplitude (standard deviation). Thus an attempt was made to simulate the situation which Lorenz sought unsuccessfully in the actual atmosphere. The "error" (instantaneous standard deviation temperature difference between the states of the pair of runs, at corresponding times) first decreased from 0.5 to 0.2 due to an internal adjustment with the undisturbed wind field. Thereafter, the error increased exponentially for about a week, with a doubling time of about $2\frac{1}{2}$ days, and then grew more slowly. After 21 days it was still appreciably smaller than the difference between two randomly selected states at the same season.

Those who perform such numerical experiments interpret them to imply that the ultimate limit of deterministic predictability

may be at least 3 weeks. The present-day practical limit, deduced by similarly comparing such forecasts with the actual weather, is about half that time. It is hoped that improvements in models and data will help to close this gap, and that increases in computer capability will eventually allow routine operational predictions for such extended ranges.

References

Charney, J. G., 1969: Predictability, in Plan for U.S. Participation in the Global Atmospheric Research Program, National Academy of Sciences, Washington, pp. 8-14.

Fultz, D., et al., 1959: Studies of thermal convection in a rotating cylinder with some implications for large-scale atmospheric motions, Meteor. Monographs, Amer. Meteor. Soc., Boston, 104 pp.

Gavrilin, B. L., 1965: Numerical experiments on the general circulation of the atmosphere, Izvestia, Atmos. and Ocean. Phys., 1, 1229-1259.

Greenspan, H. P., 1968: The Theory of Rotating Fluids, Cambridge University Press.

Lorenz, E. N., 1967: The Nature and Theory of the General Circulation of the Atmosphere, World Meteorological Organization, Geneva, 161 pp.

Lorenz, E. N., 1969: The predictability of a flow which possesses many scales of motion, Tellus, 21,289-307. (See also Bull. Amer. Met. Soc., 50, 345-351.)

Phillips, N. A., 1970: Models for weather prediction, in Ann. Rev. Fl. Mech., ed. M. van Dyke, 2, 251-292.

Smagorinsky, J., 1969: Problems and promises of deterministic extended range forecasting, Bull. Amer. Meteor. Soc., 50, 286-311.

Thompson, P. D., 1959: Numerical weather analysis and prediction, Macmillan, New York, 170 pp.

Lectures 7 and 8

Geostrophic Vortex Motion and Applications

G. K. Morikawa

The large-scale, nearly horizontal motions of the earth's atmosphere are approximately in hydrostatic and geostrophic balance. That is, 1) in the vertical direction, the fluid acceleration is small compared to both the acceleration of gravity and the vertical pressure gradient, viz., there is approximate hydrostatic equilibrium, and 2) in the horizontal direction, the fluid acceleration is small compared to both the Coriolis acceleration due to the earth's rotation and the horizontal pressure gradient, viz., the motion is approximately geostrophic. The horizontal balance is valid primarily in middle latitudes, away from the equator where, strictly, there is no Coriolis effect. If we incorporate these meteorological approximations in a proper way into the equations of motion of an inviscid, adiabatic atmosphere, we can derive simpler, more manageable equations which succinctly describe these large-scale motions; this turns out to be an asymptotic description for large time of the original equations. This approximate theory of geostrophic vortex motion can be applied to problems related to the study of short range weather forecasting[1], valid for predictions over a period of a few days. Two such problems will be considered here. We remark that this theory of kinematic motion (dynamically balanced) may be applicable to other physical phenomena over a large range of length

scales, i.e., from atomic scale motions such as those that occur in superconductivity [2] to astrophysical motions such as interacting galactic nebulae.

Derivation of the Geostrophic Vorticity Equation [3]

In order to simplify the derivation of the geostrophic conservation equation, we consider a simpler model, that of a homogeneous, incompressible atmosphere as our original model; an analogous conservation equation results from the geostrophic approximation of the adiabatic atmosphere [4]. In the homogeneous atmosphere model, the hydrostatic approximation has already been incorporated; these shallow water (or long wave) equations are:

(1) $$\frac{dh}{dt} + h(u_x + v_y) = 0 \qquad \text{(continuity)}$$

(2.1) $$\frac{du}{dt} + gh_x - fv = 0 \qquad \text{(x-momentum)}$$

(2.2) $$\frac{dv}{dt} + gh_y + fu = 0 \qquad \text{(y-momentum)}$$

where h is the depth of the homogeneous atmosphere, (u,v) is the horizontal velocity, g is the acceleration of gravity, $f \equiv 2\Omega_e \sin\phi$ (Ω_e = earth's rotational velocity and ϕ = latitude angle), and $d(\ )/dt \equiv (\ )_t + u(\ )_x + v(\ )_y$ (subscripts are partial derivatives). For describing meteorological motions, we replace the continuity equation (1) by the potential vorticity equation obtained by combining (1) with the curl of (2):

(3) $\frac{d}{dt}\left(\frac{\zeta+f}{h}\right) = 0$ (potential vorticity)

where $\zeta = (v_x - u_y)$ is the vertical component of vorticity. Equations (2) and (3) [or (1) and (2)] are a system of hyperbolic equations for (h, u, v). In addition, the pressure, p, and vertical velocity, w, are given by

(4.1) $p = g\rho(h-z)$ (hydrostatic equilibrium)

and

(4.2) $w = -z(u_x + v_y)$.

We incorporate the geostrophic approximation into (2) and (3) [or (1) and (2)] by the following formal procedure: 1) the time, t, is scaled by a small parameter, ε, where $\varepsilon \ll 1$; and 2) the solution (h, u, v) is expressed as a power series expansion, perturbed on the atmosphere at rest:

(5) $(h, u, v) = (h_o, 0, 0) + \varepsilon(h^{(1)}, u^{(1)}, v^{(1)}) + O(\varepsilon^2)$

where h_o = constant, the height of the homogeneous atmosphere at rest. The first order approximation for $(h^{(1)}, u^{(1)}, v^{(1)})$ yields

(6.1) $\frac{d^{(1)}}{d\tau}[(\zeta^{(1)} + fh^{(1)})/h_o] = 0$, $\tau = \varepsilon t$, f = const.

(6.2) $gh_x^{(1)} - fv^{(1)} = 0$

(6.3) $gh_y^{(1)} + fu^{(1)} = 0$

(geostrophic balance)

where $d^{(1)}(\ )/d\tau \equiv (\ )_\tau + u^{(1)}(\ )_x + v^{(1)}(\ )_y$. We call (6.1) the "geostrophic conservation equation". The system of equations (6) can be written in a neater form by replacing $h^{(1)}$ by $\psi \equiv gh^{(1)}/f$:

$$\frac{d^{(1)}}{d\tau}(\Delta - \kappa^2)\psi = 0 \tag{7.1}$$

$$(u^{(1)}, v^{(1)}) = (-\psi_y, \psi_x) \tag{7.2}$$

where $\Delta(\ ) \equiv (\ )_{xx} + (\ )_{yy}$, is the two dimensional Laplacian, and $\kappa^2 \equiv f^2/gh_o$. The geostrophic equation (7.2) shows that ψ is the stream function, viz., the flow is divergence-free to this order of approximation; and the first order vertical velocity $w^{(1)} = 0$ from (4.2). If we compare the asymptotic equation (6.1) [or (7.1)] with (3), we see that the essential consequence of the approximation procedure is that the potential vorticity, $(\zeta+f)/h$, has been linearized to yield $(\zeta^{(1)} + fh^{(1)}/h_o) \equiv (\Delta - \kappa^2)\psi$; however, (7.1) retains the nonlinearity of the first order material derivative operator, $d^{(1)}(\ )/d\tau$. For the linearized potential vorticity operator, we can obtain singular solutions which we call rectilinear geostrophic vortices; such a single vortex at $\vec{r} = \vec{r}_o$ is the solution of

$$(\Delta - \kappa^2)\psi_o = \delta(|\vec{r}-\vec{r}_o|) \tag{8.1}$$

where $|\vec{r}-\vec{r}_o| = [(x-x_o)^2 + (y-y_o)^2]^{1/2}$. The solution of (8.1) is

$$\psi_o = -\frac{\gamma}{2\pi} K_o(\kappa|\vec{r}-\vec{r}_o|) \tag{8.2}$$

where $\gamma/2\pi$ is the vortex strength in which we have chosen the sign of γ so that positive γ corresponds to a counter-clockwise rotating vortex (cyclonic, in meteorological terminology), and K_o is a Bessel function. The vortex solution (8.2) alone is a stationary solution of (7); in fact, any axially symmetric solution of (7) is stationary. Since $(\Delta - \kappa^2)\psi_o = 0$ everywhere except at $\vec{r}_o$, the vorticity distribution of a geostrophic vortex is

$$(8.3) \qquad \zeta^{(1)} = \Delta\psi_o = \kappa^2\psi_o = -\frac{\gamma\kappa^2}{2\pi} K_o(\kappa|\vec{r}-\vec{r}_o|)$$

and $\zeta^{(1)}$ and ψ_o have the same sign. With respect to the vortex center, $\vec{r}_o$, the tangential velocity distribution is

$$(8.4) \qquad \frac{\partial\psi_o}{\partial r} = -\frac{\gamma\kappa}{2\pi} K_o'(\kappa|\vec{r}-\vec{r}_o|) = \frac{\gamma\kappa}{2\pi} K_1(\kappa|\vec{r}-\vec{r}_o|) \; .$$

Near the origin, $(\vec{r} \to \vec{r}_o)$,

$$(8.5) \qquad \frac{\partial\psi_o}{\partial r} \sim \frac{1}{|\vec{r}-\vec{r}_o|}$$

which behaves like the classical logarithmic vortex. At large distances from $\vec{r}_o$ $(|\vec{r}-\vec{r}_o| \to \infty)$,

$$(8.6) \qquad \frac{\partial\psi_o}{\partial r} \sim (\kappa|\vec{r}-\vec{r}_o|)^{1/2} \exp\left[-(\kappa|\vec{r}-\vec{r}_o|)\right]$$

which dies out faster than the classical vortex. Equations (8) show that the geostrophic vortex has the qualitative features of a closed low (or high) pressure system, such as a hurricane. We

mention here that with an adiabatic atmosphere we can obtain a geostrophic vortex which has vertical structure.[4]

Representation of a Hurricane by a Rectilinear Geostrophic Vortex[5]

We can use (7) in the problem of short-range weather prediction in middle latitudes of large-scale atmospheric motions, far enough above the ground where real gas effects, such as viscosity, can be ignored. Ordinarily, this involves numerical calculations on electronic computers since (7.1) is a third-order nonlinear partial differential equation. The availability of a vortex solution (8) facilitates such calculations in the problem of following hurricane trajectories. We write ψ as the sum of two terms

$$\psi(x,y,\tau) = \psi_o(\kappa|\vec{r}-\vec{r}_o|) + \psi_1(x,y,\tau) \tag{9}$$

where ψ_o is given by (8.2) with $\vec{r}_o = \vec{r}_o(t)$ and represents the hurricane centered at $\vec{r}_o$ and ψ_1 is the remaining part of the flow field. If we put (9) in (7), we obtain (as in the classical vortex motion case)

$$\frac{d^{(1)}}{d\tau}(\Delta - \kappa^2)\psi_1 = 0 \tag{10.1}$$

and

$$\left(\frac{dx_o}{d\tau}, \frac{dy_o}{d\tau}\right) = \left(-\frac{\partial\psi_1}{\partial y}, \frac{\partial\psi_1}{\partial x}\right)\Bigg|_{(x_o,y_o)} \tag{10.2}$$

where $d^{(1)}(\ )/d\tau = \frac{\partial(\ )}{\partial\tau} + u^{(1)}\frac{\partial(\ )}{\partial x} + v^{(1)}\frac{\partial(\ )}{\partial y}$, $u^{(1)} = -\frac{\partial}{\partial y}(\psi_o + \psi_1)$.

and $v^{(1)} = \frac{\partial}{\partial x}(\psi_o + \psi_1)$. The point $[x_o(\tau), y_o(\tau)]$ is taken as the position of the hurricane eye at time, τ. Equations (10) are a coupled system of a partial differential equation for ψ_1 and two ordinary differential equations for (x_o, y_o). Given the initial conditions $\psi_1(x,y,0)$, $x_o(0)$ and $y_o(0)$ (and boundary conditions) we obtain $\psi_1(x,y,\tau)$ and $[x_o(\tau), y_o(\tau)]$ at any later time τ, usually by numerical computation. We show the results of calculations for Hurricane Betsy(6), 13-19 August, 1956. During this time the hurricane was in a relatively mature state and the trajectory stayed over the Atlantic Ocean without landfall. The initial data (originally from the U.S. Weather Bureau) was taken at the 500 mb. pressure level (ground level is approximately 1000 mb.) and prepared in the Meteorology Department, University of Chicago. The height data was available on a 22×22 mesh, with 300 km. mesh width at 12 hour intervals. The original runs were made with one hour time steps for 48 hours on the UNIVAC computer and later rerun at one-half hour time steps on the IBM 704 and 7090. The finite difference scheme(7) and computer program(8) were developed by Eugene Isaacson and David Levine. Using the available initial data at each 12 hour interval, two runs were made: 1) one run with $\gamma = 0$ (non-interacting vortex) and 2) one run with γ and κ chosen so that the resulting initial ψ_1, after the hurricane, ψ_o, was subtracted out, was as smooth as possible in the vicinity of $[x_o(0), y_o(0)]$. The calculated hurricane trajectories are shown in Fig. 1. The trajectories with non-zero γ, viz., ψ_o interacting nonlinearly with ψ_1, always move to the

left of the trajectories with $\gamma = 0$ (non-interacting, as previously assumed by meteorologists). However, comparing with the actual hurricane trajectory, there are certain deficiencies of the model (with $\gamma \neq 0$): 1) the model is slower than the actual motion, 2) for the initial data for 14 August, 1956, the vortex, moving initially in a northwesterly direction does not change its direction to the northeast as it should. The run with $\gamma = 0$ does make the turn (called "recurvature" by meteorologists) but not rapidly enough. The problem of predicting recurvature is still unsolved. The vortex trajectories simulate the actual trajectories best after recurvature; and the time development of ψ_1 is also good for these runs.

Interacting Motion of Rectilinear Geostrophic Bessel Vortices[9]

In (8) and in the problem of calculating hurricane trajectories, we considered only a single geostrophic vortex. Now we study the interacting motion of N (or (N+1)) vortices. The equations of motion can be derived[3] from (7). For N vortices at positions (x_i, y_i), the stream function satisfies

$$(11.1) \qquad (\Delta - \kappa^2)\psi = \sum_{i=1}^{N} \delta(|\vec{r}-\vec{r}_i|)$$

and the solution of (11.1) is

$$(11.2) \qquad \psi = -\frac{1}{2\pi}\sum_{i=1}^{N} \gamma_i K_o(\kappa|\vec{r}-\vec{r}_i|)$$

where $|\vec{r}-\vec{r}_i| = [(x-x_i)^2 + (y-y_i)^2]^{1/2}$. If the only elements in the

entire flow field are the N vortices, the velocity of the k-th vortex is obtained by differentiating

$$\psi_{(k)} = -\frac{1}{2\pi}\sum_{\substack{i\neq k\\ i=1}}^{N} \gamma_i K_o(\kappa|\vec{r}-\vec{r}_o|) \tag{11.3}$$

which is the non-singular part of (11.2) at (x_k, y_k), yielding

$$u^{(1)}_{(k)} = -\frac{\partial}{\partial y}\psi_{(k)} = \frac{dx_k}{d\tau} = \frac{\kappa}{2\pi}\sum_{\substack{i\neq k\\ i=1}}^{N} \gamma_i \frac{(y_k-y_i)}{|\vec{r}_k-\vec{r}_i|} K_o'(\kappa|\vec{r}_k-\vec{r}_i|) \tag{11.4}$$

and

$$v^{(1)}_{(k)} = \frac{\partial}{\partial x}\psi_{(k)} = \frac{dy_k}{d\tau} = -\frac{\kappa}{2\pi}\sum_{\substack{i\neq k\\ i=1}}^{N} \gamma_i \frac{(x_k-x_i)}{|\vec{r}_k-\vec{r}_i|} K_o'(\kappa|\vec{r}_k-\vec{r}_i|)\ . \tag{11.5}$$

Equations (11.4) and (11.5) are a coupled system of 2N first order, ordinary differential equations for $[x_k(\tau), y_k(\tau)]$, given the initial positions, $[x_k(0), y_k(0)]$. These equations can be expressed in a more symmetric form,

$$\gamma_k\left(\frac{dx_k}{d\tau}, \frac{dy_k}{d\tau}\right) = \left(\frac{\partial W}{\partial y_k}, -\frac{\partial W}{\partial x_k}\right) \tag{11.6}$$

where

$$W = \frac{1}{4\pi}\sum_{\substack{i\neq j\\ i,j=1}}^{N} \gamma_i\gamma_j K_o(\kappa|\vec{r}_i-\vec{r}_j|)\ . \tag{11.7}$$

Kirchhoff[10] first noticed this form for $\kappa = 0$. Equations (11.6) and (11.7) are reminiscent of Hamilton's equations of motion of interacting particles; however, significant differences are that 1) these equations are in the two dimensional configuration space,

(x_k, y_k), whereas Hamilton's equations are in the full configuration-momentum phase space, and 2) W can be positive or negative depending on the sign of the γ_i's. The integral invariants of Equations (11.6) and (11.7) are

$$W = \text{const.} \ (\gtrless 0) \ , \tag{11.8}$$

$$\sum_{k=1}^{N} \gamma_k x_k = \text{const.}, \qquad \sum_{k=1}^{N} \gamma_k y_k = \text{const.} \ , \tag{11.9}$$

$$\sum_{k=1}^{N} \gamma_k r_k^2 = \text{const.} \ , \tag{11.10}$$

$$\sum_{k=1}^{N} \gamma_k r_k^2 \dot{\theta}_k = \frac{\kappa}{4\pi} \sum_{\substack{i \neq k \\ i,k=1}}^{N} \gamma_i \gamma_k |\vec{r}_i - \vec{r}_k| \, K_1[\kappa |\vec{r}_i - \vec{r}_k|] = \text{const.} \tag{11.11}$$

where $(x_k, y_k) = r_k(\cos\theta_k, \sin\theta_k)$, and $(\dot{\ })$ means differentiation with respect to time. Equations (11.9) are related to the centroid of the vortices; and (11.10) and (11.11) are reminiscent of momentum invariants. For $\kappa = 0$, (11.11) reduces to the classical result:

$$\sum_{k=1}^{N} \gamma_k r_k^2 \dot{\theta}_k = \sum_{\substack{i \neq k \\ i,k=1}}^{N} \gamma_i \gamma_k \ . \tag{11.12}$$

We study the linear and nonlinear stability of the interacting, kinematic motion of (N+1) geostrophic vortices. Initially the vortices are positioned near a uniformly rotating equilibrium configuration which consists of N vortices of equal strength, γ, equally spaced on a circle of radius, a, and one vortex of strength, γ_o, at the center of the circle. All (N+1) vortices have the same horizontal length scale κ^{-1}, where the

limiting case, $\kappa = 0$, corresponds to potential (logarithmic) vortices. The ranges of the parameters N, (γ_o, γ), and (κa) are: $N \geq 2$, $-\infty < (\gamma_o/\gamma) < \infty$, and $0 \leq (\kappa a) < \infty$. We normalize the continuous parameters by setting $\gamma = 1$ and $a = 1$ to simplify the notation. For the equilibrium motion, $r_k = 1$ ($\dot{r}_k = 0$) and $\theta_k = \Omega t + \frac{2\pi k}{N}$ ($\dot{\theta}_k = \Omega$, const.) where

$$\Omega = \gamma_o \kappa K_1(\kappa) + \frac{1}{2} \sum_{\substack{i \neq k \\ i,k=1}}^{N} \sigma_{ki} K_1(\sigma_{ki}) \tag{12}$$

where $\sigma_{ki} = \kappa[2(1 - \cos w_{ki})]^{1/2}$ and $w_{ki} = (w_k - w_i) = \frac{2\pi(k-i)}{N}$. For the linear stability analysis, a mixed coordinate representation of the equations of motion is appropriate, viz., polar coordinates for the circle vortices and Cartesian coordinates for the center vortex. The linearized equations of motion have constant coefficients in a frame of reference rotating with angular velocity, Ω. Then the solution $(r_k^{(1)}, \theta_k^{(1)}, x_o^{(1)}, y_o^{(1)})$ can be sought that has time dependence in exponential form $e^{\lambda_i t}$; and if an eigenvalue λ_i has a real part that is positive, the motion becomes exponentially unstable with respect to the equilibrium motion. The results are summarized by the neutral stability curves in the (γ_o, κ) parameter space; in Fig. 2 a circle vortex is stable on the unhatched (right) side of each curve; in Fig. 3 the center vortex is stable on the unhatched (left) side. In particular, Table I gives the γ_o-range of linear stability for $\kappa = 0$. But, a complication arises because of the presence of a double zero eigenvalue for all values of the parameters N, γ_o and κ. This difficulty is

partially overcome by the use of two linear integral invariants:
1) by linearizing (11.10) we get

$$\sum_{k=1}^{N} r_k^{(1)} = \text{const.} = 0 \,, \tag{13.1}$$

and 2) upon linearizing (11.11) we get

$$\sum_{k=1}^{N} \theta_k^{(1)} = \text{const.} \neq 0 \tag{13.2}$$

which cannot be set equal to zero usually. Since these first order (linear) invariants do not include the center vortex position $(x_o^{(1)}, y_o^{(1)})$, which only appears to second (and higher) order, the double zero eigenvalues can be strictly nullified only for $\gamma_o = 0$. For $\gamma_o \neq 0$, the double zero eigenvalues allow solutions which increase linearly with time, implying that the motion of the center vortex is nonlinear. Numerical integrations of the nonlinear equations of motion were carried out. The numerical computations show that nonlinear effects are important in a relatively small transition region embracing both the stable and unstable sides of the neutral stability curves for the circle vortices (Fig. 2), even for small perturbations of the initial position; otherwise Fig. 2 represents valid results concerning the stability of the circle vortices. However, the stability of the center vortex is not well-represented by the neutral stability curves shown in Fig. 3; and the numerical computations are essential for the study of the stability of the center vortex.

References

1. A. S. Monin, "Hydrodynamic Theory of Short-Range Weather Forecasts", Soviet Physics Uspekhi, 11, 746-766 (March-April, 1969), (English translation).

2. A. C. Fetter, P. C. Hohenberg, and P. Pincus, "Stability of a Lattice of Superfluid Vortices", Physical Review 147, 140-152 (8 July 1966).

3. G. K. Morikawa, "Geostrophic Vortex Motion", J. of Meteorology, 17, 148-158 (April 1960).

4. ———————, "Asymptotic Behavior of Planetary-Scale Motions of the Atmosphere", NYU-CIMS Report No. IMM 348, (April 1966), Appendices I and II.

5. ———————, "On the Prediction of Hurricane Tracks Using a Geostrophic Point Vortex", Proc. of Intern. Symp. on Numerical Weather Prediction in Tokyo, Ed. S. Syono, 344-360 (March 1962).

6. A. Kasahara and G. W. Platzman, "Interaction of a Hurricane with the Steering Flow and its Effect upon the Hurricane Trajectory", Tellus, 15, 321-335 (1963).

7. E. Isaacson and H. Keller, Analysis of Numerical Methods, (Wiley, New York, 1966), p. 388.

8. D. A. Levine, "A Report on the Numerical Solution of the Geostrophic Conservation Equation", NYU Report NO. NYU IMM-247 (1958).

9. G. K. Morikawa and E. V. Swenson, "Interacting Motion of Rectilinear Geostrophic Vortices", to be published in Physics of Fluids, 14, 1058-1073 (1971).

10. H. Lamb, Hydrodynamics, (Cambridge Univ. Press, London, 1932), 6th edition, p. 230.

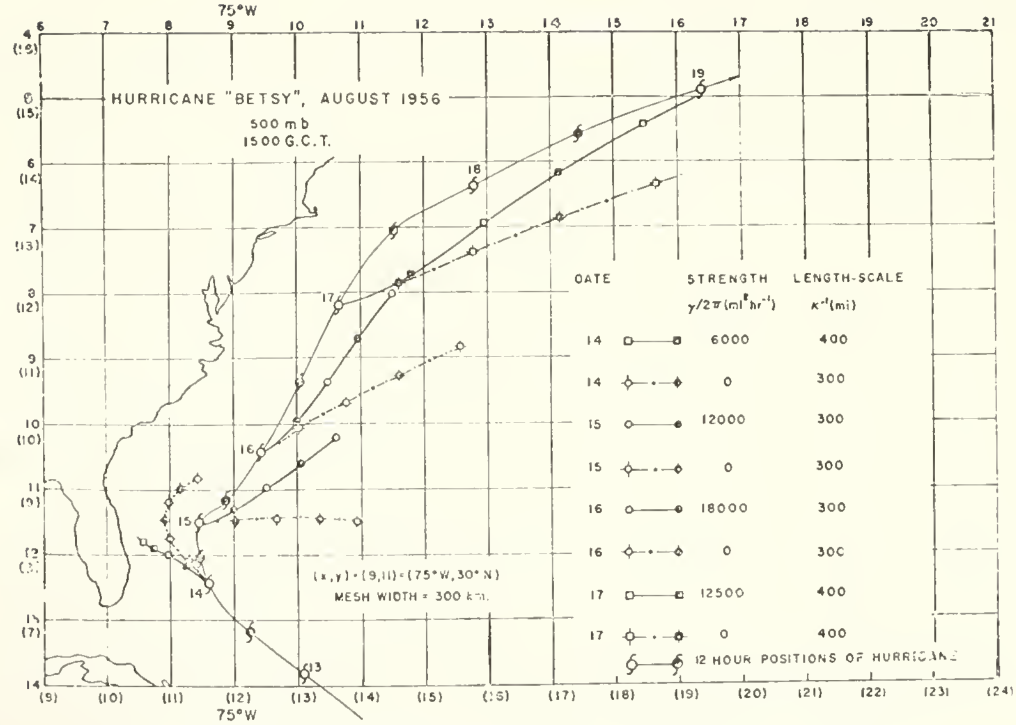

Fig. 1. Geostrophic point vortex trajectories for hurricane "Betsy" initial data.

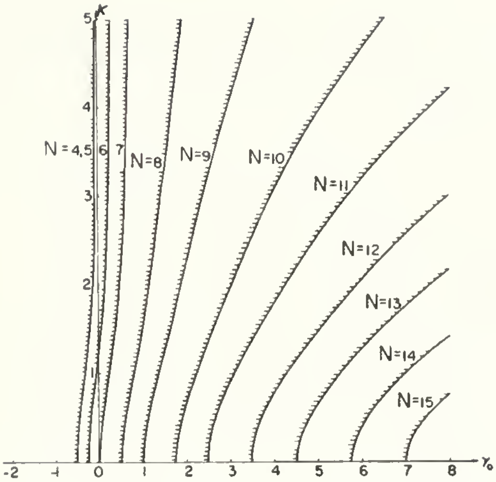

FIG. 2 Neutral stability curves for circle vortices (stable region on right side of eacb curve).

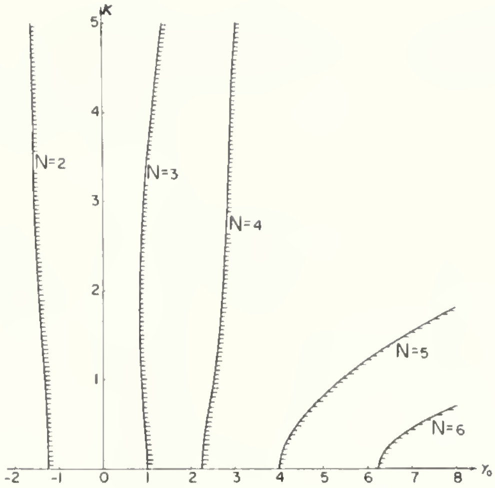

FIG. 3 . Neutral stability curves for center vortex (stable region on left side of each curve).

TABLE I. Range of exponential stability for free center vortex case, $\kappa=0$.

N	Lower stability limit[a]	Upper stability limit[b]
2	$\gamma_0^l = -\infty$	$\gamma_0^u = -1.25$
3	$-\infty$	1
4	−0.5	2.25
5	−0.5	4
6	−0.25	6.25
7	0	9
8	0.5	12.25
9	1	16
10	1.75	20.25
11	2.5	25
12	3.5	30.25
13	4.5	36
14	5.75	42.25
15	7	49

[a] A circle vortex is unstable for γ_0 less than the lower stability limit.
[b] The center vortex is unstable for γ_0 greater than the upper stability limit.

Lecture 9

The Upper Boundary Condition for Gravity Waves in the Atmosphere

Michael Yanowitch

The linearized theory of waves in an inviscid isothermal fluid in a half space serves as a simple model for the study of atmospheric gravity waves. Two boundary conditions are appropriate for this model: a boundary condition on the vertical velocity at the ground, and an "upper boundary condition", which depends on the form of the solution. If the solution is nonoscillatory in the vertical (z) coordinate, one imposes the condition that the kinetic energy in an infinite vertical column of fluid should be finite. If the solution is wavelike in the x-coordinate, a radiation condition is customarily imposed, i.e. it is assumed that the energy propagates upward to infinity without reflection. Unfortunately, the validity of this model is open to question since the velocities increase exponentially with altitude and thus violate the assumptions underlying the basic linearization. To overcome this deficiency we will study a viscous fluid model. It will be seen that the solutions to this problem are uniformly small, consistent with the small amplitude assumption, and that the radiation condition is, in general, not correct since waves may be reflected downward. For our purpose it suffices to consider an incompressible, but horizontally stratified, fluid.

The undisturbed incompressible fluid occupying the half-space $z > 0$ is assumed to have a constant dynamic viscosity ε, and a

stratified density $\rho(z)$, a specified function. The wave motion has a velocity u in the horizontal direction x and a velocity w in the vertical direction z, with a density perturbstion $\tilde{\rho}$ and a pressure perturbation $\tilde{p}$. The linearized differential equations governing the motion are

$$\frac{\partial}{\partial x} u + \frac{\partial}{\partial z} w = 0$$

$$\frac{\partial}{\partial t} \tilde{\rho} + \frac{d\rho}{dz} w = 0$$

$$\rho \frac{\partial}{\partial t} u + \frac{\partial}{\partial x} \tilde{p} = \varepsilon \left(\frac{\partial^2}{\partial x^2} + \frac{\partial^2}{\partial z^2} \right) u$$

$$\rho \frac{\partial}{\partial t} w + \frac{\partial}{\partial z} \tilde{p} + g\tilde{\rho} = \varepsilon \left(\frac{\partial^2}{\partial x^2} + \frac{\partial^2}{\partial z^2} \right) w$$

where g is the acceleration of gravity. The stream function Ψ, so defined that $u = \frac{\partial \Psi}{\partial z}$ and $w = -\frac{\partial \Psi}{\partial x}$, satisfies

$$\frac{\partial^2}{\partial t^2} \left[\rho \frac{\partial^2}{\partial x^2} \Psi + \frac{\partial}{\partial z} \rho \frac{\partial}{\partial z} \Psi \right] - g \frac{d\rho}{dz} \frac{\partial^2}{\partial x^2} \Psi = \varepsilon \left(\frac{\partial^2}{\partial x^2} + \frac{\partial^2}{\partial z^2} \right)^2 \frac{\partial}{\partial t} \Psi$$

upon elimination of the density and pressure perturbations.

For a wave propagating in the x-direction, we look for a solution such that $\Psi = \Phi(z) e^{ikx - i\omega t}$. The complex-valued amplitude $\Phi(z)$ then satisfies

$$i \frac{\varepsilon}{\omega} \left(\frac{d^2}{dz^2} - k^2 \right)^2 \Phi - \frac{d}{dz} \rho \frac{d}{dz} \Phi + k^2 \left(\rho + \frac{g}{\omega^2} \frac{d\rho}{dz} \right) \Phi = 0 .$$

The no-slip condition at the lower boundary requires that $u = 0$ and $w = \text{const.}\ e^{ikx - i\omega t}$ at $z = 0$, i.e.

$$\Phi\Big|_{z=0} = \text{const.} \ , \qquad \frac{d\Phi}{dz} = 0 \ .$$

Since the density in the atmosphere decreases very rapidly, by a factor of 10^6 in the lowest 100 km. (while the viscosity varies only slightly), we shall assume that the density is stratified exponentially, viz.,

$$\rho(z) = \rho_o e^{-z/H}$$

where H is a scale height for the stratification. Accordingly, Φ satisfies

$$\varepsilon\left(\frac{d^2}{dz^2} - k^2\right)^2 \Phi + i\omega\rho_o e^{-z/H}\left[\frac{d^2}{dz^2}\Phi - \frac{1}{H}\frac{d}{dz}\Phi + k^2\left(\frac{g}{\omega^2 H} - 1\right)\Phi\right] = 0 \ .$$

Instead of the radiation condition, we shall impose a "dissipation condition": the average rate of energy dissipation in an infinite vertical column of fluid ($0 < z < \infty$) of unit cross-section area must be finite. Namely,

$$\int_0^\infty |\Phi|^2 dz < \infty \ , \quad \int_0^\infty \left(\frac{d\Phi}{dz}\right)^2 dz < \infty \ , \quad \int_0^\infty \left(\frac{d^2\Phi}{dz^2}\right)^2 dz < \infty \ ,$$

as the dissipation function depends on the square of the space derivatives of velocities.

At very high altitudes ($z \to \infty$) the viscous term dominates. Hence in this "viscous region"

$$\left(\frac{d^2}{dz^2} - k^2\right)^2 \Phi \approx 0$$

thus, Φ is a linear combination of e^{-kz} and ze^{-kz} in order to satisfy the dissipation condition. Separated from the viscous region by a "transition region" (where $\varepsilon^{-1}e^{-z/H} = O(1)$) is an "inviscid region", where the viscous effect is negligible, hence

$$\frac{d^2}{dz^2}\Phi - \frac{1}{H}\frac{d}{dz}\Phi + k^2\left(\frac{g}{\omega^2 H} - 1\right)\Phi \approx 0$$

thus

$$\Phi \approx Ae^{z/2H-i\beta z} + Be^{z/2H+i\beta z}$$

with

$$\beta = [k^2(gH/\omega^2 - H^2) - \tfrac{1}{4}]^{1/2} .$$

The inviscid region is connected to the lower boundary $z = 0$ by a "boundary layer" which reduces $\frac{d\Phi}{dz}$ to zero as $z \to 0$. The problem is, therefore, to find a solution which is valid uniformly in the inviscid, transition, and viscous regions. (The boundary layer can always be fitted in later.)

To obtain the solution it is advantageous to transform to the independent variable: $\xi = (-i/\varepsilon)e^{-z/H}$. The transformed equation (in dimensionless quantities) is

$$\left(\xi^2\frac{d^2}{d\xi^2} - 4k^2\right)^2\Phi - \xi^2\left(\xi^2\frac{d^2}{d\xi^2} + 2\xi\frac{d}{d\xi} + 4r\right)\Phi = 0$$

where r is a constant. The only singular points of the differential equation are $\xi = 0$ and $\xi = \infty$, with $\xi = 0$ being a regular singular point, $\xi = \infty$ an irregular one. It is possible to obtain the unique solution satisfying the dissipation condition in the

form of a Frobenius series about $\xi = 0$. The coefficients of the series satisfy a two term recursion formula, which enables one to convert the series to a complex integral by the Cauchy summation method. The behavior in the inviscid region as $\varepsilon \to 0$ corresponds to the behavior for large ξ, with $\arg \xi = -i\pi/4$, which can be obtained by evaluating the residues at the poles of the integrand.

The solution does not tend to a limit as $\varepsilon \to 0$ in the fixed x, z coordinate system, but does so in a coordinate system which moves upward as $\varepsilon \to 0$ in such a way that $\varepsilon^{-1} e^{-z/H} = \text{const}$. The magnitude of the reflection coefficient, $|B/A|$, however, tends to the limit $\exp(-2\pi^2 H/\lambda)$, where λ is the vertical wavelength. Thus there is substantial reflection when the vertical wavelength is large and the solution approaches the form of a standing wave as $\lambda \to \infty$. The radiation condition becomes more and more accurate as $\lambda \to 0$.

Reference

M. Yanowitch, Effect of viscosity on gravity waves and the upper boundary condition, J. Fluid Mech. (1967), Vol. 29, pp. 209-231.

Lecture 10

Numerical Simulation of the Life Cycle of Tropical Cyclones

Katsuyuki Ooyama

The tropical cyclone is a solitary creature of the tropical oceans accompanied by violent rotating winds and torrential rain. Observational studies and diagnostic analyses leave little doubt that the energy required for driving the vortex comes from the latent heat of condensation released by tall convective clouds around the center, and that the frictionally induced inflow in the vortex plays a major role in supporting the continued activity of convective clouds. This dual character with respect to important scales of motion poses a great difficulty in investigating the dynamics of tropical cyclones as time-dependent phenomena. However, in order to understand the large-scale aspects of tropical cyclones, one may formulate the role of convective clouds in terms of cyclone-scale variables with only implicit consideration of the dynamics of individual clouds. The present study is an attempt to understand the basic mechanism of tropical cyclones by constructing a numerical-dynamical model on such a basis.

The model assumes that the large-scale hydrodynamical aspects of a tropical cyclone may be represented by an axisymmetric, quasi-balanced vortex in a stably stratified incompressible fluid, while the effects of moist convection may be formulated through the first

law of thermodynamics applied to an implicit model of penetrative convective clouds. The air-sea exchange of angular momentum as well as latent and sensible heat is explicitly calculated in the model with the use of conventional approximations.

Results of numerical integration show that the model is capable of simulating the typical life cycle of tropical cyclones, including the mature hurricane stage, with a remarkable degree of reality. The response of the model cyclone to changes in such parameters as the sea surface temperature, the coefficient of air-sea energy exchange, and the initial conditions is tested in a number of numerical experiments to show quite plausible results. A detailed diagnosis of the energy budget of the simulated tropical cyclone is also carried out. The rate of total rainfall, the production and dissipation of kinetic energy, and other energetic characteristics of the computed cyclone compare very well with available estimates for observed tropical cyclones.

Because of the restrictive assumption of axisymmetry and other weak approximations, the model is not realistic enough to predict behavior of individual tropical cyclones in nature. The limitation of the present model in this regard is also discussed.

Figure 1 shows the characteristic scales (lengths, times, and speeds) for various meteorological phenomena.

References

K. Ooyama, Numerical simulation of the life cycle of tropical cyclones, J. Atmos. Sci. (1969), Vol. 26, pp. 3-40.

Characteristic Time Scale T in Seconds

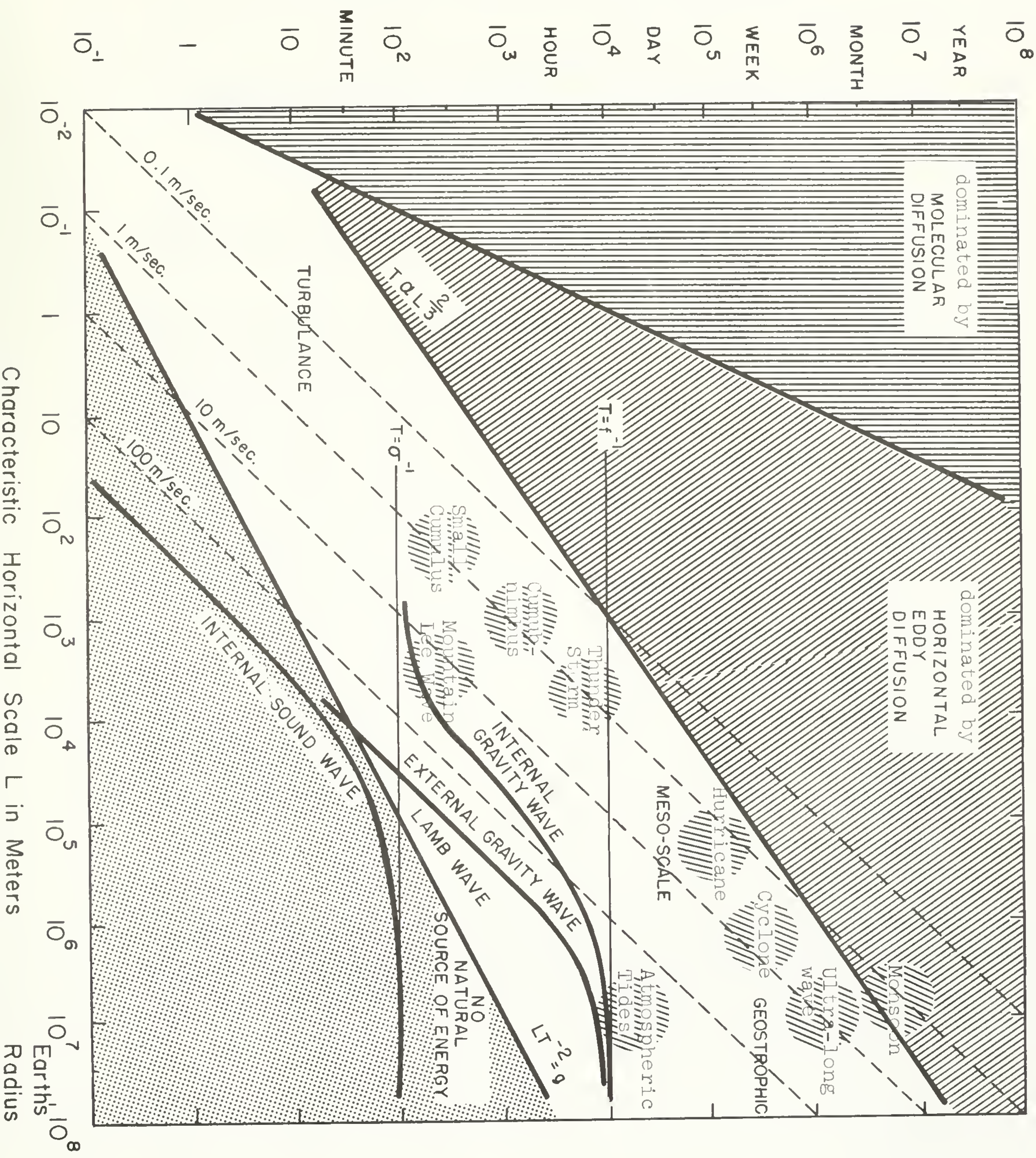

Characteristic Horizontal Scale L in Meters

Lecture 11

A Mountain Building Model

(A presentation of the Ph.D. Thesis of Jay Wolkowisky)

Chester B. Sensenig

The mountain building model treated in the Ph.D. thesis of Jay Wolkowisky [1] was proposed by J. J. Stoker. It is based on the observation that in a number of instances relatively high mountain ranges and/or deep ocean troughs occur near the edge of a continent, and the continent is relatively flat except for these variations in elevation near its edge. Since the earth's crust over a continent is much thicker than over most of the ocean floor but is thin relative to the radius of the earth, the continent can be thought of as a thin shell with its edge at or near the ocean shore. Stoker then posed the question, "Can the relatively flat interior and rippled edge of the continent be explained as the lowest buckled mode of a thin elastic plate resting on an elastic foundation?" For simplicity, a thin circular plate resting on an elastic foundation is considered, and a compressive edge force is applied with the edge clamped, or pinned (zero bending moment). Values of foundation stiffness, plate thickness, and edge thrust are sought for which the lowest buckled mode is relatively flat in the interior with relatively large ripples near the edge.

The buckling problem is treated by using the plate theory of v. Karman and Föppl [2] with a term added which corresponds to the elastic foundation. The differential equations are

$$(1)\qquad \begin{cases} \gamma^2 h^2 E \Delta^2 w = \phi_{yy} w_{xx} - 2\phi_{xy} w_{xy} + \phi_{xx} w_{yy} - \frac{k}{h} w \\ \frac{1}{E} \Delta^2 \phi = w_{xy}^2 - w_{xx} w_{yy} \end{cases}$$

where

x and y are the independent variables with $x^2 + y^2 \leq R^2$ (R = the radius of the plate),

$w = w(x,y)$ is the vertical deflection,

$\phi = \phi(x,y)$ is the Airy stress function,

$\tau_{xx} = \phi_{yy}$, $\tau_{xy} = -\phi_{xy}$, $\tau_{yy} = \phi_{xx}$ are the longitudinal stresses averaged through the thickness of the plate,

$\gamma^2 = \dfrac{1}{12(1-\nu^2)}$ (ν = Poisson's ratio),

E = Young's modulus,

h = the plate thickness,

k = the foundation stiffness (kw = restoring force per unit area),

$\Delta = \dfrac{\partial^2}{\partial x^2} + \dfrac{\partial^2}{\partial y^2}$,

and the subscripts x and y indicate partial derivatives except in the case of the longitudinal stresses.

In the books of Jeffry (The Earth, 3rd Ed.), and Heiskanen (The Earth and Its Gravity Field), it is stated that elastic instability of the earth's crust when under compressive stress never can occur because the stress required would be much greater than the crushing strength of the material of the crust. This follows, however, only because these writers assume buckled forms for the crust of the earth that have very small wavelengths, of the order of roughly three times the thickness of the crust. They use the Euler theory of buckling of columns in their discussion, but this theory applies only for long slender columns (having lengths of the order of at least 50 times the thickness, say) and gives far too large values for thick columns. In addition there seems no reason not to investigate the elastic stability of the crust under compression when it is assumed to be a plate of the size of a continent. There is, for example, a geosyncline in a large portion of the interior of continental North America, with a wavelength of something like 1500 miles. It is assumed here that such a plate buckles under compression into a cylinder with generators in the north-south direction, so that (1) applies when w and ϕ depend only upon x. It is assumed further — as was done by the two writers mentioned above — that the ends of plate on the east and west sides are free of bending moments, which implies that $\frac{d^2w}{dx^2} = 0$ there, and that the effect of the support of the earth under the crust can be ignored.

Only the onset of buckling is to be determined, and that can be done by linearizing (1) (as will be explained in more detail later), and setting $\phi_{yy} = -\tau_{xx}$, $\phi_{xy} = \phi_{yy} = 0$ in which τ_{xx} is the

compressive stress assumed to exist in the x-direction (east-west). The weight of the earth is neglected. The result is the following problem. The differential equation

$$\frac{h^2 E}{12(1-\nu^2)} \frac{d^4 w}{dx^2} = -\tau_{xx} \frac{d^2 w}{dx^2} , \qquad 0 \leq x \leq \ell ,$$

is to be integrated under the boundary conditions $w = 0$, and $\frac{d^2 w}{dx^2} = 0$ at $x = 0$ and $x = \ell$. This is a linear eigenvalue problem for the determination of the buckling stress τ_{xx}, i.e. the smallest value of τ_{xx} for which a nonvanishing solution of the mathematical problem exists. The solution is well known and is given by

$$\tau_{xx} = \frac{\pi^2}{\ell^2} \frac{h^2 E}{12(1-\nu^2)} .$$

If $\nu = 0.3$, $\ell = 1500$ miles, $E = 12 \times 10^6$ lbs/in^2, and $h = 21$ miles are taken, the value of τ_{xx} is found to be

$$\tau_{xx} \sim \pi^2 (\frac{1}{75})^2 \frac{12 \times 10^6}{12(0.9)}$$

$$\sim 2100 \text{ lbs/in}^2$$

which is negligible. For $\ell = 1000$ miles, for which the theory would still be valid ($\frac{\ell}{h} \sim 50$), $\tau_{xx} \sim 4800$ lbs/in^2 holds. Even for $\ell = 500$ miles, the buckling stress is only 19000 lbs/in^2. These values are, of course, far under the crushing stress for materials of the type making up the crust of the earth. Thus it would seem not reasonable to reject buckling of the earth's crust due to elastic instability as a possible effect in interesting special cases.

For simplicity, radially symmetric deformations of the plate are considered. Thus the partial differential equations (1) become ordinary differential equations.

These equations (with $k = 0$) were used by Friedrichs and Stoker [3] to study the lowest buckled mode of a circular plate due to a compressive edge force with pinned edge. It was discovered that the solution depends essentially on $N = \frac{\overline{p}}{p^o}$ where $\overline{p}$ is the pressure applied at the edge and p^o is the lowest pressure at which the plate buckles. The solution was calculated for $1 \leq N \leq 2.5$ by using a perturbation method, for $2.5 \leq N \leq 15$ by using power series, and for $N \to \infty$ by using asymptotic methods.

Higher buckled modes were studied by others including H. Keller, J. Keller, and Reiss [4] and Conn [5].

From these treatments it is known that the plate is relatively flat in the interior with large variations in w near the edge if the compressive edge force is sufficiently large. The lowest mode of buckling will look like a plain with a cliff at the edge, but the higher modes of buckling will have hills and valleys near the edge. However, the higher modes of buckling certainly will not occur in nature. The question being raised is whether the <u>lowest</u> buckled mode will be relatively flat in the interior and have hills and valleys near the edge for some parameter values when the plate is on an elastic foundation.

The following quantities are introduced:

R = radius of the plate,

$r^* = \sqrt{x^2 + y^2}$,

$\bar{p}$ = edge thrust,

$$q = q(r^*) = -\sqrt{\frac{E}{\bar{p}}}\,\frac{R}{r^*}\,\frac{dw}{dr^*},$$

$$p = -\frac{1}{\bar{p}r^*}\,\frac{d\phi}{dr^*} \text{ (mean radial stress)},$$

$$W = -\sqrt{\frac{E}{\bar{p}}}\,\frac{1}{Rr^{*2}} \int_0^{r^*} tw(t)dt,$$

$$r = \frac{r^*}{R}, \quad 0 \leq r \leq 1,$$

$$\alpha^2 = \frac{\bar{p}R^2}{\gamma^2 h^2 E},$$

$$K^2 = \frac{R^4 k}{\gamma^2 h^2 E},$$

$$G = \frac{1}{r^3}\,\frac{d}{dr}\left(r^3 \frac{d}{dr}\right).$$

The differential equations then become

$$(2) \qquad \begin{cases} Gq + \alpha^2 pq = K^2 W \\ Gp = \frac{1}{2} q^2 \\ GW + q = 0 \,. \end{cases}$$

To obtain (2) the equations (1) are integrated and integration constants are eliminated by using regularity and symmetry of stress and displacement at the center of the plate.

The boundary conditions are:

$$
(3) \quad \begin{cases} q'(0) = p'(0) = W'(0) = 0 \text{ from symmetry,} \\ p(1) = 1 \text{ (edge pressure is } \overline{p}\text{),} \\ W'(1) + 2W(1) = 0 \text{ (} w = 0 \text{ at edge),} \\ q'(1) + (1+\nu)g(1) = 0 \text{ for pinned edge,} \\ q(1) = 0 \text{ for clamped edge.} \end{cases}
$$

It is seen that the problem depends essentially on the parameters α and K.

A perturbation method is used to determine the critical value of the parameters. Since an exact solution to (2) and (3) is $p \equiv 1$, $q \equiv W \equiv 0$, we assume an expansion

$$
\begin{aligned}
q &= \varepsilon q_1 + \varepsilon^2 q_2 + \dots \\
p &= 1 + \varepsilon p_1 + \varepsilon^2 p_2 + \dots \\
W &= \varepsilon W_1 + \varepsilon^2 W_2 + \dots
\end{aligned}
$$

where ε is a perturbation parameter.

From (2) and (3) we obtain

$$
(4) \quad \begin{cases} Gq_1 + \alpha^2 q_1 = K^2 W_1 , \\ Gp_1 = 0 \\ GW_1 + q_1 = 0 \end{cases}
$$

and

$$(5)\qquad \begin{cases} q_1'(0) = p_1'(0) = W_1'(0) = 0 \ , \\ p_1(1) = 0 \ , \\ W_1'(1) + 2W_1(1) = 0 \ , \\ q_1'(1)+(1+\nu)q_1(1) = 0 \text{ for a simply supported edge,} \\ q_1(1) = 0 \text{ for a clamped edge.} \end{cases}$$

These imply $p_1 \equiv 0$, and leave two differential equations for q_1 and W_1. Special solutions can be found such that $q_1 = \lambda^2 W_1$ where λ is a constant. From (4)

$$GW_1 + (\alpha^2 - \frac{K^2}{\lambda^2})W_1 = 0 \ ,$$

$$GW_1 + \lambda^2 W_1 = 0 \ ,$$

so that

$$\lambda^2 = \alpha^2 - \frac{K^2}{\lambda^2} \ .$$

The solutions λ are

$$(6)\qquad \begin{cases} \lambda_1 = \sqrt{\dfrac{\alpha^2}{2} + \dfrac{1}{2}\sqrt{\alpha^4 - 4K^2}} \ , \\ \lambda_2 = \sqrt{\dfrac{\alpha^2}{2} - \dfrac{1}{2}\sqrt{\alpha^4 - 4K^2}} \end{cases}$$

where we are now limiting ourselves to parameter values such that

$$(7)\qquad \begin{cases} \alpha^2 > 2K \ , \quad \text{or} \\ \bar{p}^2 > 4\gamma^2 h^2 Ek \end{cases}$$

so that λ_1 and λ_2 are real.

The general solution for q_1 and W_1 is

$$W_1 = \frac{1}{r}[AJ_1(\lambda_1 r) + BY_1(\lambda_1 r) + CJ_1(\lambda_2 r) + DY_1(\lambda_2 r)] ,$$

$$q_1 = \frac{1}{r}[A\lambda_1^2 J_1(\lambda_1 r) + B\lambda_1^2 Y_1(\lambda_1 r) + C\lambda_2^2 J_1(\lambda_2 r) + D\lambda_2^2 Y_1(\lambda_2 r)] ,$$

where J_1 and Y_1 are the usual Bessel functions and A, B, C, D are arbitrary constants.

If we substitute W_1 and q_1 into the boundary conditions (5), we obtain 4 homogeneous linear equations in A, B, C, D. In order that there be a non-zero solution, the determinant of the coefficients must vanish. This gives

$$(8) \quad \begin{cases} \lambda_1 \dfrac{J_1(\lambda_1)}{J_o(\lambda_1)} - \dfrac{\lambda_1^2}{1-\nu} = \lambda_2 \dfrac{J_1(\lambda_2)}{J_o(\lambda_2)} - \dfrac{\lambda_2^2}{1-\nu} \text{ for a pinned edge ,} \\[2ex] \lambda_1 \dfrac{J_1(\lambda_1)}{J_o(\lambda_1)} = \lambda_2 \dfrac{J_1(\lambda_2)}{J_o(\lambda_2)} \text{ for a clamped edge .} \end{cases}$$

Equations (8) determine the relationship between α and K at the onset of buckling. For each K there will be a sequence $\alpha_n(K)$ of values of α such that (8) is satisfied. We let $\lambda_{1n}(K)$ and $\lambda_{2n}(K)$ be the values of λ_1 and λ_2 which correspond to $\alpha_n(K)$ and K. We also let q_{1n} and W_{1n} be the functions q_1 and W_1 corresponding to $\alpha_n(K)$, K, and we let w_{1n} be the corresponding perturbed vertical deflection. Then

$$(9)\begin{cases} q_{1n} = \frac{a_n}{r}[\lambda_{1n}J_o(\lambda_{2n})J_1(\lambda_{1n}r) - \lambda_{2n}J_o(\lambda_{1n})J_1(\lambda_{2n}r)] , \\ W_{1n} = \frac{a_n}{r}[\lambda_{2n}J_o(\lambda_{2n})J_1(\lambda_{1n}r) - \lambda_{1n}J_o(\lambda_{1n})J_1(\lambda_{2n}r)] , \\ w_{1n} = b_n[J_o(\lambda_{2n})J_o(\lambda_{1n}r) - J_o(\lambda_{1n})J_o(\lambda_{2n}r)] , \end{cases}$$

where a_n and b_n are arbitrary constants.

From (8) and (6) it follows that as $K \to 0$, $\alpha_n(K)$ goes to the n^{th} critical value for the plate without an elastic foundation. Hence, although in (7) we restricted the range in which we looked for critical values of α, we still have a critical value of α which corresponds to each of those when the elastic foundation is missing. Since the elastic foundation is expected to have a stiffening effect on the plate, we believe we have all the critical values of α despite the restriction (7).

From (9c)

$$w_{11} = b_1[J_o(\lambda_{21})J_o(\lambda_{11}r) - J_o(\lambda_{11})J_o(\lambda_{21}r)] .$$

Since $\lambda_{11} \to \infty$ as $K \to \infty$, it is seen that w_{11} can be made to have as many ripples as one pleases by picking K appropriately, i.e. the lowest mode of buckling can be made to have as many ripples as one pleases by picking K appropriately and then picking the edge thrust slightly larger than $\alpha_1(K)$.

Numerical results have been obtained for the clamped edge case. Figures 1 and 2 show $\lambda_{1n}(K)$ and $\alpha_n(K)$. Figures 3 through 9 show the dimensionless vertical deflection for a variety of values of α and K and for n = 1,2,3.

By studying Figs. 3-9 one concludes that if K is held fixed and α is increased, the zeros of w disappear or move near to the edge of the plate while the interior of the plate approaches a flat configuration. In particular, all zeros of the lowest buckled mode disappear as $\alpha \to \infty$ with K fixed. Consequently, this procedure does not lead us to a solution of the type sought, i.e. a lowest buckled mode with a relatively flat interior and ripples near the edge.

The next step is to see what happens if we let $\alpha \to \infty$ and $K \to \infty$ together. Since the critical values of α are all in the range $\alpha^2 > 2K$ and since we want α to go to ∞ in such a way that α is slightly greater than $\alpha_1(K)$ but not too much greater, we consider values of $\alpha^2 > 2K$ or $0 < K/\alpha^2 < 1/2$. Letting $\bar{k} = K^2/\alpha^4$, this range becomes $0 < \bar{k} < 1/4$. It is natural therefore to try letting $K \to \infty$ with $\bar{k}$ a constant in the interval $(0, \frac{1}{4})$. Numerical results were obtained using various values of $\bar{k}$ for the first and second modes of buckling. No significant qualitative differences were obtained except that limiting values were approached more rapidly as $K \to \infty$ if $\bar{k}$ was small. Figures 10 and 11 show the dimensionless radial bending stress and vertical deflection for large values of α and K with $\bar{k} = .01$. The solution shown in Fig. 11 is of the type being sought. It is very nearly flat with many small ripples in the interior and has two relatively large hills or mountains near the edge.

The thesis also contains a formulation and discussion of the boundary layer problem which results if $\alpha \to \infty$ with K fixed or if $\alpha \to \infty$ and $K \to \infty$ with $\bar{k}$ fixed. It is observed that in the former case the boundary layer problem is exactly the same as that treated by Friedrichs and Stoker. It is concluded that, as α increases with K held fixed, the plate behaves like a plate without elastic foundation. The boundary layer problem corresponding to the second case could not be treated by the methods used by Friedrichs and Stoker, and it remains unsolved.

References

1. Wolkowisky, Jay H., Buckling of the Circular Plate Embedded in Elastic Springs. An Application to Geosphysics, Comm. Pure Appl. Math., Vol. 22, 1969, pp. 639-667.

2. Föppl, A., Vorlesungen über Theoretische Mechanik, Vol. 5 (1907). Von Karman, Theodor., Festigkeitprobleme im Maschinenbau, Enz. d. math. Wiss., B.IV, 4 (1910).

3. Friedrichs, K. O., and Stoker, J. J., The Non-Linear Boundary Value Problem of the Buckled Plate, American Journal of Mathematics, Vol. LXIII, No. 4, 1941, pp. 839-888.

4. Keller, H. B., Keller, J. B., and Reiss, E. L., Buckled States of Circular Plates, Quart. of App. Math., 20, 1962, pp. 55-65.

5. Conn, Joan A., Some Buckling and Boundary Layer Problems of a Circular Plate, Ph.D. Thesis, 1964, N.Y.U.

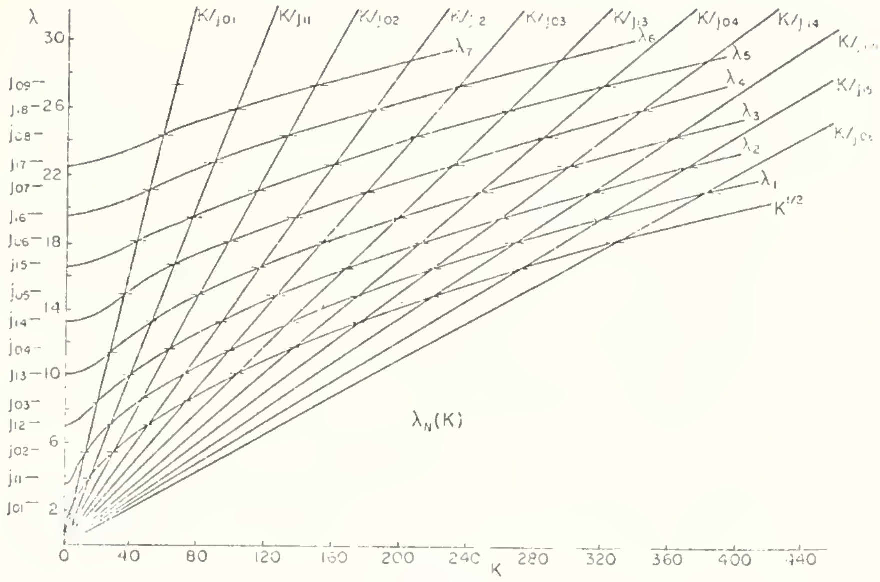

Figure 1

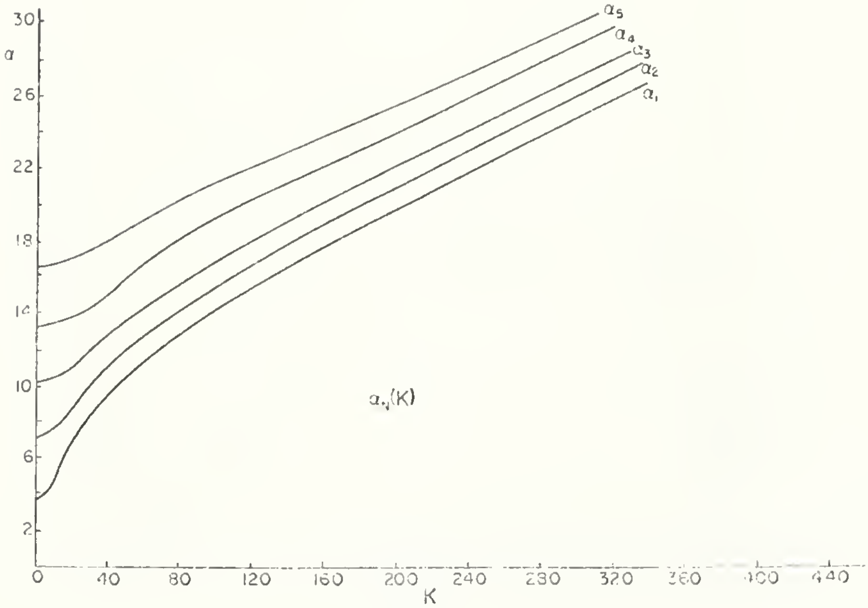

Figure 2

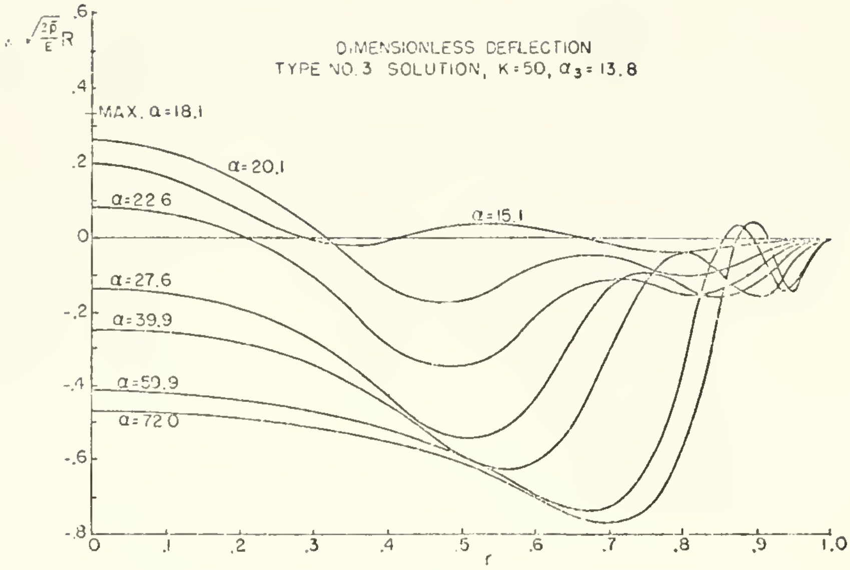

Figure 3

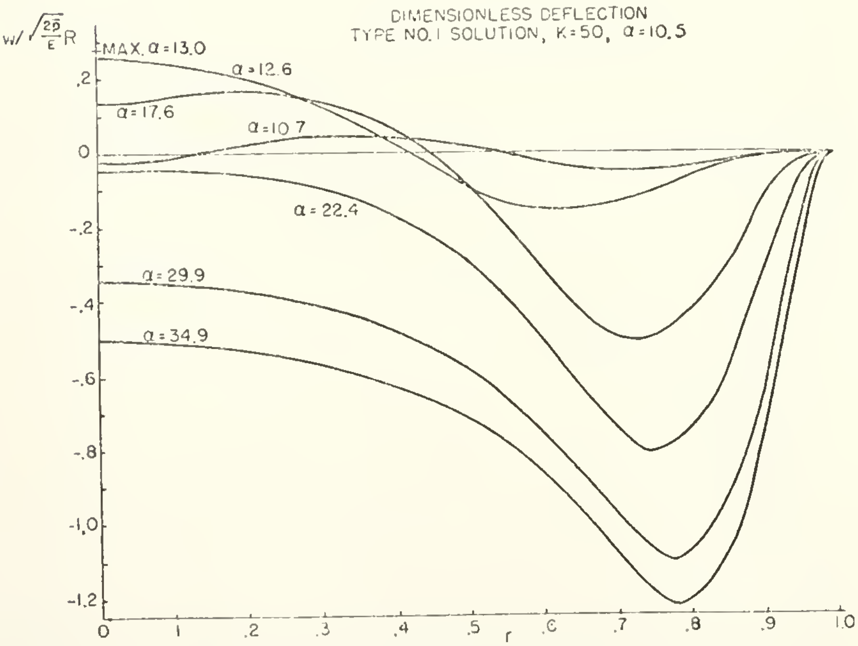

Figure 4

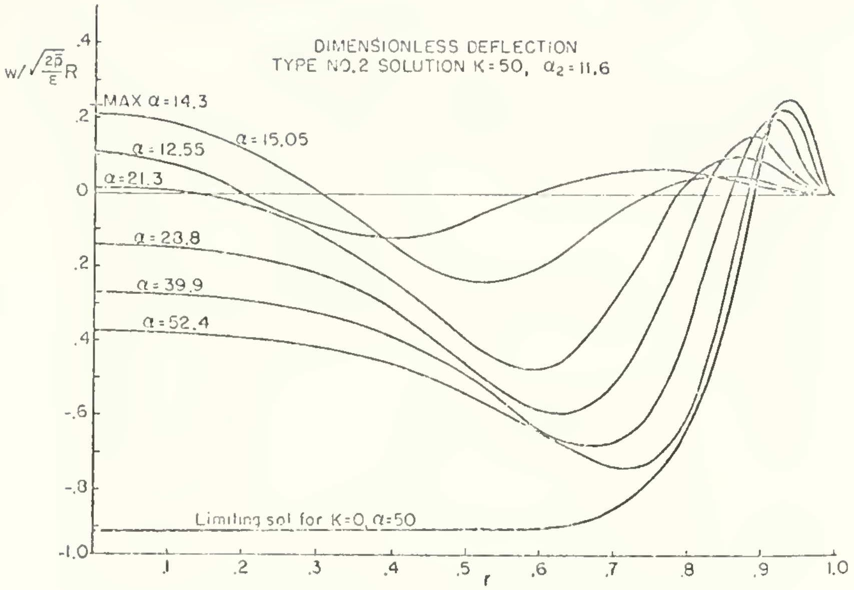

Figure 5

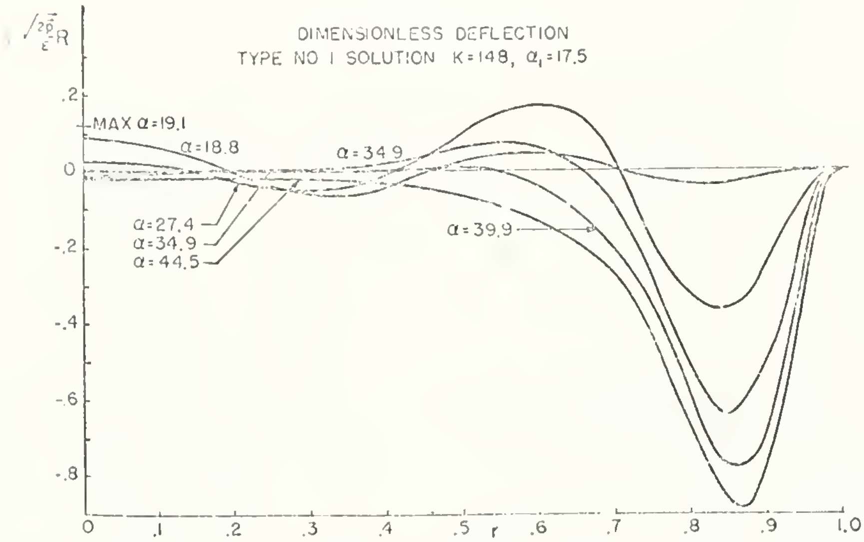

Figure 6

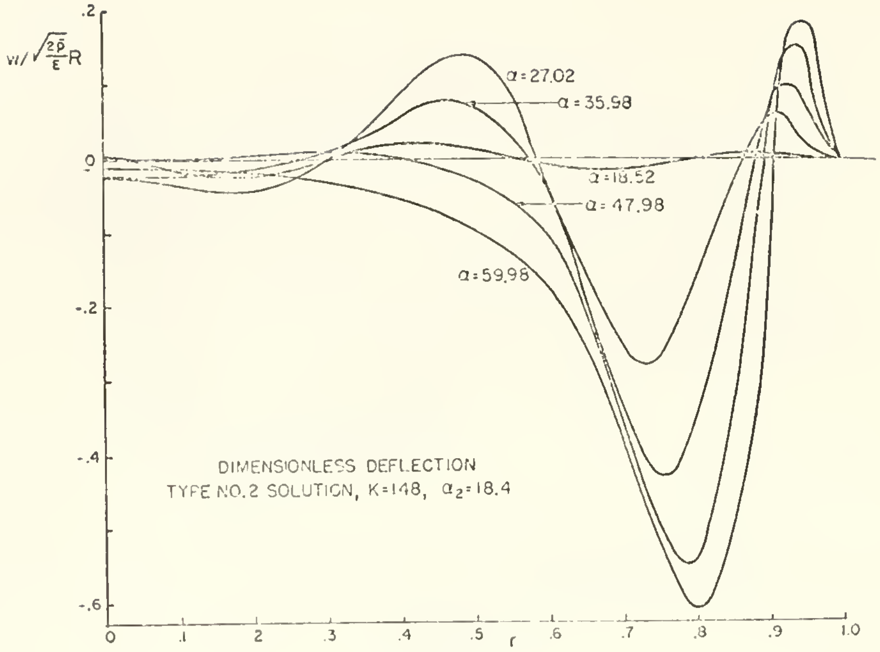

Figure 7

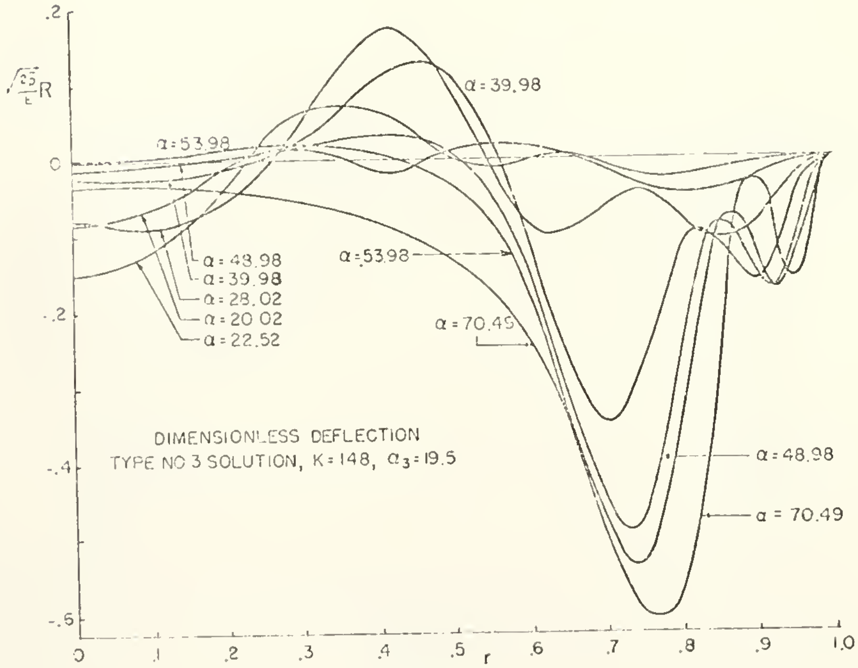

Figure 8

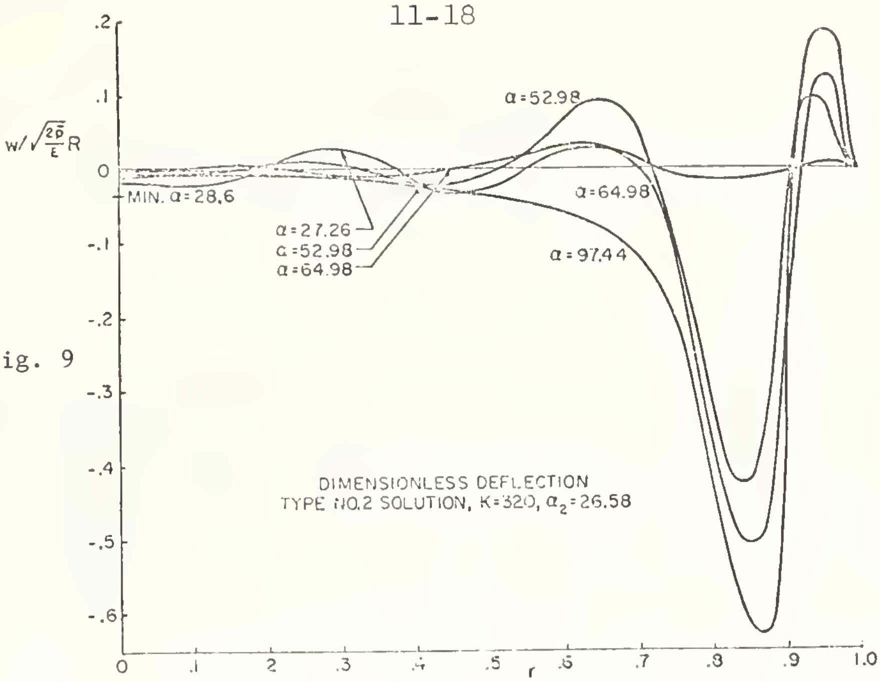

Fig. 9

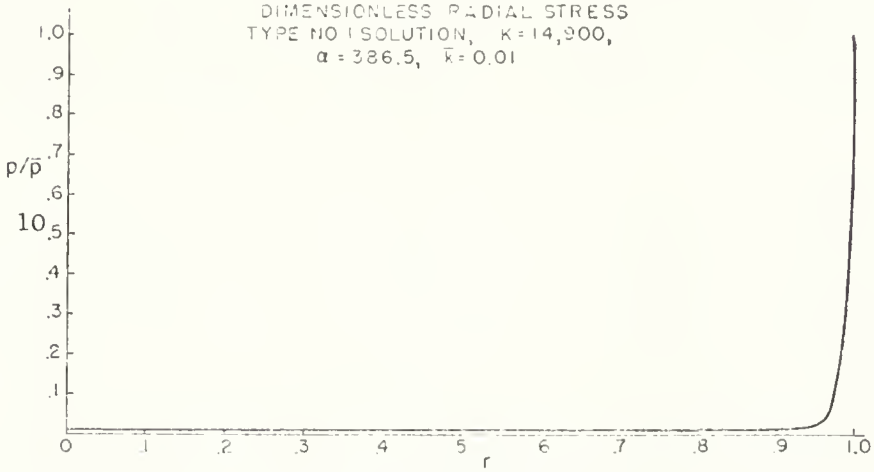

Fig. 10

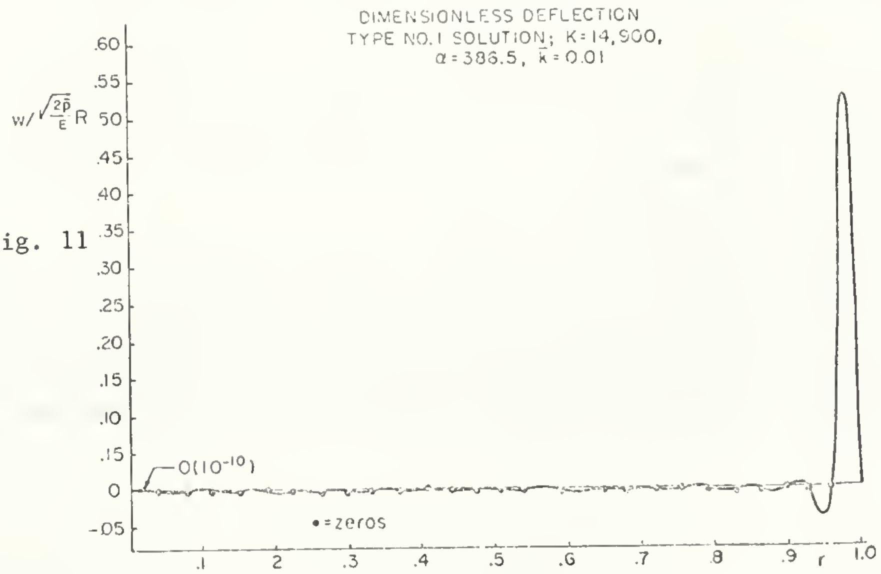

Fig. 11

Lecture 12

Turbulence

J. B. Keller

At low velocities the fluid motion appears as a laminar flow. It may be steady or it may change slowly if the external conditions are changed. At high velocities the flow becomes turbulent. It changes rapidly in time even when the external conditions are constant. For each flow configuration, there is a critical value of the Reynolds number $R = UL/\nu$, (U is a typical velocity, L is a typical length and ν is the kinematic viscosity) such that the flow is turbulent if the Reynolds number exceeds the critical value.

The first problem of the theory of turbulence is to account for the phase transition of a flow from the laminar state to the turbulent state, and to provide a procedure for determining the transition point, i.e. the critical Reynolds number R_c. The linear stability theory offers the answer. The laminar state is stable if $R < R_c$ and unstable if $R > R_c$. Therefore when $R > R_c$, any small fluctuation in the initial velocity of the flow or in the velocity of a boundary of the fluid will grow and convert the laminar flow into a turbulent flow.

A second problem of the theory of turbulence is to determine the behavior of flows with R slightly larger than R_c. These flows can be viewed as laminar flows combined with a few unstable modes

having small amplitudes. Bifurcation theory shows that the number of steady solutions increases with the Reynolds number. Thus, according to the nonlinear stability theory the turbulent flow may be regarded as approximating one solution for a while, then another, etc.

The main problem of turbulent theory is to describe flows with R much larger than R_c. The formulation of a theory of fully developed turbulence is the major goal of turbulence theory, but that goal is nowhere near being achieved.

Fully developed turbulence occurs in various fluid flows in geophysics and astrophysics. The lack of a theory of such flows is a major barrier to progress in all these fields.

<u>Reference</u>

J. B. Keller, Survey of the theory of turbulence, Contemporary Physics, vol. I, International Atomic Energy Agency, Vienna, 1969.

Lecture 13

Progressive Gravity Waves on a Sphere

A. S. Peters

A remarkable example of an axisymmetric disturbance which propagates on the surface of a sphere is the atmospheric pressure wave exhibited during the eruption [1] of the volcano Krakatoa in 1883. In that event, the disturbance originated at a pole point (Krakatoa). It propagated over the surface of the earth almost axisymmetrically. Then the pressure wave was reflected at the antipodal point located in Venezuela. Several passages of the disturbance were recorded.

Progressive waves on a sphere can be studied using a linear model with an incompressible, inviscid, gravitating fluid. In spherical coordinates (r,θ,ϕ) the elevation of the free surface $\psi(\theta,t)$ satisfies the wave equation on a sphere

$$\frac{1}{\sin\theta}\frac{\partial}{\partial\theta}\sin\theta\frac{\partial}{\partial\theta}\psi = \frac{1}{c^2}\frac{\partial^2}{\partial t^2}\psi$$

where $c = \sqrt{gh}/a$, g being the gravitational acceleration, h being the depth of the shallow fluid, and a being the radius of the sphere. The initial conditions to be satisfied are

$$\psi\Big|_{t=0} = 0\ , \qquad \frac{\partial\psi}{\partial t}\Big|_{t=0} = f(\theta)$$

where $f(\theta)$ is the initial disturbance.

Formally the solution can be obtained as an eigenfunction expansion in Legendre polynomials. But the intrinsic nature of wave propagation is not revealed by an infinite series of functions involving the time. However, by applying the Laplace transform with respect to the time the solution can be expressed as the sum of a finite number of terms. In this way a clearer picture of the wave motion can be obtained. For detailed calculations see IMM-NYU Report 271, June 1960, Waves on a sphere, by A. S. Peters.

[1] "Eruption of Krakatoa and Subsequent Phenomena". Report of the Krakatoa Committee of the Royal Society of London (1888).

Lecture 14

Turbulence Spectra and Vortex Formation

Alexandre Joel Chorin

Introduction. It is well known that the energy spectrum $E(k,t)$ of a turbulent flow has, for large wave number k, a universal form, i.e. a form common to a variety of flows whose larger scale features have little in common. This fact is often explained by the universal equilibrium hypothesis, well summarized in Batchelor[1]: The range of wave numbers k which contain most of the energy ("the energy containing eddies") can be regarded as a definite group, with characteristic velocity $u = (\overline{\underline{u}^2})^{1/2}$ and characteristic length $\ell = k_{en}^{-1}$, where $\underline{u}$ is the velocity vector, the bar under $\underline{u}$ denotes a vector, the bar above $(\overline{\underline{u}^2})$ denotes an appropriate average, and k_{en} is a typical wave number in the group. The characteristic time of these eddies is ℓ/u, and the time scale of their decay is $u/|\frac{du}{dt}|$; these times are experimentally found to be comparable, and thus this range of k's has no feature resembling an equilibrium. It may however be assumed, under conditions to be determined, that for large k the spectrum has a characteristic time small in comparison with the scale of the over-all decay, and thus will be associated with degrees of freedom in approximate statistical equilibrium. Let $\hat{\underline{u}}(\underline{k})$ be the Fourier transform of $\underline{u}(\underline{x})$, let $\underline{k}_{eq}$ be a wave number typical of the equilibrium range, with magnitude $k_{eq} = |\underline{k}_{eq}|$, and let $\hat{u}_{eq}$ be a

typical amplitude of $\hat{\underline{u}}(\underline{k})$, $k = |\underline{k}|$ in the equilibrium range, for example $\hat{u}_{eq} = |\hat{\underline{u}}(\underline{k}_{eq})|$. Put

(1) $$K = k_{eq}/k_{en}\ , \quad U = \hat{u}_{eq}/u\ ;$$

The characteristic time of $\hat{u}_{eq}$ is $(k_{eq}\hat{u}_{eq})^{-1} = (KU)^{-1}(k_{en}u)^{-1}$, and the assumption of equilibrium reads

$$(KU)^{-1}(k_{en}u)^{-1} << u/|\frac{du}{dt}|$$

or

(2) $$(KU)^{-1}|\frac{du}{dt}| << k_{en}u^2\ .$$

The quantity u in (2) is the result of an averaging operation; consider this average to be an ensemble average; it is reasonable, and consistent with experience in classical statistical mechanics, to assume that if (2) holds on the average, it holds for most systems in the ensemble, i.e., for most flows there exists a range of k's typified by k_{eq} such that

$$(KU)^{-1}|\frac{du}{dt}| << k_{en}u^2\ , \quad u = \sqrt{\int u^2 dx}\ .$$

This further assumption will be at least partially justified below.

The purpose of the present lecture is to derive a number of conclusions from the assumption (2), used in conjunction with the equations of motion. In particular, the form of the inertial range spectrum, i.e. the equilibrium range spectrum in the limit of very small viscosity, will be derived, and a physical

explanation of the reasons for its existence will be presented. The inertial range spectra will be studied in three cases: The one-dimensional Burgers equation, and the Navier-Stokes equations in two as well as three space dimensions.

Equilibrium and inertial ranges of the Burgers equation. Consider an ensemble of solutions of the Burgers equation

$$(3) \qquad u_t + uu_x - \nu u_{xx} = 0 , \quad -\infty \leq x \leq +\infty , \quad t \geq 0 ,$$

with $u(x,0)$ in C_0^{∞}. ν is a small viscosity. The behavior of the Fourier transform $\hat{u}(k)$ of $u(x)$, in the limit as $\nu \to 0$ and $k \to \infty$ (in that order) can be readily determined. As ν tends to zero, the solutions of (3) tend to the solutions of the inviscid equation

$$(4) \qquad u_t + uu_x = 0$$

in L_1; $\hat{u}(k)$ thus tends to the transform of the solution of (4) pointwise, and uniformly on every bounded segment of the k-axis. Hence as $\nu \to 0$ the behavior of $\hat{u}$ is determined by the behavior of the solution of (4).

The solutions of (4) exhibit collections of shocks separated by intervals of smooth u; their transforms are thus of the form

$$(5) \qquad o(k^{-1}) + \sum_j C_j(t) e^{ia_j(t)} k^{-1} ;$$

the C_j, a_j are functions of t and depend on the initial data;

they are in this sense random. The form (5) is universal, i.e. independent of the particular initial data. For large k the energy spectrum E(k) is thus of the form

(6) $$E(k) = O(k^{-2}) ,$$

which is a well known result.

Let us now rederive (5) and (6) using the assumption (2). Take the Fourier transform of (3). We already know that if we are interested in the inertial range, i.e. in the equilibrium range in the limit of decreasing viscosity, we may set $\nu = 0$ in the resulting equation, obtaining

(7) $$\hat{u}_t + ik \int \hat{u}(k')\hat{u}(k-k')dk' = 0 ,$$

where $\hat{u}(k)$ is the complex conjugate of $\hat{u}(-k)$.

Let k be in the inertial range, i.e. of order k_{eq}, and make the change of variable

(8) $$\hat{u}^* = \hat{u}/U , \quad k^* = k/K ,$$

U, K defined in the introduction. Substitution into (7) yields

(9) $$(KU)^{-1}\hat{u}^*_t = ik^* \int \hat{u}^*(k')\hat{u}^*(k-k')dk' .$$

The right-hand side is of order $k_{en}u^2$, the left-hand side of order $(KU)^{-1} \frac{du}{dt}$; by (2), for most flows

(10) $$ik \int \hat{u}^*(k')\hat{u}^*(k-k')dk' = 0 .$$

The energy-containing eddies have been relegated to the neighborhood of the origin, and the integral must in general be interpreted in a principal part sense. In the unstarred variables (10) reads

$$\lim_{k\to\infty} ik \int \hat{u}(k-k')\hat{u}(k')dk' = 0 . \tag{11}$$

Equation (10) is readily solved: $\hat{u}^*$ is the transform of u^*, which satisfies

$$(u^{*2})_x = 0$$

$$u^{*2} = C^{*2} , \quad C^* = \text{constant},$$

or

$$u^* = \pm C^*$$

where different signs may be assumed on distinct parts of the x-axis. Only a solution with a single change of sign can satisfy the entropy condition; its Fourier transform is of the form

$$\hat{u}^* = Ce^{iak}k^{-1} , \tag{12}$$

where C, a may depend on t. We now observe that any superposition of solutions of the form (12) satisfies (11); indeed let

$$\hat{u} \sim C_1 e^{ia_1 k} k^{-1} + C_2 e^{ia_2 k} \quad \text{as} \quad k \to \infty ,$$

Then

$$\int \hat{u}(k')\hat{u}(k-k')dk' = (C_1 e^{ia_1 k} + C_2 e^{ia_2 k}) \int \frac{1}{k'} \frac{1}{k-k'}\, dk'$$

$$+ 2C_1 C_2 e^{ia_2 k} \int e^{i(a_1-a_2)k'} \frac{1}{k'} \frac{1}{k-k'}\, dk' .$$

Perform the change of variables $k' = Kk^{*'}$, $k = Kk^*$; we obtain

$$\int \hat{u}(k')\hat{u}(k-k')dk' = \frac{1}{K}\Big[(C_1 e^{ia_1 k} + C_2 e^{ia_2 k}) \int \frac{1}{k^{*'}} \frac{1}{k^*-k^{*'}}\, dk^{*'}$$

$$+ 2C_1 C_2 e^{ia_2 k} \int e^{i(a_1-a_2)Kk^{*'}} \frac{1}{k^{*'}} \frac{1}{k^*-k^{*'}}\, dk^{*'}\Big]$$

as $k \to \infty$, $K \to \infty$, the last integral is negligible compared to the first, and (11) is satisfied. Thus the solution of (11) is

$$o(k^{-1}) + \sum_j C_j(t) e^{ia_j(t)} k^{-1} \quad \text{as} \quad k \to \infty ,$$

in agreement with (5). By comparison of two arguments which lead to (5) we see that the equilibrium hypothesis holds for all flows; we have furthermore an interpretation of the equilibrium hypothesis: As the flow evolves and the values of u on each side of a shock vary, the shock adjusts to the change instantaneously. It is readily seen that (5) represents an equilibrium in wave number space.

<u>Two dimensional Navier-Stokes equations</u>. It has been shown in some generality (see Ebin and Marsden[2] and the references therein) that as the viscosity ν tends to zero in the absence of

boundaries the solutions of the Navier-Stokes equations with smooth initial data tend to the corresponding solutions of the Euler equations strongly, as well as in L_1. The respective Fourier transforms then tend to each other uniformly on every bounded region in $\underline{k}$-space and the limit $\nu \to 0$ may be studied by setting $\nu = 0$. One then performs the scaling analogous to (1)

$$(13) \qquad \underline{k}^* = \underline{k}/K\ , \quad \underline{\hat{u}}^* = \underline{\hat{u}}/U\ ,$$

appeals to the equilibrium hypothesis (2), and obtains the steady inviscid equation

$$(14) \qquad ik_\delta P_{\alpha\gamma} Q_{\delta\gamma} = 0$$

where

$$Q_{\delta\gamma} = \int \hat{u}^*_\delta(\underline{k}-\underline{k}')u^*_\gamma(\underline{k}')dk'\ ,$$

$$P_{\alpha\gamma} = \delta_{\alpha\gamma} - \frac{k_\alpha k_\gamma}{k^2}\ , \quad (\delta_{\alpha\gamma} \text{ the Kronecker delta}),$$

and the summation convention is in use. $\underline{\hat{u}}^*(\underline{k})$ is the complex conjugate of $\underline{\hat{u}}^*(-\underline{k})$, and the pressure has been eliminated through the use of the equation of continuity

$$(15) \qquad k_\alpha \hat{u}^*_\alpha = 0\ ,$$

giving rise, in the well known manner, to the projection $P_{\alpha\gamma}$. The integrals $Q_{\delta\gamma}$ must of course be interpreted in a principal-part sense. As before, (14) can be solved by application of the Fourier

transform: it is the transform of the steady Euler equations, which admit an infinite number of solutions, in particular circular vortices whose stream function has a Fourier transform of the form

(16) $\hat{u}_1^* = -ik_2/k^{2\beta}$, $\hat{u}_2^* = ik_1/k^{2\beta}$, $k = \sqrt{k_1^2 + k_2^2}$, β constant;

given β, the energy spectrum is

$$E(k) = O(k^{-\sigma}) , \quad \sigma = 4\beta - 3 .$$

These vortices play the role played by the shocks in the one dimensional problem. A lower bound for σ can be readily found: The H_1 norm of $\underline{u}$ is constant (by conservation of vorticity), thus

$$\int_1^\infty k^2 E(k)dk$$

is uniformly bounded, and $\sigma > 3$. The following conjecture appears natural: in any particular flow vortices will appear with spectra of the form

$$E(k) = O(k^{-3-\varepsilon}) , \quad \varepsilon = \varepsilon(t) > 0 .$$

When $E(k)$ decays as fast as k^{-3} or faster, finite-difference computations have a chance of yielding reasonable results; such computations have been carried out, e.g. by Zabuski and Deem[3], and lend support to the conjecture. In an ensemble of flows, the behavior of $E(k)$ for large k will be determined by the vortices whose transforms decay most slowly, and should then be

indistinguishable from $O(k^{-3})$, as postulated by Leith[4] and Kraichnan[5].

The three dimensional Navier-Stokes equations. In three space dimensions, the existence of solutions of the Navier-Stokes and Euler equations for all time, and a fortiori, the convergence of the former to the latter, have not been established. We have to assume that the solutions exist and that such convergence takes place. These assumptions, together with the equilibrium assumption (2), lead to the three-dimensional analogue of (14).

It can be shown that if grad $\underline{u}^{*2} \neq 0$, equations (14) in three dimensions admit only two dimensional solutions. It should be remembered that $\hat{\underline{u}}^*$ characterizes the behavior of $\hat{\underline{u}}$ for large k. The fact that $\hat{\underline{u}}^*$ is two-dimensional does not imply that $\hat{\underline{u}}$ (and $\underline{u}$) are two-dimensional. The $\hat{\underline{u}}^*$ are vortices; their "two-dimensionality" means that their radius of curvature is of order k_{en}^{-1} and that the flow parallel to their axis is relatively smooth. Vortex-stretching is thus allowed.

We consider now solutions of the form (16). The non-increasing character of the energy implies that $\sigma > 1$. If it were known that the integral

$$\int_1^\infty k^\alpha E(k)dk$$

remains uniformly bounded for $\alpha < \alpha_o$ while it may become unbounded for $\alpha \geq \alpha_o$, then we could conclude that $\sigma = \alpha_o + 1$. Such results

are unfortunately unavailable. A more precise determination of σ requires a heuristic argument, in the absence of a rigorous one. Consider the question, which vortices can arise from smooth initial data. Clearly only vortices which are in some sense stable can develop. We are in presence of an unusual stability problem. $\underline{\hat{u}}^*$ characterizes the behavior of $\underline{\hat{u}}$ for large k only. We have thus to look for vortices $\underline{\hat{u}}^*$ with the following property: When they are imbedded in a flow $\underline{\hat{u}}$, and when that flow is perturbed, the behavior of the transforms $\underline{\hat{u}}$ for large k, i.e. the form of $\underline{\hat{u}}^*$, is unaffected. The shock solutions of (10) have such a property: if a flow with shocks in one dimension is perturbed, it remains a flow with shocks, with transform of the form (5). Perturbations containing a bounded set of Fourier components are of no significance when applied to equation (14), since a scaling will relegate them to a neighborhood of $\underline{k}^* = 0$ and will leave (14) unaffected. To formulate a reasonable problem, appeal must be made to physical intuition. A flow encountered in nature will have a definite scale, based either on the scale of the driving mechanism or in the size of the container. $\underline{\hat{u}}(\underline{k})$ will then have for support not the whole $\underline{k}$-space but only a lattice of wave numbers which can be excited. Let h be a length typical of the lattice. The integrals in (14) become sums over the lattice points; let us write the resulting equation in the symbolic form

$$F_h[\underline{\hat{u}}^*] = 0 \, . \tag{17}$$

Formally, as $h \to 0$, (17) converges to (14). In analogy with (16), we seek solutions of (17) of the form

$$\hat{u}^*_{h,1} = -ik_2/H(\underline{k},h) \ , \quad \hat{u}^*_{h,2} = ik_1/H(\underline{k},h) \ ,$$

$$\underline{k} = (k_1,k_2) \ , \quad k = \sqrt{k_1^2 + k_2^2} \ ,$$

where $\underline{\hat{u}}^*_h$ is defined only at the nodes of the lattice, and H is a function of $\underline{k}$ and h. To each h will correspond a spectrum $E(k,h)$; if H is a homogeneous function of $\underline{k}$ the spectrum will be of the form

$$E(k) = O(k^{-\sigma_h}) \ ,$$

where σ_h depends on h. The question is: as $h \to 0$, does σ_h tend to a definite value of σ, independent of the lattice? The answer appears to be affirmative, with $\sigma_h \to \sigma$, $\sigma = 1.7 \pm 0.1$, a result compatible with the Kolmogorov law (see Chorin[6]).

<u>Conclusion</u>. We have made plausible a picture of turbulent flow as a disorderly process in which small scales are dominated by a tangle of vortices, whose presence explains the existence of an inertial range and the form of the corresponding spectrum.

References

1. G. K. Batchelor, The Theory of Homogeneous Turbulence, Cambridge University Press, (1960).

2. D. G, Ebin and J. Marsden, <u>Annals of Math</u>., <u>92</u>. 102 (1970).

3. N. J. Zabuski and G. Deem, to appear in <u>J. Fluid Mech</u>.

4. C. E. Leith, <u>Physics of Fluids</u>, <u>11</u>, 671, (1968).

5. R. H. Kraichnan, <u>Physics of Fluids</u>, <u>10</u>, 1417, (1967).

6. A. J. Chorin, Turbulence Spectra, Equilibrium and Vortex Formation, to appear.

Lecture 15

Dynamo Theory

Stephen Childress

Introduction

In 1919 Larmor put forward the idea that magnetic fields found in nature may in some cases be maintained against dissipative losses by magnetohydrodynamic induction within an isolated homogeneous fluid region, in much the same way that a magnetic field is generated in a laboratory dynamo. In particular, it is believed that the earth's magnetic field is generated and maintained in this way.

The dynamo models of geomagnetism may be distinguished mathematically from other problems of magnetohydrodynamics by the fact that the equations and boundary conditions permit "trivial" solutions with zero magnetic field. The interesting problems therefore have an eigenvalue or bifurcation character. Also, in the absence of a detailed description of the velocity field within the earth's fluid core, the theory is in some ways concerned with the inverse problem of determining the structure of the dynamo from surface measurements of the resulting field.

Magnetic surveys over the last 150 years indicate that the surface field is almost completely of internal origin, and that it may be regarded as consisting of two parts, namely a main dipole field and an irregular non-dipole field. From studies of

magnetization in sea floor sediments and volcanic rocks it is known that the main field has reversed in polarity about 200 times over the last 80 million years. Periods of uniform polarity may be divided into "events" lasting 10^4-10^5 years, and "epochs" lasting 10^6 years or so; there appears to be no preferred polarity. The time scale of events is roughly equal to that of the free decay of the magnetic field that would occur if the dynamo process was not occurring. The non-dipole field undergoes "secular variations" with time scales from 10^2-10^4 years. A portion of this can be interpreted as a westward drift of an otherwise "rigid" field, at a rate of about .2° long./year. The non-dipole field has in some studies been represented by 8 or 10 regional sources within the core, convected relative to the mantle by a motion consistent with the observed westward drift velocity. It has also been suggested that the secular variation includes hydrodynamic waves moving relative to the mantle.

The kinematic problem

Most work in dynamo theory has been concerned with the kinematic version of the problem, wherein the velocity field $u(x,t)$ is prescribed throughout the core region D and the dynamical equations are discarded. The rationale here is that, if u generates a non-decaying magnetic field $h(x,t)$, then u, h is consistent with <u>any</u> dynamical model for <u>some</u> distribution of externally imposed forces; of course it could well be that the required forces are not at all realistic, so the usefulness of the

method depends on a shrewd a priori choice of the class of u to be considered.

The problem is defined as follows: For the given solenoidal $u(x,t)$, determine real functions $h(x,t)$ and $E(x,t)$ (electric field) satisfying

$$\nabla \times h = \sigma E + \sigma\mu u \times h$$

$$\nabla \times E = -\mu \frac{\partial h}{\partial t} , \quad \nabla \cdot h = 0$$

in D, (σ, μ = electrical conductivity and magnetic permeability of the core = constants),

$$\nabla \cdot h = \nabla \times h = \nabla \cdot E = 0$$

$$\nabla \times E = -\mu \frac{\partial h}{\partial t} , \quad r^2 |E| \text{ and } r^3 |h| \text{ bounded}$$

in the region D' exterior to D, with h and the tangential components of E continuous on ∂D, such that the total magnetic energy exceeds some $\delta > 0$ for arbitrarily large t. Presumably u represents a source-free motion of an incompressible fluid with zero flux through the boundary.

If u, h, and E are regarded as independent of time, the equation for h in D may be written

$$\nabla^2 h + \sigma\mu \, \nabla \times (u \times h) = 0 \, .$$

In this case the kinematic dynamo problem reduces to an eigenvalue

problem, with a typical speed of the dynamo appearing as the eigen-parameter.

It is known that in a sphere of radius L, u is a dynamo only if $R \equiv u_m \sigma \mu L \geq \pi$, where u_m is the maximum of $|u|$ over D and time. Apart from the flexibility obtained from parameters implicit in u, this inequality limits asymptotic solutions of the eigenvalue problem to the case of large magnetic Reynolds number R. Cowling (1934) and others have shown that u cannot be a dynamo if the associated h is axisymmetric. Also it is known that certain simple choices of u, for example a purely "toroidal" motion of the form

$$u = \nabla \times T(x)x$$

cannot maintain any steady field (Bullard and Gellman (1954). See also Roberts, P. H. (1967)). In the steady case Herzenberg (1958), and in the non-steady case Backus (1958) have provided examples of kinematic dynamos in a spherical core. Backus' model consists of three time intervals of rigorous motion separated by sufficiently long periods of free decay of h. The initial field is decomposed into a principal part f and an arbitrary, bounded residual r. The velocity fields are then chosen so that, after one full cycle, the solution of the dynamo equations has a similar decomposition f+r' where r' is no larger than r. Herzenberg's model consists of a finite number of small, rigid rotating spheres imbedded in an otherwise stationary core. For small ratio of sphere to core radius the eigenvalue problem can be solved. In either case the analysis is

based upon the different rates of decay (with respect to space or time) of the functions used to represent h.

Another approach utilizes a complete analysis in an infinite core of induction by space-periodic motions (Childress 1970, Roberts, G. 1970). The periodic dynamos obtained from such an analysis can be easily imbedded in a sphere, and the resulting steady-state dynamo problem can be solved by perturbing a comparison eigenvalue problem. An example of a spherical dynamo of this kind is

$$u = \varepsilon \nabla \times \omega(|x|) v(x/\varepsilon)$$

where ω is a scalar cut-off and $v(x) = (\sin x_2 + \cos x_3, \sin x_3 + \cos x_2, \sin x_1 + \cos x_2)$. The parameter ε is the ratio of the scale of the periodic field to the radius of the core. If ε is sufficiently small, such a motion interacts with a large scale h to produce, upon averaging over the small scale, a mean current roughly parallel to h.

Almost symmetric dynamos

A formal asymptotic procedure for R >> 1 has been devised by Braginskii (1964a,b). In these models deviations of u, h from axial symmetry are of order $R^{-1/2}$, a typical choice of u being of the form (now using dimensionless variables)

$$u = W(z,r) i_\phi + R^{-1/2} u'(z,r,\phi) + R^{-1} \nabla \times [\psi(z,r) i_\phi] \ .$$

Here (z,r,ϕ) denote cylindrical polar coordinates and u' has zero

ϕ-mean. Braginskii shows that the ϕ-mean of the dynamo equations in D reduce, to leading order in R, to the following system:

$$\frac{\partial A_e}{\partial t} + r^{-1}u_e \cdot \nabla(rA_e) - \nabla^2 A_e = \Gamma B ,$$

$$\frac{\partial B}{\partial t} + ru_e \cdot \nabla(r^{-1}B) - \nabla^2 B = [\nabla(r^{-1}W) \times \nabla(rA_e)]_\phi .$$

Here the ϕ-mean of h is equal to $h_o = B(z,r)i_\phi + R^{-1}\nabla \times [A(z,r)i_\phi]$, $u_e = \nabla \times [\psi_e(z,r)i_\phi]$, and Γ, $\frac{\psi_e - \psi}{W}$, and $\frac{A_e - A}{B}$ are each ϕ-means of a function quadratic in u'.

Braginskii's equations are remarkable in that, if the term involving Γ is deleted, the resulting system is identical to the equations for an axially-symmetric dynamo involving the "effective" quantities ψ_e and A_e. The surviving term involving the toroidal velocity field W acts as a source of the azimuthal component B of h_o. (This "W-effect", which can be interpreted as a drawing out of the lines of force of the meridional component $\nabla \times (A_e i_\phi)$, is likely to be an important one in a rotating spherical core, since W will then contain the geostrophic component of velocity.) The new "Γ-effect" provides a corresponding source of meridional field, thus completing the cycle. Numerical solution of the eigenvalue problem for steady dynamos has been carried out for several choices of W and ψ_e. In certain cases the ratio of the non-axisymmetric to axisymmetric part of the exterior meridional field is found to be of order $R^{-1/2}$, in which case $R^{-1/2}$ can be interpreted as the order of magnitude of the tilt of the geomagnetic dipole relative to the earth's axis of rotation.

References

Backus, G., Ann. Phys. 4, (1958), 372.

Braginskii, S. I., Soviet Physics JETP, 20 (1965), (a) 726 and (b) 1462.

Bullard, E. C. and Gellman, H., Philos. Trans. Roy. Soc., London, Ser. A, 247, (1954), 213.

Childress, S., Jour. Math. Phys., 11, (1970), 3063.

Cowling, T. G., Month. Not. Roy. Astron. Soc., 94, (1934), 39.

Herzenberg, A., Philos. Trans. Roy. Soc., London, Ser. A, 250, (1958), 543.

Roberts, G., Philos. Trans. Roy. Soc., London, Ser. A, 266, (1970), 535.

Roberts, P. H., An Introduction to Magnetohydrodynamics, American Elsevier Publishing Co. Inc., New York, (1967), Chapter 3.

Lecture 16

Linear and Nonlinear Magneto-Elastic Wave Motion

J. Bazer

The following is an abstract of a talk on magneto-elastic wave motion based on the papers [1]-[3] listed below in the reference section.

An account is given of some work dealing with wave motion, linear and nonlinear, in an electrically neutral, infinitely conducting, elastic medium subject to magnetic as well as elastic stresses. The analysis is based on the fact that the governing equations of such a physical system share with the equations of conventional elasticity, gasdynamics and magnetogasdynamics the property of being representable as a first-order symmetric-hyperbolic system of conservation laws. This property implies, in advance, that the linearized magneto-elastic equations possess a geometrical theory analogous to geometrical optics and that the nonlinear equations possess a theory of shocks and simple waves similar to that of gasdynamics and magnetogasdynamics.

A complete solution of the following basic problem in the geometrical theory is presented: Let $\mathcal{S}_0$ denote a surface bounding a small disturbance in an otherwise undisturbed medium. Suppose the discontinuity across $\mathcal{S}_0$ of the magnetic, velocity and strain fields are specified. The problem is to determine the

wave fronts which evolve from $\mathcal{S}_0$ — there will be six of them in general — and to ascertain the orientations of the field quantities and the strengths of the discontinuities carried on these fronts. Insofar as the propagating fronts are concerned, the presence of the magnetic field is reflected in the fact that their propagation speeds are direction-dependent. Specifically, these speeds depend upon the angle between the direction of propagation and that of the local magnetic field. As to the orientation of the field quantities on the fronts, these are found to be unambiguously determined by the direction of propagation and the local magnetic field, provided these are not parallel. Moreover, in only one of the three waves that may propagate in a given direction, the so-called intermediate wave, are the velocity and displacement vectors purely transverse, that is, parallel to the wave front. In the remaining 'slow' and 'fast' fronts both longitudinal and transverse components are present. These results are completely analogous to those of geometrical hydromagnetics and in sharp contrast to those of conventional geometrical elasticity both of which incidentally are limiting cases of the present theory.

As in gas dynamics the nonlinear theory is restricted to one-dimensional wave motion. This means that all physical quantities are required to depend on only one space variable and time. No restriction is placed on the orientations of the magnetic, velocity and strain fields. In the simplest case considered, the stress-strain relation is assumed to be that given as Hooke's law. The nonlinearity is then due to the interaction

of the magnetic field with itself and with the velocity and strain fields. Despite the complexity of the equations, it is possible to obtain almost completely explicit simple wave solutions. As in magnetogasdynamics it turns out there are slow, fast and Alfvén-like simple waves which together with the corresponding magneto-elastic shocks enable one to solve one-dimensional propagation problems with sufficiently simple initial and boundary conditions. One interesting result of the nonlinear theory is that magneto-elastic simple wave motion affords a mechanism for generating intense magnetic fields.

References

[1] Geometrical Magnetoelasticity - J. Bazer, Geophys. J. R. astr. Soc. (1971) 25, 207-237.

[2] Simple Wave Motion in Magnetoelasticity - F. Karal and J. Bazer, Geophys. J. R. astro. Soc. (1971) 25, 127-156.

[3] Magnetoelastic Shocks - W. B. Ericson and J. Bazer, to appear.

Lecture 17

Viscosity of the Earth's Crust

Gerald Grube

Introduction

Geophysicists have observed that for forces of long duration the earth behaves like a fluid with a very high viscosity. This phenomena is not surprising when we notice that ice, pitch, and glass have the same property. Viscosities for many substances commonly thought of as solids may be found in various handbooks.

During the last ice age, vast ice sheets covered large portions of the earth for an extended period of time. In 1928, Nansen published his detailed study of the Scandanavian ice sheets and the resulting deformation of the earth's surface. Haskell derived a formal solution for a viscous fluid in 1935 and, using Nansen's data, determined a kinematic viscosity for the earth's crust of 3×10^{21} cm^2/sec.

Until recently, only a few other attempts were made to calculate a viscosity for the earth. Haskell's results have been used by many geophysicists in their theories of the earth's interior. Particularly, the value of viscosity is critical to understanding the continental drift. In the following, Haskell's work will be summarized and a discussion of how one might try to improve upon his results will be presented.

Formulation

We will consider a semi-infinite, incompressible highly viscous fluid with the z = 0 plane as the equilibrium surface. Cylindrical coordinates will be used and only circularly symmetrical disturbances will be considered. Because the viscosity ν is large, we may neglect inertial and nonlinear terms; the equations of motion are:

$$\nu\left[\frac{1}{r}\frac{\partial}{\partial r}\left(r\frac{\partial}{\partial r}V_r\right) - \frac{1}{r^2}V_r + \frac{\partial^2}{\partial z^2}V_r\right] = \frac{\partial}{\partial r}P\ ,$$

$$(1) \qquad \nu\left[\frac{1}{r}\frac{\partial}{\partial r}\left(r\frac{\partial}{\partial r}V_z\right) + \frac{\partial^2}{\partial z^2}V_z\right] = \frac{\partial}{\partial z}P\ ,$$

$$\frac{1}{r}\frac{\partial}{\partial r}(rV_r) + V_z = 0$$

where V_r and V_z are radial and horizontal velocity, respectively, $P = \rho^{-1}p - gz$ with p the pressure, ρ density, and g the gravitational force. The positive z axis is downward. Assuming small surface deflections $\xi(r,t)$, we may linearize the usual boundary conditions of zero stress at the surface:

$$2\nu\frac{\partial}{\partial z}V_z - P - g\xi = 0\ , \qquad z = 0\ ,$$

$$(2) \qquad \frac{\partial}{\partial r}V_z + \frac{\partial}{\partial z}V_r = 0\ , \qquad z = 0\ ,$$

$$\frac{\partial}{\partial t}\xi = V_z\ , \qquad z = 0\ .$$

We now apply the Hankel transform:

$$\tilde{f}_n(\lambda, z, t) = \int_0^\infty rJ_n(\lambda r)f(r, z, t)dr \ .$$

With n = 1 for V_r and n = 0 for the other variables, one may transform (1) and (2) and solve the resulting problem directly. In particular one obtains:

$$\text{(3)} \quad \begin{aligned} V_z(r, z, t) &= \int_0^\infty K(\lambda)(1 + \lambda z)e^{-\lambda z - gt/2\nu\lambda} \ J_o(\lambda r)d\lambda \ , \\ \xi(r, t) &= \frac{2\nu}{g} \int_0^\infty \lambda K(\lambda)e^{-gt/2\nu\lambda} \ J_o(\lambda r)d\lambda \end{aligned}$$

where $K(\lambda)$ is as yet undetermined. Notice that K is known if either $\xi(r,0)$ or $V_z(r,0,0)$ is given.

<u>Geological Data</u>

Nansen has determined past surface elevations and rate of uplift at two sites, Oslo and Ångermanland, about 500 km. apart; the latter having been near the center of the ice sheet. We assume a reasonable surface form:

$$\text{(4)} \qquad \xi(r, 0) = \beta e^{-b^2r^2}(1 - b^2r^2) \ .$$

Substituting (4) into (3), one may solve for ν:

$$\text{(5)} \qquad \nu = -.22 \frac{g\beta}{bV_z(0, 0, 0)} \ .$$

The parameters b and β are determined so that (4) fits the surface

elevations given by Nansen, then the rate of uplift determines ν. Using data from various times in the past, Haskell obtains $\nu = 2.9 \times 10^{21}$ cm^2/sec as an average value.

Acceleration Terms

One may justify not including the acceleration terms in (1) by means of a singular perturbation (a new unstretched time is defined by multiplying the old time by a large parameter). Of course, now one is restricted in terms of initial conditions; either $\xi(r,0)$ or $V_z(r,0,0)$ completely determines the solution.

However, one may include the time derivative terms in (1) and still obtain a closed form for the solution. We proceed as before but now the Laplace as well as the Hankel transform must be applied:

$$\tilde{f}_n(\lambda, z, s) = \int_0^\infty rJ_n(\lambda r) \int_0^\infty e^{-st} f(r,z,t)\,dt\,dr \, .$$

We use Haskell's solutions (3) to provide initial values for V_z. Then, the solution becomes:

$$V_z(0,0,t) = \frac{1}{2\pi i} \int_0^\infty \lambda d\lambda \int_{-i\infty}^{i\infty} e^{st}\, \tilde{V}_{z,o}(\lambda, 0, s)\,ds$$

$$\tilde{V}_{z,o}(\lambda, 0, s) = \left(\frac{\ell}{g}\right)^{1/2} K(\lambda)\left(\frac{1}{\lambda s} - \frac{\ell}{\Delta s}\right) \tag{6}$$

$$\Delta = \lambda + (2\lambda^2 + s)^2 - 4\lambda^3(\lambda^2 + s)^{1/2} \, .$$

The function Δ is common in viscous problems and has been studied by Lamb (p. 627) and Miles. By bending the contour of integration and using asymptotic expressions for the zeroes of Δ, one can simplify (6) into a form more suitable for numerical evaluation on a computer.

From Nansen's data, additional values of viscosity may be computed by studying the evolution of the solution. The viscosities obtained in this manner have an average value of 3.1×10^{21} cm^2/sec.

Lake Bonnevile

The difficulty in computing a viscosity from the recovery of the earth from the Scandinavian ice sheet was due to meager data. The flooding of the Lake Bonneville basin in Utah, however, was an event for which we have some idea not only of the deflections involved but also the history of the surface loading. If one adds the normal stress due to the loading in (2a), then a solution for the free surface similar to (6) may be derived. Viscosities may now be computed numerically by using the observed deflection of the earth's surface near the lake center (see Grube). In this manner, an average viscosity of 3.6×10^{20} cm^2/sec was computed.

Conclusions

Although Haskell's approach is self-consistent, it is a singular perturbation technique and all the initial conditions

cannot be used. When the acceleration terms are included, we still may derive a closed form for the solution, which may easily be evaluated on a computer. Thus, if one possesses enough data, solutions to the linearized Navier-Stokes equations may be derived and evaluated numerically.

References

Crittenden, J. Geophys. Res., 68 (1963), pp. 5517-5530.

Grube, Doctoral Dissertation, New York University, 1972.

Haskell, Physics, 6 (1935), pp. 265-269.

Lamb, Hydrodynamics, Dover, New York, 1945.

Miles, J. Fluid Mech., 34 (1968), pp. 359-370.

Nansen, The Earth's Crust.........., Oslo, 1928.

Lecture 18

Nonexistence of Shear Waves in the Earth's Core

J. J. Stoker

It is a well-known fact of seismology that the core of the earth does not transmit shear waves. In geophysics this is commonly explained by postulating that the core of the earth behaves like a liquid, in spite of the fact that other phenomena indicate that the core is more rigid than steel. In this lecture it will be shown that according to a nonlinear theory of elasticity, shear waves cannot propagate in an elastic medium if the compression is sufficiently large

We shall consider an elastic medium with plane strain. Let x, y be the Lagrange-coordinates when the medium is unstrained, and X, Y be the Euler-coordinates when the medium is strained. The local deformation is described by the Jacobian matrix

$$\underline{P} \equiv (P_{ij}) = \begin{bmatrix} \frac{\partial X}{\partial x}, & \frac{\partial X}{\partial y} \\ \frac{\partial Y}{\partial x}, & \frac{\partial Y}{\partial y} \end{bmatrix} .$$

When the distortion is a rigid body displacement, $\underline{P}^* \underline{P}$ (an asterisk denotes the transpose) is equal to $\underline{I}$, the identity matrix, there is no strain. According to linear theory of elasticity, when the distortion produces small extensions, $\underline{P}^* \underline{P}$ is approximately $\underline{I} + 2\underline{E} + \ldots$ where $\underline{E}$ is the stress matrix, given by $E_{ij} = \frac{1}{2} \frac{\partial}{\partial x_j} (X_i - x_i) + \frac{1}{2} \frac{\partial}{\partial x_i} (X_j - x_j)$. Thus, in the nonlinear theory of elasticity, when the distortion

produces large extensions, $\underline{P}^* \underline{P}$ should be related to $\underline{E}$ as $\underline{E} = f(\underline{P}^* P)$, the function $f(\xi)$ should have the properties $f(1) = 0$ and $f'(1) = \frac{1}{2}$ so the nonlinear theory will cover the linear theory. We shall choose $f(\xi) = \sqrt{\xi} - 1$. Thus, we assume the following relationship between $\underline{E}$ and $\underline{P}$

$$\underline{E} = \sqrt{\underline{P}^* \underline{P}} - \underline{I} \ .$$

Note that $\underline{P}^* P$ is a symmetric matrix, hence there exists an orthogonal matrix

$$\underline{C} = \begin{bmatrix} \cos\theta & \sin\theta \\ -\sin\theta & \cos\theta \end{bmatrix}$$

such that $\underline{P}^* \underline{P} = (\underline{P}\ \underline{C})^2$. Hence

$$\underline{I} + \underline{E} = \underline{P}\,\underline{C} \ .$$

The local angle of rotation θ is given by $\tan\theta = (\frac{\partial Y}{\partial x} - \frac{\partial X}{\partial y})/(\frac{\partial X}{\partial x} + \frac{\partial Y}{\partial y})$ so that $\underline{E}$ is a symmetric matrix.

It is assumed that the elastic property is characterized by a strain energy density function W such that the potential energy of the elastic body in the strained state is $\iint W\,dxdy$. The Lagrange stress matrix $\underline{Q}$ is defined by $Q_{ij} = \partial W/\partial P_{ij}$. Then, using the principle of virtual work, it can be shown that the strain matrix $\underline{\tau}$ is related to $\underline{P}$ and $\underline{Q}$ by

$$\underline{\tau} = (\det \underline{P})^{-1}\,\underline{Q}\,\underline{P}^* \ .$$

Newton's second law of motion shows that in the absence of body forces the equations of motion are

$$\rho \frac{\partial^2 X}{\partial t^2} = \frac{\partial Q_{11}}{\partial x} + \frac{\partial Q_{12}}{\partial y} ,$$

$$\rho \frac{\partial^2 Y}{\partial t^2} = \frac{\partial Q_{21}}{\partial x} + \frac{\partial Q_{22}}{\partial y} ,$$

where ρ is the mass density in the unstrained state.

For an isotropic medium the dependence of W on $\underline{P}$ must be such that W is a function of the invariants of $\underline{P}$ under rotation. Thus

$$W = W(r,s) ,$$

where

$$r = \mathrm{tr}\sqrt{\underline{P}^* \underline{P}} = \left[\left(\frac{\partial X}{\partial x} + \frac{\partial Y}{\partial y}\right)^2 + \left(\frac{\partial Y}{\partial x} - \frac{\partial X}{\partial y}\right)^2\right]^{1/2} ,$$

$$s = \det\sqrt{\underline{P}^* \underline{P}} = \frac{\partial X}{\partial x}\frac{\partial Y}{\partial y} - \frac{\partial X}{\partial y}\frac{\partial Y}{\partial x} .$$

Here tr and det refer to the trace and the determinant of a matrix. Accordingly, $\underline{Q}$ and $\underline{\tau}$ are given by

$$\underline{Q} = \frac{\partial W}{\partial r}\underline{C}^* + s\frac{\partial W}{\partial s}\underline{P}^{*-1} ,$$

$$\underline{\tau} = \frac{1}{s}\frac{\partial W}{\partial r}(\underline{I} + \underline{E}) + \frac{\partial W}{\partial s}\underline{I} .$$

The function W(r,s) should satisfy the condition $\frac{\partial W}{\partial r} + \frac{\partial W}{\partial s} = 0$ at $r = 2$, $s = 1$ so that zero stress will correspond to zero strain. Now, τ is given by

$$\left(\frac{\partial W}{\partial r} + \frac{\partial W}{\partial s}\right)\underline{I} + \frac{\partial W}{\partial r}\underline{E} + \left(\frac{\partial^2 W}{\partial r^2} + 2\frac{\partial^2 W}{\partial r \partial s} + \frac{\partial^2 W}{\partial s^2} - \frac{\partial W}{\partial r}\right)(\mathrm{tr}\,\underline{E})\underline{I} + \ldots$$

when $W(r,s)$ is expanded at $r = 2$, $s = 1$. On the other hand, in the linear theory ($\underline{P}^* \underline{P} \rightarrow \underline{I}$ hence $r \rightarrow 2$, $s \rightarrow 1$), τ is equal to $\lambda(\text{tr } \underline{E})\underline{I} + 2\mu\underline{E}$, where $\lambda = E\nu(1+\nu)^{-1}(1-2\nu)^{-1}$ and $\mu = \frac{1}{2} E(1+\nu)^{-1}$ are the two Lamé constants defined with respect to Young's modulus E and Poisson's ratio ν. The corresponding function $W(r,s)$ in the limit of the linear theory is $\frac{\lambda}{2}(r-2)^2 + \mu(r^2 - 2r - 2s + 2)$, which is equal to $\frac{\lambda}{2}(\text{tr } \underline{E})^2 + \mu(\underline{E}\,\underline{E})$.

For a harmonic medium, as defined by F. John, $W(r,s)$ has the following form

$$W(r,s) = 2\mu[F(r) - s] \ .$$

At $r = 2$, the function $F(r)$ should satisfy the conditions $F(2) = 1$, $F'(2) = 1$, $F''(2) = (\lambda + 2\mu)/2\mu$ in view of the fact that $F(r) \rightarrow 1 + (r-2) + \frac{\lambda+2\mu}{4\mu}(r-2)^2 + \ldots$ in the limit of linear theory. In addition, $F(r)$ should satisfy the conditions $\frac{d}{dr}\frac{1}{r}\frac{dF}{dr} > 0$ and $\frac{d^2F}{dr^2} > 1$. The first condition follows from the fact that the stress should increase monotonically with the strain in a state of uniform stress. The second condition follows from the fact that when a long rectangular bar is stretched, the decrease in its lateral thickness is slower than the increase in its axial length. In terms of $F(r)$ the relations for $\underline{Q}$ and $\underline{\tau}$ are

$$\underline{Q} = 2\mu F'(r)\underline{C}^* - 2\mu s \underline{P}^{*-1}$$

$$\underline{\tau} = 2\mu \frac{F'(r)}{s}(\underline{I} + \underline{E}) - 2\mu\underline{I}$$

and the equations of motion are

$$\frac{\rho}{2\mu}\frac{\partial^2 X}{\partial t^2} = \frac{\partial A}{\partial x} - \frac{\partial B}{\partial y}$$

$$\frac{\rho}{2\mu}\frac{\partial^2 Y}{\partial t^2} = \frac{\partial A}{\partial y} + \frac{\partial B}{\partial x}$$

where $A \equiv F'(r)\cos\theta$ and $B \equiv F'(r)\sin\theta$, with $\theta(x,y)$ the angle introduced earlier with reference to the rotation matrix $\underline{C}$. When a harmonic medium is in equilibrium, A and B clearly satisfy the Cauchy-Riemann equations, hence they are a pair of conjugate harmonic functions of x and y. It follows that θ and $\frac{1}{2}\log\,[F'(r)]^2$, equal to $\arctan\frac{B}{A}$ and $\log\,(A^2+B^2)^{1/2}$ respectively, are another pair of conjugate harmonic functions.

There is in general one value r_o of r at which $F'(r) = 0$; it corresponds in general to a very large strain — of the order $\frac{1}{2}$, say. Since $A + iB$ is an analytic function of $x + iy$ and $F'(r)$ vanishes at $r = r_o$, the zeros of $F'(r)$ in the body must be isolated, unless $F'(r)$ is identically zero; it then follows that $r \geq r_o$ everywhere or $r \leq r_o$ everywhere inside a harmonic medium which is in equilibrium without body forces.

Now consider wave motions in a strained elastic medium with X equal to ax, and Y equal to by, correspondingly, r equal to $r^o \equiv a+b$, and θ equal to 0. Let

$$X = ax + u(x,y,t) + \ldots\,,$$

$$Y = by + v(x,y,t) + \ldots\,.$$

The equations of motion linearized with respect to the strained equilibrium state are

$$\frac{\rho}{2\mu}\frac{\partial^2 u}{\partial t^2} = F''(r^o)\left(\frac{\partial^2 u}{\partial x^2}+\frac{\partial^2 v}{\partial x\partial y}\right) + \frac{1}{r^o}F'(r^o)\left(\frac{\partial^2 u}{\partial y^2}-\frac{\partial^2 v}{\partial x\partial y}\right) \quad ,$$

$$\frac{\rho}{2\mu}\frac{\partial^2 v}{\partial t^2} = F''(r^o)\left(\frac{\partial^2 u}{\partial x\partial y}+\frac{\partial^2 v}{\partial y^2}\right) - \frac{1}{r^o}F'(r^o)\left(\frac{\partial^2 u}{\partial x\partial y}-\frac{\partial^2 v}{\partial x^2}\right) \quad .$$

Plane wave solutions $u,v \sim \exp i(\xi x + \eta y - ct)$ exist only if the wave speed c is equal to $c_T \equiv [(2\mu/\rho)F'(r^o)/r^o]^{1/2}$ or equal to $c_L \equiv [(2\mu/\rho)F''(r^o)]^{1/2}$. In the first case, the displacement vector (u,v) is perpendicular to the wave normal (ξ,η); it represents a transverse (shear) wave. In the second case, the displacement is parallel to the wave normal; it represents a longitudinal (dilatation) wave. We remark that $c_L > c_T$ because $\frac{d}{dr}\frac{1}{r}\frac{dF}{dr} > 0$. If the initial equilibrium position is without strain ($a = 1$, $b = 1$), the two wave speeds are real $c_T = \sqrt{\mu/\rho}$, $c_L = \sqrt{(\lambda+2\mu)/\rho}$; these are the classical results from the linear theory of elasticity. Since $F''(r^o)$ is always positive, longitudinal waves can always propagate whatever the initial strain is. However, if the initial state of equilibrium has a sufficiently large compression strain so that the medium is in a subcritical state $r^o < r_o$ hence $F'(r^o)/r^o$ is negative, then c_T is imaginary and no shear waves can propagate at all.

References

J. J. Stoker, Topics in nonlinear elasticity, Lecture Notes 1964, Courant Institute of Mathematical Sciences, New York Univ.

F. John, Plane strain problems for a perfectly elastic material of harmonic type, Comm. Pure Appl. Math., 13, 239 (1960).

Lecture 19

Gravity Waves in a Thin Sheet of Viscous Fluid
(work of C. C. Mei)

E. Isaacson

Let us consider a two dimensional incompressible viscous flow down a plane inclined at an angle θ. The governing equations are

$$\frac{\partial}{\partial x} u + \frac{\partial}{\partial y} v = 0 ,$$

$$\frac{\partial}{\partial t} u + u \frac{\partial}{\partial x} u + v \frac{\partial}{\partial y} u + \rho^{-1} \frac{\partial}{\partial x} p = g \sin \theta + \rho^{-1} \mu \left(\frac{\partial^2}{\partial x^2} + \frac{\partial^2}{\partial y^2} \right) u ,$$

$$\frac{\partial}{\partial t} v + u \frac{\partial}{\partial x} v + v \frac{\partial}{\partial y} v + \rho^{-1} \frac{\partial}{\partial y} p = -g \cos \theta + \rho^{-1} \mu \left(\frac{\partial^2}{\partial x^2} + \frac{\partial^2}{\partial y^2} \right) v .$$

Here u is the velocity in the x-direction along the inclined plane, v is the velocity in the y-direction normal to the plane, p is the pressure. The constants ρ, g, and μ are the density, the gravitational acceleration and the coefficient of viscosity. The boundary conditions to be satisfied are

$$u = 0 , \quad v = 0 , \text{ on the inclined plane } \quad y = 0 ;$$

while on the free surface, $y = \eta(x,t)$, we have the kinematic condition,

$$\frac{\partial}{\partial t} \eta + u \frac{\partial}{\partial x} \eta = v , \text{ on } \quad y = \eta(x,t) ,$$

and the condition of no stress, which for the two components yields,

$$(p - 2\mu \frac{\partial}{\partial x} u) \frac{\partial}{\partial x} \eta + \mu(\frac{\partial}{\partial y} u + \frac{\partial}{\partial x} v) = 0 , \quad \text{on} \quad y = \eta(x,t) ,$$

$$p - 2\mu \frac{\partial}{\partial y} v + \mu(\frac{\partial}{\partial y} u + \frac{\partial}{\partial x} v) \frac{\partial}{\partial x} \eta = 0 \quad , \quad \text{on} \quad y = \eta(x,t) .$$

The above set of equations admits the following solution:

$$\eta = h ,$$

$$u = U(y) \equiv \mu^{-1} \rho g \sin \theta \ (hy - \tfrac{1}{2} y^2) ,$$

$$v = 0 ,$$

$$p = P(y) \equiv \rho g \cos \theta \ (h-y) ,$$

which represents a steady, stratified flow of constant depth.

To consider a nonlinear time-dependent flow superposed on this steady flow, we let

$$u = U(y) + u' ,$$

$$v = v' ,$$

$$p = P(y) + p' .$$

Now consider a flow with time scale T, length scales L and H in the x- and y-directions (with $H \equiv h$), velocity scale V and such that $\varepsilon \equiv H/L << 1$ (shallow fluid), the Reynolds number $\rho\mu^{-1}LV = \varepsilon$, the Froude number $V(gL)^{-1/2} = \varepsilon^{1/2}$ (whence $V = (gH)^{1/2}$), and the

Strouhal number $LT^{-1}V^{-1} = \varepsilon^2$. It can be shown that this implies that the steady flow is slow, i.e. $U(y) = O(\varepsilon^2(gH)^{1/2})$, and that $\frac{\partial}{\partial t} u'$ and $\frac{\partial}{\partial t} v'$ are $O(\varepsilon^3)$, $u \frac{\partial}{\partial x} u' + v' \frac{\partial}{\partial y} u$ and $u \frac{\partial}{\partial x} v + v' \frac{\partial}{\partial y} v'$ are $O(\varepsilon)$, $\frac{\partial}{\partial x} p'$, $\frac{\partial}{\partial y} p'$, $\mu\nabla^2 u'$ and $\mu\nabla^2 v'$ are $O(\varepsilon^0)$. Accordingly, it can be found by a formal expansion procedure first in powers of the variable y and then in powers of the parameter ε, that

$$\varepsilon^2 \frac{\partial\eta}{\partial t} + \sin\theta\ \eta^2 \frac{\partial\eta}{\partial x} = \frac{1}{3}\cos\theta \frac{\partial}{\partial x}\left(\eta^3 \frac{\partial\eta}{\partial x}\right) + O(\varepsilon^5) .$$

For a progressing wave of permanent form, in which η is a function of $\xi = x - Ct$, η satisfies the following equation

$$\frac{d}{d\xi}\left(-C\varepsilon^2\eta + \frac{1}{3}\sin\theta\ \eta^3 - \frac{1}{3}\cos\theta\ \eta^3 \frac{\partial\eta}{\partial\xi}\right) = 0 .$$

Suppose that $d\eta/d\xi$ vanishes at $\eta = \varepsilon$, then

$$\cos\theta\ \eta^3 \frac{d\eta}{d\xi} = \sin\theta\ (\eta^3 - \varepsilon^3) - 3C\varepsilon^2(\eta - \varepsilon) .$$

Since $d\eta/d\xi$ is negative when η is between ε and $b \equiv \frac{\varepsilon}{2}[-1 + (12C/\sin\theta - 3)^{1/2}]$, η decreases montonically between these two values. In the critical case, $b = 0$ (which occurs for $C = \frac{1}{3}\sin\theta$), the free surface is normal to the bottom (i.e., $d\eta/d\xi$ becomes infinite at $\eta = 0$). This solution represents a bore invading a dry bed. The equations described above, govern the "large" perturbations about the uniform flow. Such a theory may be of interest in connection with the flow of glaciers. Other, "smaller" perturbation equations and progressing wave solutions are also studied in C. C. Mei, (1966), Journal of Mathematics and Physics, 45, pp. 266-288.

Lecture 20

Temperature Profile of the Solar Wind

Tyan Yeh

The solar wind is the most important discovery in space physics in the last decade. It refers to charged particles moving quickly away from the sun in the interplanetary space. This solar corpuscular radiation is emitted from the surface of the sun due to its high temperature (about 2×10^6 K) in all directions and at all times. The operating mechanism of heating in the outer corona is so effective that the high temperature of the corona extends well into interplanetary space. The particles in the solar wind are accelerated in their flight by the pressure gradient just like a gas discharged into a low pressure region through a de Laval nozzle. At the orbit of the earth the solar wind has a flow velocity of about 300 km/sec with a particle density of about 5 ions/cm^3 and a temperature of about 10^5 K. The interaction of the supersonic solar wind with the geomagnetic field produces a magnetosphere. Thus the dipole geomagnetic field is distorted considerably into a configuration with a magnetic tail, and the geomagnetic field is confined inside the magnetosphere.

The characteristic supersonic expansion of the solar wind was predicted successfully by Parker's theory of coronal expansion. Space-probe measurements confirmed that the solar corpuscular radiation forms a wind rather than a breeze as proposed in the evaporation theory. In the hydrodynamic theory of coronal

expansion, the velocity profile of the solar wind is represented by a critical solution of the momentum equation, assuming that the temperature is known. The temperature profile itself is determined by the energy equation. Beyond several solar radii, thermal conduction is effectively the sole means of transport of heat. Thus the governing equations for a steady state, spherically symmetric solar wind are

$$\frac{d}{dr}(nur^2) = 0 \,, \tag{1}$$

$$(m_p+m_e)nu\frac{du}{dr} + \frac{d}{dr}(2kTn) + (m_p+m_e)GM\frac{n}{r^2} = 0 \,, \tag{2}$$

$$\frac{1}{r^2}\frac{d}{dr}\left(r^2\left(\frac{m_p+m_e}{2}nu^2 + 3kTn\right)u\right) + \frac{1}{r^2}\frac{d}{dr}\left(r^2(2kTn)u\right) + (m_p+m_e)GM\frac{n}{r^2}u = \frac{1}{r^2}\frac{d}{dr}\left(r^2KT^{5/2}\frac{dT}{dr}\right) . \tag{3}$$

Here r is the distance from the center of the sun, n is the number density of protons or electrons, u is the flow velocity, T is the temperature. The constants m_p, m_e and M are the masses of a proton, an electron and the sun, k is the Boltzmann constant, and G is the gravitational constant. The thermal conductivity of a fully ionized gas depends on the temperature $\kappa = KT^{5/2}$, K being a constant. The pressure is equal to 2kTn, the internal energy is equal to 3kTn.

The continuity equation (1) can be integrated to give

$$nur^2 = F \,. \tag{4}$$

The constant $4\pi F$ is the total particle flux. Then the momentum equation (2) can be written

(5) $$\frac{r}{u}\frac{du}{dr} = \frac{2 - (r/T)(dT/dr) - (m_p+m_e)GM/2kTr}{(m_p+m_e)u^2/2kT - 1} .$$

The left side of equation (3) is equal to $2k(\frac{3}{2}\ nu\ dT/dr - Tu\ dn/dr)$ by virtue of equations (1) and (2). Thus the heat-flow equation (3) can be written

(6) $$\frac{K}{2kF}\frac{d}{dr}\left(r^2T^{5/2}\frac{dT}{dr}\right) - \frac{3}{2}\frac{dT}{dr} - \frac{T}{r}\left(2+\frac{r}{u}\frac{du}{dr}\right) = 0 .$$

With the temperature profile assumed known, equation (5) was used by Parker to demonstrate the supersonic expansion of the solar wind. The coupled equations (5) and (6) for u and T have not yet been completely solved analytically. So far only special solutions for some values of the parameters have been obtained by numerical integrations. In carrying out the numerical methods, difficulties in computation do not arise from the coupling between the energy equation and the momentum equation; they arise rather from the singular boundary condition at infinity for the energy equation. These numerical solutions are isolated, because it is not clear at all how they are imbedded in all possible solutions. However by assuming that the velocity profile is known, equation (6) can be used to study the temperature variation in the solar wind.

When u is regarded as a known function of r, equation (6) is a second order differential equation for T, and $ru^{-1}\ du/dr$ as

given by equation (5) contains no second derivative of T. Thus, the mathematical structure of equation (6) is effectively independent of the variation of the term ru^{-1} du/dr, particularly so when du/dr is everywhere positive for the solar wind. We shall exploit this mathematical remark by assuming that ru^{-1} du/dr is equal to a constant. The value of this positive constant does not affect the solutions qualitatively. Hence we shall set it to zero. Formally such an approximation is justifiable when the right side of equation (5) is small, namely, if the solar wind has a small logarithmic expansion rate. At large distances, where the solar wind attains a large velocity and a small temperature, this approximation is certainly valid.

We proceed to solve the approximate heat-flow equation

$$\frac{K}{2kF}\frac{d}{dr}\left(r^2T^{5/2}\frac{dT}{dr}\right)-\frac{3}{2}\frac{dT}{dr}-2\frac{T}{r}=0 . \tag{7}$$

Two boundary conditions are required to fix the solution. One of them arises naturally, viz., T vanishes at infinity. The other one can be chosen as prescribing the temperature at some distance, say $T = T_0$ at $r = r_0$.

A direct verification will show that $(2K/35kF)rT^{5/2} = 1$ is an exact solution of equation (7). This isolated solution is useless, because it cannot satisfy the arbitrarily prescribed temperature at some distance, although it satisfies the singular condition at infinity. However, upon introduction of the following new variables

$$x \equiv \frac{2K}{35kF} rT^{5/2} , \tag{8}$$

$$y \equiv - \frac{2K}{35kF} r^2 \frac{dT^{5/2}}{dr} , \tag{9}$$

the second order differential equation (7) is split into two simultaneous first order differential equations:

$$r \frac{dx}{dr} = x - y , \tag{10}$$

$$r \frac{dy}{dr} = \frac{14y^2 + 6y - 20x}{35x} . \tag{11}$$

The advantageous feature of the simultaneous equations is that elimination of r results in a single first order equation

$$\frac{dy}{dx} = \frac{14y^2 + 6y - 20x}{35x(x-y)} . \tag{12}$$

And according to definitions (8) and (9) we have

$$\frac{r}{T} \frac{dT}{dr} = - \frac{2}{5} \frac{y}{x} . \tag{13}$$

Thus, after solving equation (12) to obtain y in terms of x, we can solve equation (10) to obtain x in terms of r, then T can be found in terms of r by solving equation (13). In this way. all possible solutions of equation (7) are found; and the particular solution which satisfies the appropriate boundary conditions is revealed.

The detailed calculation will be published shortly in the Journal of Geophysical Research.

Security Classification

DOCUMENT CONTROL DATA - R & D

(Security classification of title, body of abstract and indexing annotation must be entered when the overall report is classified)

1. ORIGINATING ACTIVITY (Corporate author) Courant Institute of Mathematical Sciences New York University	2a. REPORT SECURITY CLASSIFICATION not classified 2b. GROUP none
3. REPORT TITLE Some Problems in Geophysics	
4. DESCRIPTIVE NOTES (Type of report and inclusive dates) Technical Report April 1973	
5. AUTHOR(S) (First name, middle initial, last name) J. J. Stoker	

6. REPORT DATE April 1973	7a. TOTAL NO. OF PAGES 149	7b. NO. OF REFS 68
8a. CONTRACT OR GRANT NO. N00014-67-A-0467-0030 b. PROJECT NO. NR 041-446 c. d.	9a. ORIGINATOR'S REPORT NUMBER(S) IMM 394 9b. OTHER REPORT NO(S) (Any other numbers that may be assigned this report) none	
10. DISTRIBUTION STATEMENT Distribution of this document is unlimited.		
11. SUPPLEMENTARY NOTES none	12. SPONSORING MILITARY ACTIVITY Mathematics Branch Office of Naval Research Washington, D. C. 20360	

13. ABSTRACT

This report gives somewhat abbreviated versions of talks in a seminar on geophysics that was held once a week during the academic year 1970-71 at the Courant Institute of Mathematical Sciences of New York University.

The talks were presented for the most part by applied mathematicians rather than by professionals in the field of geophysics, but a number of professionals attended the seminar. It was hoped that both groups would find it interesting and rewarding to look at the problems together, based on the well-founded experience in science that progress has often resulted by bringing disciplines together that at first sight might not seem to have much in common. It was also thought desirable to examine a rather wide variety of physical problems, which in turn required the use of a variety of mathematical ideas and methods. For example, more emphasis was put on problems with formulations from the theory of elasticity in its linear version than is usual in the literature on geophysics.

The table of contents indicates rather clearly the nature of the material presented in this report.

DD FORM 1 NOV 65 1473 (PAGE 1)

S/N 0102-014-6600

Security Classification

14 KEY WORDS	LINK A		LINK B		LINK C	
	ROLE	WT	ROLE	WT	ROLE	WT

DD FORM 1 NOV 65 1473 (BACK)
(PAGE 2)

SEP 18 1973

DATE DUE

OCT 2 2 1973			
1973			
DEC 3 1973			
SEP 2 1974			

GAYLORD PRI